Author's responses for the paper "Implementation and Performance of Adaptive Mesh Refinement in the Ice Sheet System Model (ISSM v4.14)"

Thiago Dias dos Santos, Mathieu Morlighem, Hélène Seroussi, Philippe Remy Bernard Devloo and Jefferson Cardia Simões

December 11th

Response notes

We appreciate the comments and the suggestions given by the reviewers and by the Topical Editor. We reproduced below all their comments.

Attached are:

Pages 2 to 12: author's comment to the reviewers;
Pages 13 to 49: manuscript highlighting the modifications suggested by the reviewers;
Pages 50 to 53: author's comment to the Topical Editor;
Pages 54 to 90: manuscript highlighting the modifications suggested by the Topical Editor.

Author's responses for the paper "Implementation and Performance of Adaptive Mesh Refinement in the Ice Sheet System Model (ISSM v4.14)"

Thiago Dias dos Santos, Mathieu Morlighem, Hélène Seroussi, Philippe Remy Bernard Devloo and Jefferson Cardia Simões

December 5th

Response notes

We appreciate the comments and the suggestions given by the reviewers. We reproduced below all their comments. **The author's responses are in blue and bold**.

Attached are:

(a) the original manuscript highlighting the modifications, and
(b) the new manuscript version.

Note 1: In **(a)**, the deleted words or phrases are in red and in a strikethrough way. **Words or phrases inserted in the manuscript are in blue and bold** (e.g., ~~scheme~~ **schemes**).

Note 2: all modifications are referred to the file **(a)**. Example: **(AMR) approach** ~~approach (AMR)~~, line 6, page 1 (in file (a)).

---

1) Response to Anonymous Referee #1 (RC1)

The paper entitled "Implementation and Performance of Adaptive Mesh Refinement in the Ice Sheet System Model (ISSM v4.14)" by Thiago Dias dos Santos et al., presents the implementation of adaptive mesh refinement (AMR) in the finite element ice flow model ISSM.

The performances of the implementation in terms of accuracy and computing time are assessed using the setups of two recent marine ice sheet intercomparison exercises. Accurate modelling of the grounding line dynamics is particularly important to assess the dynamical contribution of the Antarctic Ice-Sheet to sea-level rise. The recent marine ice sheet model intercomparisons (MISMIPs) have confirmed the sensitivity of the results to the mesh resolution. Saving numerical resources while maintaining accuracy is then essential for simulations at the scale of the whole ice-sheet. Thus this paper address an interesting question for the community.

I find the paper well written and the experiments clearly described and discussed, so I have no general nor specific comments. Previous works on the subjects are clearly detailed in the introduction. Many models use an heuristic criterion based on the distance to the grounding line to prescribe areas of high mesh resolution. Here, this heuristic is compared with the results obtained using an error estimator. It is shown that for complex bed topographies the results based on the distance-to-GL criterion are also sensitive to the distance of refinement, advocating for the use of proper error estimators as refinement criteria. This result is important to motivate further theoretical work on such estimators. The implications for real bed topographies (usually no smooth and not noise free) are discussed in the last section and will motivate further numerical studies.

We would like to thank the Anonymous Referee #1 for his/her positive comments and support for publication.

2) Response to D. Martin (RC2)

Overview

Adaptive mesh refinement (AMR) is a useful numerical tool in ice sheet modeling due to the wide range of resolution requirements, particularly for accurately modeling marine ice sheet dynamics. A large body of evidence points toward the need for very fine model resolution concentrated near grounding lines (GLs), which can migrate over hundreds of kilometers in long-time simulations. AMR provides the capability to efficiently deploy the required fine resolution adaptively only where needed, resulting in potentially large savings in computational resource requirements. This paper describes an approach taken to add adaptive mesh refinement to the finite-element-based ISSM ice sheet model. The authors present a description of the algorithm in use, including examples incorporating two different pre-existing remeshing packages. The paper is fairly well-written and quite readable, although could use some editing to fix some English-grammar issues. It does a fairly good job of representing the details of the approach taken and represents a useful addition to the literature. I support publication after some relatively minor changes.

We thank D. Martin for his positive comments and careful reviews. He pointed out important details, and his comments helped to improve the manuscript.

The movies in the supplement are very short and fast, making it hard to see the details of what is happening. I'd suggest slowing them down somewhat (maybe by a factor of 2 or so?). They do look impressive, however.

We apologize for the very short and fast movies. We tried to avoid uploading very large files. We slowed them down and we also improved the resolutions of the files.

Another general comment – all of the results are presented in terms of GL position, which can be a bit tricky to work with. I'd suggest supplementing with an integrated quantity like ice volume, grounded area, or volume above flotation if that presents a clearer picture.

We added plots with ice volume above flotation (VAF), since this is an integrated quantity that represents potential sea level. The values of VAF depends on the grounding line positions. Therefore, the same AMR mesh-dependency is observed in the VAF plots. Please, see Figure 5, page 31, and Figure 7, page 33.

Also, see

- page 13, line 31

- page 11, line 13

- page 10, line 10

- page 10, line 19

Specific comments

1. p1, line 9: You say here that you use different combinations of the two error estimators, but I didn't see any combinations in the paper – the examples appeared to use either distance from the GL or the ZZ error estimator, but never both. In practice, we've found that the combination of the two works best (although as is pointed out elsewhere in the text, we generally use the undivided Laplacian of the velocity field as a proxy for the truncation error).

This is a good point, we actually did not run the combination of the criteria, since the AMR ZZ produced accurate results in comparison to uniform meshes. We decided to run AMR R5+ZZ and we inserted the results in a table, comparing with AMR ZZ and uniform meshes. Please, see Table 4, page 37.

2. p2, line 10: You might also want to mention the role of ice-shelf buttressing for completeness.

Agreed. Please, see page 2, line 10.

3. p2, line 16: I'd suggest changing "high grid resolution" to "sufficiently high grid resolution" (or "sufficiently fine") – the whole point here is to (locally) apply sufficient resolution to resolve the dynamics in play. What is "sufficient" depends on where you are.
Done, page 2, line 17.

4. p3, line 5: BISICLES is actually at its heart a 2D model, although "2 1/2 D" might be more descriptive due to the vertical reconstruction entailed by the Schoof-Hindmarsh scheme along with the fully 3D temperature/enthalpy discretization.
We thank the reviewer for this information. We changed to "2 1/2 D".
Please, see page 3, line 6.

5. p4, line 20: It would be helpful if you could add a figure showing examples of how the mesh refinement occurs for the two schemes (start with a coarse base mesh, then show how the mesh is evolved in a picture or two). It's too hard to see that level of detail in your figures and animations. I think I can imagine it, but a picture would be helpful here.
We added a figure showing the coarse mesh and the AMR meshes using Bamg and NeoPZ. We also slowed down the animations, and we also changed the other figures according to reviewer suggestions (please, see text below).
Please, see Figure 3, page 25.
Also, see the cross-reference: page 4, line 26, and page 5, line 2.

6. p4, line 21: "numerical perturbations" – what you're really talking about is "numerical errors" (so it would be good to say that explicitly) introduced due to interpolation. It's important to call this out as a source of error that is introduced by the AMR scheme. The reality is that AMR schemes introduce errors; the goal is to ensure that these errors are outweighed by the improved accuracy and efficiency. The fact that you're able to minimize these by minimizing the need to interpolate from old fine-mesh region to new fine-mesh region as the mesh evolves is an important advantage of your approach.
Agreed. We changed that term on page 4, line 23 and line 32.

7. p5, line 21: Are you saying that you are reducing all of the interpolated fields (thickness, bedrock, etc) to processor 0 and then broadcasting them all out? If so, this all-to-one reduction will eventually overwhelm you as you push to larger problems at much higher concurrencies. If that's not what you're doing, please clarify which fields you're talking about here.
Your interpretation is correct, we reduce all fields in CPU #0, and then we broadcast to the other CPUs, such that each CPU takes care of the interpolation process related to their respective nodes/elements. This is done because the mesh partition changes every time AMR is called (the goal is to keep a balanced number of elements among partitions). Then, to interpolate the fields from the old mesh to the new adapted mesh, CPU #0 broadcasts the fields to the others; and each CPU performs the interpolation in its own partition.

The reviewer is right, this all-to-one reduction may be a bottleneck for large models. We optimized this by doing only one big MPI call, compacting the data structure and avoiding multiple MPI communications. Another way to overcome this problem is to perform AMR each X time steps, where X is a user-definition parameter ("AMR frequency", in the ISSM interface). Just to have an idea about the size of the MPI data transmission, we show a simple calculation. A mesh with ~100,000 elements has ~50,000 vertices. Then, we have: 50,000 x 8 bytes = 0.4 Mb per interpolated field. This size is relatively small considering the transmission rate of current InfiniBands (>10 Gb/s).

It is important to note that we are not advocating the AMR strategy used in ISSM is a procedure that should be applied to any Finite Element code or Ice Sheet model. This is

specific for the ISSM architecture. Besides that, our AMR strategy has a minimum impact in the ISSM data structure.

We added some explanations about our optimization scheme on page 5, line 24.

8. p7, line 9: I suspect that the ZZ error estimator will be much more useful when applied to either the velocity field or the stress tensor, since this will indicate where there is instantaneous error in the dynamics (which is what will be improved via AMR). Since ice thickness is essentially a time-integral of the divergence of the velocity field, applying an error estimator to the thickness field is likely to indicate where errors have accumulated over time; adding refinement in those regions is likely too late.

Yes, we agree with the reviewer that the ZZ error estimator is useful for the elliptic part of the ice sheet problem, the SSA equations in this manuscript. Applying the ZZ estimator to the velocity field or stress tensor is a natural approach. In fact, this estimator was proposed by Zienkiewicz and Zhu (*Int J Numer Meth Eng* 1987) for a linear elasticity problem.

We extend the estimator to the ice thickness since this field depends on the bedrock elevation. Basically, the bedrock defines the "vertical geometry" of the problem, which impacts the solutions (ice thickness and velocity field). Then, the ZZ estimator for the ice thickness could be an indicator of areas where the bedrock geometry should be improved in terms of resolution, mainly in transient simulations (where the grounded area changes with time). We suspect that the ZZ for the ice thickness could be also useful if applied together with the other one (ZZ for the deviatoric stress). This should be assessed in the future, for real bedrock elevation, where noise is present.

In order to make it clear to the reader, we changed the order on page 7, emphasizing the implementation of the deviatoric stress tensor. We also inserted a note.
Please, see page 7, line 12 and line 13.

9. p10, line 23: Which is correct? You should use a uniform (very-)fine-mesh solution as a comparison.

The original sentence is correct, because we are referring to Figure 5 (now Figure 6). This figure compares the AMR solutions with the coarse mesh, to show how the GL positions are mesh resolution-dependent and refinement criterion-dependent. But to make it clear to the reader, we inserted the GL positions obtained with the (very-)fine-mesh (L4, uniform).
Please, see Figure 6, page 32, and page 11, line 2 to line 7.

10. p11, line 14: Stability isn't the only reason to refine your timestep – assuming your time integration scheme is consistent, you should also see an O(Δt) or possibly O(Δt^2) component of the error, which can become important if you refine only spatially without a corresponding reduction in the timestep.

Yes, we agree. We use an implicit scheme for the ice thickness evolution, then we have an O(Δt) in terms of the time-integration error. We use the same time-step in these time performance experiments only for comparison (assuming that all cases should have the same error in the time-integration discretization).

We decided to rerun the profiling experiments using the time step required to fulfill the CFL condition (0.2 yr). We apply the same time step to all simulations, such that all cases have the same order in terms of the time-integration error.
Please, see page 11, line 31.

11. p11, line 19: If I understand the approach suggested here, I think the proposal is to initialize the model using a uniform coarse-resolution solution, and then turn on AMR and add resolution as you begin to evolve the ice sheet (and justify it by stating that's how one begins a realistic simulation based on observations). This is almost certain to produce numerical artifacts due to the sudden change in the mesh setup. We have found that it's important to initialize the model (including data assimilation, inverse-problem solution, etc) with at least the resolution configuration that the model will start with to produce an initial condition with as few numerical artifacts as possible (and you actually essentially make that point in the next sentence about requiring both the steady-state and perturbation experiments be carried out using AMR). I realize that this particular sentence only applies to the performance experiments, but it represents a bad idea which might be misconstrued as a suggestion. Why doesn't it make sense to simply run each mesh configuration forward from its own self-consistent steady state? That would be more representative of how one would initialize the model in a realistic configuration.
Yes, we agree that the initial solution and the initial mesh should be carefully defined using the same AMR mesh applied in the experiments (or at least the same mesh resolution). Our idea was only to compare the processing time with AMR within a tolerance in terms of numerical error.

To avoid any misunderstanding, we decided to rerun the time-performance experiments using the same AMR mesh to reach the steady state. We also rephrased the experiment descriptions. Please, see page 12, line 1 to line 11, and Table 3, page 35.

12. section 4.2: There is one more figure which would be very useful here to supplement Figure 3 – a plot which shows both element counts and solution time for each case, each normalized against the values for the equivalent uniform fine-mesh solutions, on the same graph (along the lines of Figure 21 in Martin and Colella, JCP, 2000). This has the advantage of showing both the relative savings due to AMR while also illustrating the overhead due to AMR – as represented by the gap between the cell counts and execution times. (If fully computing the uniform fine-mesh solution is too expensive, you can likely compute a few timesteps and extrapolate).
We added a figure along the lines of Figure 21 in Martin and Colella, JCP, 2000, as the reviewer suggested.
Please, see Figure 9, page 36, and the note on page 12, line 23.

13. p12, line 6: Using estimates of the error is also commonly used in AMR models in the community. For example (as you mention elsewhere), BISICLES often uses the Laplacian of the velocity field as an estimate of the truncation error (in a second-order discretization). Others do as well, but I don't have them at hand. (You seem to imply that using an error-estimator is novel)
We changed that sentence such that it doesn't imply that this is a novel estimator.
Please, see page 12, line 30 and line 33.

14. p13, line 3: I think you can make a stronger statement than "an error estimator may be more appropriate" here – I think you could say "is more appropriate", or, if you'd prefer "is likely more appropriate". This is a nice example of why it is important to understand the error structure of your problem when constructing refinement criteria.
Good point. Done.
Please, see page 14, line 1.

15. p13, line 25: Is there a reason you don't demonstrate an example which uses the combination of refinement criteria that you recommend here?
Well, initially we didn't run the combination R5+ZZ because using the results based on ZZ only were virtually similar to uniform meshes. The idea was to show how a simple test with an error estimator produced accurate solutions with fewer elements.

Our recommendation is based on the following: we know a priori that applying high resolution around GL would reduce the error caused by the basal friction discretization within the elements. In fact, applying only an error estimator does not guarantee that the elements around the GL are refined. We noted this for the MISMIP+ setup. Interestingly, for the MISMIP+ setup, both AMR R5+ZZ and AMR ZZ produced similar results, which does not mean that it would be the case for real ice sheets. Therefore, for general ice sheets, we suspect that using both criteria (R5+ZZ) should work properly.

The results using AMR R5+ZZ are shown in a table. We also added a discussion.
Please, see Table 4, page 37.
Also, see page 14, line 23 to line 33.

16. p13, line 35: In general, actual savings due to AMR are fairly problem-dependent.
Yes, we agree. The original sentence refers to our results. We added a few words to make it clearer.
Please, see page 15, line 7.

17. p.14, line 12: "mainly in setups where bedrock induces strong buttressing" – I'm not sure that's really all that relevant here. The additional error (and hence the additional refinement) occurred due to topographical features which induced complicated stress distributions unrelated to the buttressing.
Yes, we agree. We added "complex stress distributions", and we also keep strong buttressing.
Please, see page 15, line 20.

18. Algorithm 1: It appears that in your algorithm, the initial timestep is taken on the initial coarse mesh before any refinement is implemented. Is that the case? If so, then you have the problem that the initial coarse-resolution timestep can contaminate the solution with initial-time errors. In general, as I mentioned earlier, you're a lot better off if you initialize the problem with the AMR mesh you're going to be running with.
Yes, the reviewer is right. The initial mesh is crucial for the first time steps. We also noted this issue. We wrote step 1 in Algorithm 1 thinking only in the initial configuration for the steady state phase of the MISMIP3d and MISMIP+ experiments. But for general and real applications, the initial mesh should be also defined using AMR mesh, as pointed out by the reviewer (or at least at the same resolution used in the AMR meshes).

We deleted "coarse" in step 1, Algorithm 1, and we added a footnote with this observation. We also added a new reference as examples of initial setup (Lee et al., Annals of Glaciology, 2015). We also refer to Cornford, et al., JCP, 2013.
Please, see Algorithm 1 and the footnote, both on page 26.

19. Figure 5: This figure suffers from the choice of colormaps. White lines are hard to see, particularly in the more highly-refined regions, and the choice of blue dots to represent the AMR GL position makes that hard to discern from the blue velocity colormap. The small size of the plots only adds to the difficulty. What about potentially showing the mesh lines colored by the velocity field colormap, and then using entirely different colors for the grounding lines?
The original plots in Figure 5 (now Figure 6) were saved in PDF format, so the thickness of the lines were relative to monitor configurations. We decided to save the figures in PNG format, and we changed them as the reviewer suggested.
Please, see Figure 6, page 32.

20. Figure 6. This figure is central to the entire effort, and raises a few questions/issues. I find quite a bit puzzling here:

(a) Why is the ZZ error estimator only being used for the NeoPZ case? Is it only available for the NeoPZ runs? (I couldn't find any statement to that effect in the paper, although it's possible I overlooked it).
We have performed these simulations only for NeoPZ, but the ZZ is also available for Bamg. We decided to run with Bamg as well, and we added the results on Figure 6 (now Figure 7). AMR ZZ using Bamg performs similarly to AMR ZZ using NeoPZ.

NeoPZ generates nested meshes, which is suitable to perform AMR using error estimators. In nested meshes there is a hierarchy between elements and their refined "children". Then, it is relatively easy to refine (coarsen) elements (group of elements), in the sense of Algorithm 2 in the manuscript.

For Bamg, there are different approaches to use estimators, for example: applying the desired mesh resolution in selected nodes (where element errors are high, following Algorithm 2), or applying the error as a 2D metric in the original Bamg algorithm. Here, we applied the desired resolution at the nodes according to the error of the adjacent elements, following Algorithm 2.
Please, see Figure 7, page 33.

(b) Would it be possible to use different line types (or possibly different colors) to distinguish the different lines? Seeing how the different cases follow the uniform-mesh case is part of the goal (as distinct from looking at individual data points), and that's hard to separate out when all of the lines are identical, particularly for the finer-resolution parts of the NeoPZ plot.
Done. Please, see Figure 7, page 33.

(c) Do you have any idea why R30 improves continuously with increasing resolution for the NeoPZ runs, but stagnates for the Bamg runs? Can you apply the error estimator to see what's going on there?
We suspect this is due to our parameter settings in terms of the mesh adaptation. In Bamg, we applied a big ratio between adjacent elements. This creates a "transition zone" between the highest and lowest resolutions. See Figure A below. For NeoPZ, we used a larger "transition zone", see Figure B below. These settings were a simple choice during our simulations (we did not try to find the best parameters for each mesher). Of course, NeoPZ generated more elements in this case compared to Bamg. But, for this case, the ZZ error estimator (deviatoric stress) is higher around the refined zone in Bamg mesh in comparison to the mesh generated by NeoPZ.

Also, as we extended the "transition zone" in NeoPZ, the resolution of the bedrock elevation increased more in comparison to the mesh generated by Bamg, since we calculate the MISMIP+ bed elevation in hard code. The error due to the bedrock geometry may be also affecting the results of AMR R30 with Bamg (see further discussion in the next response).

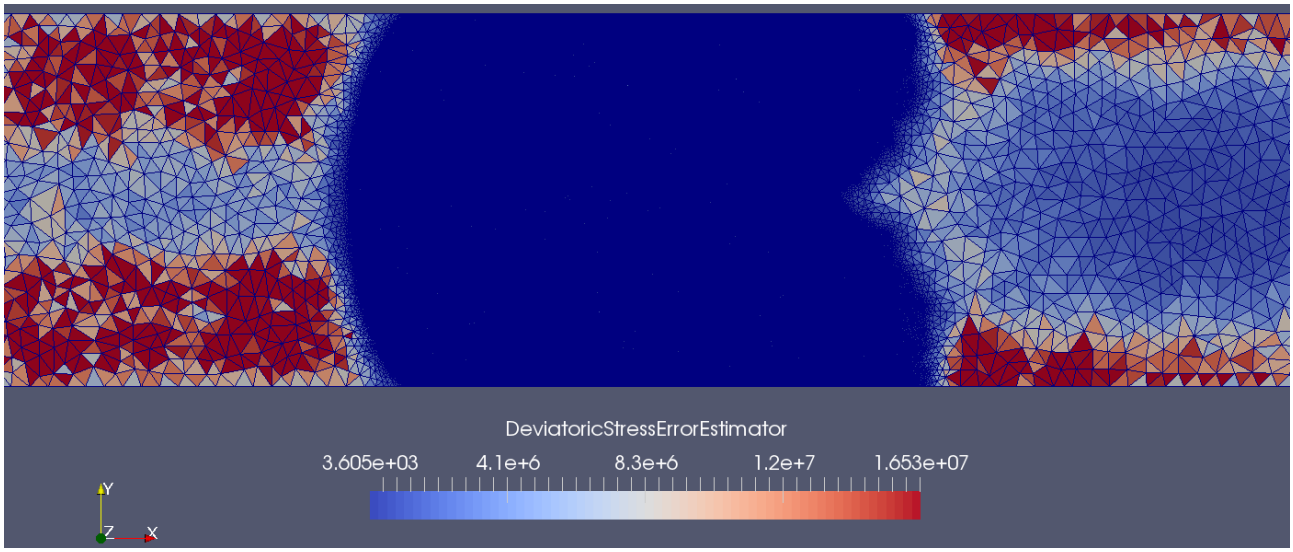

Figure A, AMR R30 using Bamg.

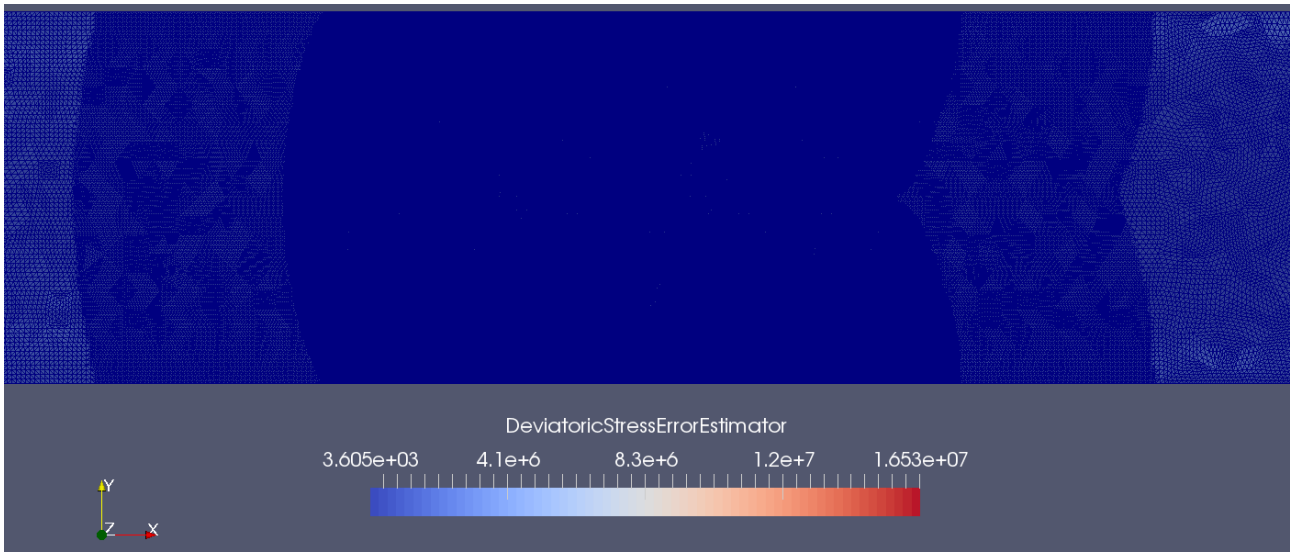

Figure A, AMR R30 using NeoPZ.

(d) The drop-off of the AMR-ZZ case at the finest resolution for the NeoPZ case is problematic, because it could represent a saturation of the ability for AMR to improve the accuracy of your solutions and provide fine-grid accuracy. There are a number of reasons why that might be the case, some of which would indicate potentially serious limitations on your scheme. One possibility, as mentioned earlier, is that temporal errors are beginning to dominate, due to the constant timestep across all resolutions. I suspect, however, that what's happening here is the saturation of your error indicator. The error threshold for refinement should scale appropriately (proportional to dx 2 , perhaps?) to match the target resolution. If you're using the same numerical value in your error-tagging criterion for all runs (you don't actually mention in the paper how you're choosing that parameter – you should say that), it will act as a switch and turn off once the solution is accurate enough to match the criterion. Trying to ask for more refinement after that won't actually add much, and so the solution improvement will stall. If that's the case, then there are two potentially useful outcomes:

i. Tightening the refinement criterion for the 0.25km case will improve the accuracy of that result and reduce or eliminate the stalling apparent in figure 6, and

ii. The corresponding loosening of the refinement criterion for coarser cases will potentially reduce the number of refined cells without a corresponding effect on the solution accuracy (improving the computational efficiency of the AMR scheme)

We actually did not mention the values of the error thresholds used in AMR ZZ simulations. We apologize about this.

For simplicity, we use the same error threshold for all levels of refinement. Probably, for the highest level (L4, resolution equal to 250 m), there is some saturation in the ZZ error indication, as the reviewer pointed out. Our goal was not to find the best parameters (error thresholds). Instead, we wanted to show how a simple simulation using an error estimator produced results very close to the uniformly refined meshes, with fewer elements than the ones produced by AMR R30 meshes.

We don't think the drop-off of the AMR-ZZ is caused by temporal errors because we run until a steady state is reached. Although the steady state in the MISMIP+ setup presents some kind of oscillations (see the movies), we don't think the time stepping would impact the "mean" steady state solution. Also, we noted that as the mesh resolution increases, the oscillations tend to vanish.

Then, we think there are other components of the numerical errors in the MISMIP+ setup. There are at least three (3) source of numerical error (which are not necessarily independent of each other):
1) Basal friction discretization within the elements around the GL;
2) High gradient changes in the velocity field near the GL;
3) Bedrock geometry.

(1) is a model-dependent. Using SEP1 and SEP2 the numerical convergence is higher than using NSEP (please, see Figure 5 for MISMIP3d). Despite that, high resolution at the GL is necessary to reduce this error component. The AMR R5 criterion should reduce this error.

(2) is a physical problem-dependent. We know that around the GL, the deviatoric stress tensor dominates the stress balance (e.g., see Schoof, C., JGR 2007). The length of the region where the velocity field changes significantly (where the deviatoric stress tensor dominates) depends on the geometry of the problem (the bedrock geometry). Refining the elements in this region will reduce the error of the deviatoric stress tensor (the derivative of the velocity field).
The AMR ZZ criterion should reduce this component.

(3) is the error due to the geometry discretization. As we mentioned in the original manuscript, the MISMIP+ bed elevation is calculated directly in the code from the input every time AMR is called. It means that the resolution of the MISMIP+ bedrock is increased during the refinement process only in the refined regions. Therefore, not necessarily applying AMR R5 or AMR ZZ (or combination of both) should improve the MISMIP+ bedrock geometry as the uniformly refinement does. This explains why applying AMR ZZ, even tightening the refinement criterion for the 0.25 km(AMR)-mesh (we did the reviewer suggestion, "i"), does not improve the solutions in comparison to the 0.5 km(AMR)-mesh and to the 0.25 km(uniform)-mesh. Probably this error component also affected the result of AMR_R30 using Bamg (0.25 km-resolution, see the last response above).

In fact, increasing the bedrock geometry resolution during the mesh adaptation makes the problem different from a mathematical point of view. But the comparison between AMR and uniform meshes are yet plausible. In this sense, the difference between AMR ZZ and uniform mesh for 0,25 km-resolution is less than 1%.

We stress that more studies should be carried out using real bedrock topographies, to analyze the weight of the component (3) of the numerical errors.

The thresholds were written in the legends of Figure 7 (page 33), Table 3 (page 35) and Figure 9 (page 36).

21. Figure 7: What does the error look like for uniform fine-mesh solutions? Also, the white mesh lines are even harder to see here than they were in Figure 5.
We inserted a figure for the uniform fine-mesh solution (same level of the AMR meshes). We modified the legend accordingly.

We decided to remove the white lines (mesh) since the goal of Figure 7 (now Figure 8) is to show the spatial distribution of the ZZ error estimator around the grounding line.
Please, see Figure 8, page 34.

Technical corrections

1. p1, line 4: “of grounding line” → “of a grounding line”
Done. Page 1, line 4.

2. p1, line 6: “adaptive mesh refinement approach, AMR” → “adaptive mesh refinement (AMR) approach”
Done. Page 1, line 6.

3. p1, line 9, elsewhere: “MISMIP3d setup” → “the MISMIP3d setup”
Done. Page 1, line 10, and elsewhere.

4. p2, line 4: “the collapse of WAIS is based on” suggest replacing with “projections of the collapse of WAIS are based on...”
Replaced as suggested. Page 2, line 1.

5. p2, line 20: “flux condition at GL...” → “a flux condition at the GL..”
Done. Page 2, line 21.

6. p2, line 24: “allows to apply resources...” → “allows resources to be applied...”
Replaced as suggested. Page 2, line 25.

7. p3, line 11: “ice flow Elmer/Ice” → “ice flow model Elmer/Ice”
Done. Page 3, line 12.

8. p4, line 25: “high adaptive” → “highly adaptive”?
Done. Page 4, line 27.

9. p5, line 4: “transient simulation” → “transient simulations”?
Done. Page 5, line 6.

10. p5. line 23: “being ρi the ice density” → something like “with ρi the ice density...”
Replaced as suggested. Page 6, line 1.

11. p5, line 24: “vertical plane view” – I’d suggest “vertical cross-section” (also in the caption for fig. 1)
Replaced as suggested (in both places). Page 6, line 2.

12. p6, line 1: “of GL” → “of the GL”
Done. Page 6, line 3.

13. p12, line 10: “what is useful...” – do you mean “which is useful...” (if not, then I’m not sure what this means)
Yes, the correct is “which is useful”. We corrected that phrase. Page 13, line 4.

14. p12, line 15: “scheme” → “schemes”
Done. Page 13, line 9.

15. p.14, line 1: "even with a hundred..." → "even with hundreds…"
Done. Page 15, line 8.

16. p.14, line 7: "implemented here dynamic..." → "implemented dynamic…"
Done. Page 15, line 15.

17. p14, line 23: "compenting" → "competing"
Done. Page 16, line 1.

Implementation and Performance of Adaptive Mesh Refinement in the Ice Sheet System Model (ISSM v4.14)

Thiago Dias dos Santos[1], Mathieu Morlighem[2], Hélène Seroussi[3], Philippe Remy Bernard Devloo[1], and Jefferson Cardia Simões[4]

[1]Department of Structures, School of Civil Engineering, Architecture and Urban Design, University of Campinas - UNICAMP, Brazil
[2]Department of Earth System Science - University of California Irvine, CA, USA
[3]Jet Propulsion Laboratory, California Institute of Technology, Pasadena, CA, USA
[4]Polar and Climate Center, Geosciences Institute, Federal University of Rio Grande do Sul - UFRGS, Brazil

Correspondence: Thiago Dias dos Santos (santos.td@gmail.com)

Abstract. Accurate projections of the evolution of ice sheets in a changing climate require a fine mesh/grid resolution to correctly capture fundamental physical processes, such as the evolution of the grounding line, the region where grounded ice starts to float. The evolution of the grounding line indeed plays a major role in ice sheet dynamics, as it is a fundamental control on marine ice sheet stability. Numerical modeling of **a** grounding line requires significant computational resources since the accuracy of its position depends on grid or mesh resolution. A technique that improves accuracy with reduced computational cost is the adaptive mesh refinement **(AMR) approach** ~~approach, AMR~~. We present here the implementation of the AMR technique in the finite element Ice Sheet System Model (ISSM) to simulate grounding line dynamics under two different benchmarks, MISMIP3d and MISMIP+. We test different refinement criteria: (a) distance around the grounding line, (b) a posteriori error estimator, the Zienkiewicz-Zhu (ZZ) error estimator, and (c) different combinations of (a) and (b). We find that for **the** MISMIP3d setup, refining 5 km around the grounding line, both on grounded and floating ice, is sufficient to produce AMR results similar to the ones obtained with uniformly refined meshes. However, for the MISMIP+ setup, we note that there is a minimum distance of 30 km around the grounding line required to produce accurate results. We find this AMR mesh-dependency is linked to the complex bedrock topography of MISMIP+. In both benchmarks, the ZZ error estimator presents high values around the grounding line. Particularly for **the** MISMIP+ setup, the estimator also presents high values in the grounded part of the ice sheet, following the complex shape of the bedrock geometry. This estimator helps guide the refinement procedure such that AMR performance is improved. Our results show that computational time with AMR depends on the required accuracy, but in all cases, it is significantly shorter than for uniformly refined meshes. We conclude that AMR without an associated error estimator should be avoided, especially for real glaciers that have a complex bed geometry.

1 Introduction

The uncertainty in projections of ice sheet contribution to sea level rise in the next century remains large, primarily due to the potential collapse of the West Antarctic Ice Sheet, WAIS (Church et al., 2013; Jevrejeva et al., 2014; Ritz et al., 2015;

DeConto and Pollard, 2016). **Projections of the collapse of WAIS are based on** ~~The collapse of WAIS is based on~~ the Marine Ice Sheet Instability (MISI) hypothesis (Weertman, 1974; Mercer, 1978; Thomas, 1979). This hypothesis refers to ice sheets grounded below sea level on retrograde bedrock slopes (as seen in Figure 1), as is the case for many glaciers in WAIS (Fretwell et al., 2013). MISI states that the grounding line (GL), the region where the ice sheet starts to float (see Figure 1), cannot remain stable on such bedrock slopes (Schoof, 2007b; Katz and Worster, 2010; Gudmundsson et al., 2012). Accordingly, the GL retreat on retrograde bedrock slopes causes increased ice discharge, which in turn leads to further GL retreat, resulting in a non-linear positive feedback. This self-sustaining GL retreat persists until a prograde bedrock slope is reached. Therefore, a change in climate or ocean can potentially force a large-scale fast migration of the GL inland (Schoof, 2007a; Favier et al., 2014; Seroussi et al., 2014b). Recently, the region of WAIS has experienced an increase in the intrusion of ocean warm deep water (Jacobs et al., 2011; Dutrieux et al., 2014) that ~~probably~~ **likely increased the ocean induced melt under the ice shelves, reduced the buttressing they provide to the inland ice, and** triggered the retreat of the GL observed over the last decades (Rignot et al., 2014; Christie et al., 2016; Kimura et al., 2016; Seroussi et al., 2017).

Modeling this positive feedback requires the coupling of different physical processes (ice sheet and ice shelf evolutions, GL migration, basal friction, etc.), and the accuracy of the results is highly dependent on the GL parameterization and the spatial discretization of the domain. Vieli and Payne (2005) compared the results of different ice sheet numerical models in terms of GL migration, and found that the numerical results have a strong dependency on horizontal grid size. Analyzing the stability and dynamics of the GL on reverse bed slopes, Schoof (2007b) pointed out that **sufficiently** high grid resolution in the GL zone is a critical element to obtain reliable numerical results. Two ice sheet model intercomparison projects later confirmed the GL dynamics dependency on spatial resolutions (Pattyn et al., 2012, 2013).

Several marine ice sheet models have employed different numerical schemes to overcome this mesh resolution requirement at the GL with reduced computational cost: by imposing **a** flux condition at **the** GL position (Pollard and DeConto, 2009, 2012; Pattyn, 2017), by treating GL and basal friction with sub-grid or sub-element schemes (Feldmann et al., 2014; Leguy et al., 2014; Seroussi et al., 2014a) or by applying high spatial resolution only in the GL region with adaptive grid refinement (Durand et al., 2009; Goldberg et al., 2009; Gladstone et al., 2010; Gudmundsson et al., 2012; Cornford et al., 2013).

The grid or mesh adaptation technique ~~allows to apply resources~~ **allows resources to be applied** only where they are required, which is very useful in transient simulations that include some discontinuity in the time-dependent solution (Devloo et al., 1987; Berger and Colella, 1989), as is the case for GL dynamics (the basal friction is only applied to grounded ice). This technique can be performed with two different methods: r-adaptivity and h-adaptivity methods (Oden et al., 1986). The r-adaptivity, also known as moving mesh method, moves progressively a fixed number of vertices in a given direction or region (Anderson et al., 1984, p. 533), while the h-adaptivity method, named in this work as adaptive mesh refinement (AMR), splits edges and/or elements, inserting new vertices into the mesh where high resolution is required (Devloo et al., 1987; Berger and Colella, 1989). The performance of each of these methods depends on the problem for which they are applied. Vieli and Payne (2005) showed that models applying moving grid to track the GL movement perform better than fixed grid models. Since the position of the GL is explicitly defined in moving grids, Vieli and Payne (2005) noticed for this method a weak grid resolution dependency in comparison to fixed grid method, for which the GL position falls between grid points. Goldberg

et al. (2009) obtained accurate solutions with fewer resources solving the time-dependent Shelfy-Stream equations with the two different mesh adaptation techniques mentioned above, moving mesh and AMR. Using a one-dimensional Shelfy-Stream model based on finite difference scheme, Gladstone et al. (2010) demonstrated that AMR and sub-grid parameterization for GL position could produce robust predictions of GL migration. Pattyn et al. (2012) found that moving grid methods tend to be the most accurate and AMR can further improve accuracy compared to models based on fixed grid. Cornford et al. (2013) implemented a block-structured AMR in BISICLES, a ~~three dimensional~~ $2^1/_2$**D** ice sheet model based on the finite volume method. They demonstrated that simulations with AMR are computationally cheaper and more efficient, even as the grounding line moves over significant distances. Jouvet and Gräser (2013) combined the Shallow Ice Approximation and the Shallow Shelf Approximation in an AMR numerical scheme involving a truncated Newton multigrid and finite volume method. Through MISMIP3d experiments (Pattyn et al., 2013), they highlighted the relevance and efficiency of AMR in terms of computational cost when high resolution ($\sim$100 m) is necessary to reproduce GL reversibility. Recently, Gillet-Chaulet et al. (2017) implemented an anisotropic mesh adaptation in the finite element ice flow **model** Elmer/Ice (Gagliardini et al., 2013). Based on **the** MISMIP+ experiment (Asay-Davis et al., 2016), they showed that combining various variables (ice thickness, basal drag, velocity, etc.) in an estimator allowed to reduce the number of mesh vertices by more than one order of magnitude compared to uniformly refined meshes, for the same level of numerical accuracy.

Here, we implement the AMR technique for unstructured meshes in the parallel finite element Ice Sheet System Model (ISSM v4.14, Larour et al., 2012). The AMR capability in ISSM relies on two different and independent mesh generators: Bamg, a bidimensional anisotropic mesh generator developed by Hecht (2006), and NeoPZ, a finite element library developed by Devloo (1997). ISSM's architecture is based on the Message Passing Interface (MPI), where models are run in a distributed memory scheme. Our AMR implementation minimizes MPI communications, avoiding overheads and latencies. Since refinement criteria are crucial to AMR performance (Devloo et al., 1987), we implement different criteria based on: (a) the distance to the grounding line, (b) the ZZ error estimator (Zienkiewicz and Zhu, 1987), and (c) different combinations of (a) and (b). To analyze the performance of AMR, we run two benchmark experiments: MISMIP3d (Pattyn et al., 2013) and MISMIP+ (Asay-Davis et al., 2016). We compare AMR results from both Bamg and NeoPZ with uniformly refined meshes in terms of GL position and computational time.

This paper is organized as follows: in Section 2, we summarize the main features of ISSM's architecture, and the strategies used to implement an efficient AMR technique for transient simulations. In Section 3, we describe both MIMISP3d and MISMIP+ experiments used to analyze the AMR performance, and in Section 4 we present the results in terms of GL position and processing time. We finish this paper with a discussion of the results and conclusions in Sections 5 and 6, respectively.

2 AMR implementation

2.1 ISSM architecture

Our AMR implementation is strongly based on the architecture of ISSM. We describe here the main ISSM features necessary to understand the AMR strategy. We refer to Larour et al. (2012) for a more detailed description of ISSM.

Several stress balance approximations are implemented in ISSM, including higher-order models (e.g., Blatter-Pattyn, Pattyn (2003), full-Stokes). The current AMR capability is supported for the 2-D vertically integrated Shallow-Shelf or Shelfy-Stream Approximation (SSA, Morland, 1987; MacAyeal, 1989). The SSA is employed for both grounded and floating ice, so membrane stress terms (which are required to correctly model the GL dynamics, Schoof, 2007b) are included but all vertical shearing is neglected (Seroussi et al., 2014a). Here, the mesh used for the SSA equations is unstructured and relies on a Delaunay triangulation.

ISSM is designed to run in parallel in a distributed memory fashion by Message Passing Interface (MPI). When a model is launched, the entire mesh is spatially partitioned over processing units or cores (CPU's), and data structures related to finite element method are built in each partition. All physical entities that vary in space (ice viscosity, ice thickness, surface, velocities, etc.) are kept within the elements.

MPI communications between the partitions (CPU's) are performed to assemble the global stiffness matrix and load vector, as well as during the solution update in the elements once the system of equations is solved. The advantage of MPI is its ability to handle larger models (i.e. for continental scale simulations) in several cores and nodes on a cluster. Its disadvantage is the cost in the communications between the partitions.

2.2 Bamg and NeoPZ

The AMR technique in ISSM is implemented for unstructured meshes and triangular elements. Here are some short descriptions of the meshers Bamg and NeoPZ.

Bamg (Hecht, 2006) is a bidimensional mesh generator based on Delaunay-like method (Hecht, 2005). This mesh generator is embedded in ISSM for static anisotropic mesh adaptation (Morlighem et al., 2010). Here, we extend Bamg capabilities for dynamic adaptation (AMR). The refinement in Bamg is carried out by specifying the desired resolution on the vertices. To reach the desired resolution, Bamg's algorithm splits triangle edges and inserts new vertices in the mesh (Hecht, 2006). The algorithm keeps new vertices and connectivities unchanged as much as possible compared to the previous mesh (Hecht, 2005). This procedure reduces the numerical ~~perturbations~~ **errors introduced by the AMR** when the solutions are interpolated into the new mesh (see Section 2.3). Regions of different resolutions are linked by a transition zone, where the element sizes are changed gradually. The spatial extent of this transition zone is also specified in the Bamg's algorithm. An example of an adapted mesh using Bamg is shown in Figure **3** ~~6~~ .

NeoPZ (Devloo, 1997) is a finite element library dedicated to ~~high~~ **highly** adaptive techniques (Calle et al., 2015). In NeoPZ's data structure, each element is refined into 4 topologically similar elements, whose resolutions are half of the refined element. To avoid hanging vertices (Calle et al., 2015), some elements are divided in specific ways such that any two elements in the mesh may have a vertex or an entire edge in common, or no vertices in common (Szabó and Babuška, 1991, p. 81). In this sense, all meshes refined by NeoPZ are nested, i.e., vertices and connectivities from the coarse mesh are kept fixed during all simulation time. This characteristic does not introduce any **numerical error induced by the AMR** ~~perturbation~~ during the interpolation process (see Section 2.3). The AMR with NeoPZ is given by specifying the level of refinement, i.e., how often

elements are refined. Therefore, the transition zone, which links regions of different resolutions, is generated stepwise through resolutions dictated by levels of refinement. Figure 3 ~~6~~ shows an example~~s~~ of adapted mesh~~es~~ using NeoPZ.

Here, we describe the algorithm to couple ISSM to Bamg and NeoPZ as well as the refinement criteria usage (Sections 2.3 and 2.4).

2.3 Parallel strategy

The solution sequence for transient ~~simulation~~ simulations with AMR is summarized in Figure 2. Details of AMR processes are itemized in Algorithm 1. In Figure 2, the AMR is the last step to be executed for a given time step. This is an explicit approach, where a new adapted mesh is built for a given solution. In Algorithm 1, all processes involved to perform the AMR in ISSM are executed in the step 'e', the remeshing core. Step 'e.1' executes the mesh adaptation (refinement or coarsening of elements) and the other steps ('e.2' to 'e.5') prepare the adapted mesh, data structures and solutions for the next simulation time step.

Bamg and NeoPZ perform the AMR (step 'e.1', Algorithm 1) in serial, considering the entire mesh. In our implementation, only one partition (which CPU rank is #0) keeps the Bamg or NeoPZ entire mesh, and is responsible to execute the AMR process.

Our AMR implementation keeps the number of partitions constant during all simulation time. The number and distribution of elements into the partitions varies every time AMR is called, since the mesh partitioning process (step 'e.2', Algorithm 1) generates partitions with similar number of elements. This process avoids memory imbalance among the CPU's and overheads during the solver phase (Larour et al., 2012).

Each time remeshing is performed, the solutions and all data fields are interpolated from the old mesh onto the new mesh. This step is executed in parallel, where each CPU interpolates the solutions just on its own partition (step 'e.4', Algorithm 1). The construction of new data structures and the adjustment of solutions (steps 'e.3' and 'e.5', respectively, Algorithm 1) are also executed in parallel, as is the computation of the refinement criteria (see Section 2.4).

All MPI communications in the remesh core (step 'e', Algorithm 1) are minimized to avoid overheads when large models are run. **In order to minimize MPI calls, we perform a single communication of a large array that includes all data structures.** In the interpolation process, for example, all relevant fields are collected by CPU #0 in one single vector structure in such a way that only one MPI broadcast is called. This approach is based on the fact that, in general, it is more efficient to perform few large MPI messages instead of carrying out many smaller ones (Reinders and Jeffers, 2015, p. 327).

2.4 Refinement criteria

The grounding line dynamics is implemented in ISSM through an implicit level set function, ϕ_{gl}, based on a hydrostatic floatation criterion (Seroussi et al., 2014a):

$$\phi_{gl} = H - H_f, \tag{1}$$

where H is the ice thickness and $H_f = -b(\rho_w/\rho_i)$ is the floating height, ~~being~~ **with** ρ_i the ice density, ρ_w the ocean density and b the bedrock elevation (negative if below sea level). Figure 1 illustrates the GL position in a vertical ~~plane view~~ **cross-section** of a marine ice sheet. The position of **the** GL is defined as:

$$\begin{cases} \phi_{gl} < 0: & \text{ice is floating} \\ \phi_{gl} > 0: & \text{ice is grounded} \\ \phi_{gl} = 0: & \text{grounding line position} \end{cases} . \tag{2}$$

The performance of AMR depends on the refinement criterion (Devloo et al., 1987). We implement the three following criteria:

(a) Element distance to the GL, R_{gl};

(b) ZZ error estimator for deviatoric stress tensor, τ and ice thickness, H;

(c) Different combinations of (a) and (b).

The criterion (a) is based on a heuristic approach commonly applied (Goldberg et al., 2009; Gudmundsson et al., 2012; Cornford et al., 2013). The second criterion, (b), is based on the fact that high changes in the gradients in the velocity field (therefore, in the deviatoric stress tensor, τ) and ice thickness, H, are expected to be present near the grounding line. Criterion (c) extends and merges the features of the other two previous criteria. We define the AMR criterion used based on binary flags θ ($= 0$ or 1) such that:

$$\begin{cases} \theta_{gl} = 1: & \text{use element distance to the GL} \\ \theta_{\tau} = 1: & \text{use ZZ error estimator for } \tau \\ \theta_{H} = 1: & \text{use ZZ error estimator for } H \end{cases} . \tag{3}$$

We propose Algorithm 2, inspired by Devloo et al. (1987), to execute the refinement and coarsening processes under different criteria (AMR core, step 'e.2' in Algorithm 1). The first 3 steps in Algorithm 2 compute the criterion according to the binary flags, θ, defined above. These steps are performed in parallel. Step '4' verifies, for each element in the mesh, if it should be refined: its distance to the GL and its ZZ errors are compared with prescribed limits (thresholds). The element is refined if at least one of the thresholds is exceeded, so long as its level of refinement is less than the maximum level chosen. This logical operation is performed by the operator "or" in the statement "if" in step '4'. Once an element is refined, it is identified as a group. Step '5' verifies for each group if it should be coarsened. To be coarsened, a group should meet all thresholds; the logical operator used in this case is "and" (statement "if" in step '5'). Algorithm 2 has two sets of thresholds (shown with max), for elements and for groups of elements. For the algorithm to work properly, these sets of thresholds should be different, following Devloo et al. (1987).

2.5 ZZ error estimator

The generic form of the ZZ (Zienkiewicz and Zhu, 1987) error estimator $\epsilon(e)$ for a given element e is:

$$\epsilon(e) = \left[\int_{\Omega_e} (\nabla u^* - \nabla u)^2 \, d\Omega_e \right]^{1/2}, \tag{4}$$

where Ω_e is the domain of the element e, ∇u is the gradient of the finite element solution u and ∇u^* is the smoothed reconstructed gradient, calculated on the element e as:

$$\nabla u^* = \sum_{i=1}^{s} \psi_i \nabla u_i^*, \tag{5}$$

and

$$\nabla u_i^* = \frac{1}{W_i} \sum_{j=1}^{k} w_j \nabla u_j, \tag{6}$$

where ψ_i is the ith P1 Lagrange shape function on element e, s is the number of shape functions of the element e (here, $s = 3$), j is the jth element connected to the vertex i, k is the number of elements connected to vertex i, w_j is the weight relative to the element j and W_i is the sum of all weights for the vertex i. Here, the weights w are defined as the geometric area of the triangular elements. We implement the ZZ error estimator for the ~~ice thickness ($u = H$) and we extend the estimator for the~~ deviatoric stress tensor (τ), written in a vectorized form, i.e., for SSA we have $\nabla u \rightarrow \boldsymbol{\tau} = (\tau_{xx}, \tau_{yy}, \tau_{xy})^\intercal$. **We also extend the estimator for the ice thickness ($u = H$). The ZZ estimator was conceived by Zienkiewicz and Zhu (1987) for linear elasticity, which involves elliptic equations. Applying the ZZ error estimator to the deviatoric stress tensor is therefore a natural extension, since the SSA equations are also elliptic. The ZZ estimator for the ice thickness highlights the regions of sharp bedrock gradient, and could be used to improve the resolution of the bedrock geometry (e.g., see Figure 8).** See Section 2.4 and Algorithm 2 for how these error estimates are combined.

3 Numerical experiments

We run 2 different benchmark experiments to evaluate the adaptive mesh refinement capabilities based on the MISMIP3D (Pattyn et al., 2013) and MISMIP+ (Asay-Davis et al., 2016) experiments. The following subsections describe briefly each setup. More details can be found in the respective references. All experiments are performed using the vertically integrated Shelfy-Stream Approximation equations (SSA, Morland, 1987; MacAyeal, 1989).

3.1 MISMIP3d setup

The MISMIP3d domain setup is rectangular, and extends from 0 to 800 km in the x direction and from 0 to 50 km in the y direction. The bed elevation (b) varies only in the x direction, as follows:

$$b(x, y) = -100 - x. \tag{7}$$

Boundary conditions are applied as follows: a symmetric condition at $x = 0$ so that ice velocity is equal to zero, a symmetric condition at $y = 0$ (which represents the centerline of the ice stream), and free slip condition at $y = 50$ km so that the flux through these surfaces is zero. Water pressure is applied at the ice front at $x = 800$ km.

The ice viscosity, μ, is considered to be isotropic and to follow the Glen's flow law (Cuffey and Paterson, 2010):

$$\mu = \frac{B}{2\dot{\epsilon_e}^{\frac{n-1}{n}}}, \tag{8}$$

where B ($= A^{1/n}$, being A the Glen's flow law factor) is the ice viscosity parameter, $\dot{\epsilon_e}$ is the effective strain rate and $n = 3$ the Glen's exponent. The ice viscosity parameter, B, is uniform and constant over the domain and the time, and its value is equal to $2.15 \times 10^8\,\mathrm{Pa\,s^{-1/3}}$. A non-linear friction (Weertman) law is applied on grounded ice:

$$\boldsymbol{\tau}_b = C\,|\boldsymbol{u}_b|^{m-1}\,\boldsymbol{u}_b, \tag{9}$$

where $\boldsymbol{\tau}_b$ is the basal shear stress, $\boldsymbol{u}_b$ is the basal sliding velocity, C is the friction coefficient, and $m = 1/3$ is the sliding law exponent. The basal friction coefficient, C, is also spatially uniform for all grounded ice, and equal to $10^7\,\mathrm{Pa\,m^{-1/3}s^{1/3}}$.

The experiments are run starting from an initial configuration with a thin layer (100 m) of ice and run until a steady state condition is reached, which occurs after 30,000 years. We compare the GL positions from different meshes at t=30,000 yr.

We investigate the sensitivity of the AMR for which the refinement method is based on the element distance to the GL, R_{gl} (criterion (a), Section 2.4). For comparison analysis, three different distances are used for the highest refinement level: $R_{gl} = 5$, 10 and 15 km. These different meshes are labeled as R5, R10 and R15, respectively. The distance R_{gl} refers to the region with the highest level of refinement. For example, R5 means that 5 km on both sides of the GL (upstream and downstream) are refined with the highest level. Table 1 summarizes the criteria used for all experiments. The coarse mesh, that has a resolution of 5 km, is used as an initial mesh for all simulations and mesh generators (Bamg and NeoPZ). To analyze the convergence, we refine the coarse mesh $1\times$, $2\times$ and $3\times$. These 3 levels of refinement are applied to both uniform and adaptive meshes, and correspond to elements with 2.5, 1.25 and 0.63 km resolution, respectively. Table 2 presents the correspondence between level and resolution at the GL used in the experiments.

We also investigate the sensitivity of the AMR to GL parameterization into the elements (Seroussi et al., 2014a). Three sub-element parameterizations are tested: no sub-element parameterization (NSEP), sub-element parameterization 1 (SEP1) and sub-element parameterization 2 (SEP2). In the NSEP method, each element of the mesh is either grounded or floating and the grounding line position is defined as the last grounded point. In SEP1 and SEP2 methods, the grounding line position is located anywhere within an element and defined by the implicit level set function, ϕ_{gl}, which is based on the floating condition (see Section 2.4). The difference between SEP1 and SEP2 is how each one of these methods computes the basal friction to match the amount of grounded ice in the element. In the SEP1 approach, the basal friction coefficient (C) is reduced as $C_g = C\,A_g/A$, where C_g is the new basal friction coefficient for the element partially grounded, A_g is the area of grounded ice of this element and A is the total area of the element. In the SPE2 technique, the basal friction is integrated (in the sense of the finite element method) only on the part where the element is grounded. This is done by changing the integration area from

the original element to the grounded part of the element. We refer to Seroussi et al. (2014a) for a complete description of these sub-element parameterizations.

3.2 MISMIP+ setup

The MISMIP+ domain is also rectangular, whose dimensions are: $0 \leq x \leq 640$ km and $0 \leq y \leq 80$ km. The bed elevation is defined as follows:

$$b(x,y) = \max\left(b_x(x) + b_y(y), b_{deep}\right). \tag{10}$$

with:

$$b_x(x) = b_0 + b_2\left(\frac{x}{\bar{x}}\right)^2 + b_4\left(\frac{x}{\bar{x}}\right)^4 + b_6\left(\frac{x}{\bar{x}}\right)^6, \tag{11}$$

and

$$b_y(y) = \frac{d}{1+\exp\left[-2(y - L_y/2 - w_c)/f_c\right]} + \frac{d}{1+\exp\left[2(y - L_y/2 + w_c)/f_c\right]}, \tag{12}$$

where $b_{deep} = -720$ m, $b_0 = -150.0$ m, $b_2 = -728.8$ m, $b_4 = 343.91$ m, $b_6 = -50.57$ m, $\bar{x} = 300$ km, $d = 500$ m, $L_y = 80$ km, $w_c = 24$ km, $f_c = 4$ km. Figure 4 shows the bed elevation calculated with Equations 10, 11 and 12.

The ice is isothermal and the ice viscosity parameter, B, is equal to $1.1642 \times 10^8\,\mathrm{Pa\,s^{-1/3}}$ (uniform and constant over the domain and the time). The boundary conditions are similar to MISMIP3d. The friction model used here is a power law, Eq. (9), with a coefficient, C, equal to $3.160 \times 10^6\,\mathrm{Pa\,m^{-1/3}s^{1/3}}$ (spatially uniform for all grounded ice) and sliding law exponent, m, equal to $1/3$.

We run the experiments starting from an initial configuration with a 100 m thick layer of ice, and run the simulations until a steady state condition is reach (after 20,000 years). The GL positions are compared at t=20,000 yr.

To investigate further the sensitivity of the GL position to the refinement distance, R_{gl}, we choose distances with the highest refinement level equal to $R_{gl} = 5$, 15 and 30 km, with meshes labeled as R5, R15 and R30, respectively (see Table 1). As for **the** MISMIP3d simulations, these distances refer to the region around the GL with the highest level of refinement. The same coarse mesh with a resolution of 4 km is used for Bamg and NeoPZ, and it is refined up to four times for both adaptive and uniform refinement approaches. The respective resolutions for the four refinement levels are 2, 1, 0.5 and 0.25 km. Table 2 summarizes the levels and the respective resolutions at the GL. All **the** MISMIP+ simulations are performed with sub-element parameterization type I, SEP1 (Seroussi et al., 2014a).

It is important to emphasize that the MISMIP+ bed elevation (Figure 4) is calculated directly in the code every time AMR is called (step 'e.5', Algorithm 1). This procedure avoids excessive smoothing of the complex bedrock topography in the refined region.

4 Results

For a given problem, the results from an AMR mesh should be as close as possible (within an acceptable tolerance) to those obtained with an uniformly refined mesh, for the same level of refinement (element resolution) in both meshes. This comparison is an indicator of the AMR performance to that given problem. Since Bamg and NeoPZ adapt the mesh in different ways, it is important to analyze how their differences impact the numerical solutions. Therefore, we first compare the results from the adaptive and uniform meshes using both Bamg and NeoPZ for the MISMIP3d and MISMIP+ experiments, and then we assess the time performance of the AMR in comparison with uniformly refined mesh.

4.1 GL position comparison

4.1.1 MISMIP3d setup

Figure 5 presents the GL positions **and the ice volume above floatation (VAF[1])** for different AMR meshes and sub-element parameterizations as a function of element resolutions. The refinement criterion used is the element distance to the GL, R_{gl} (see Table 1 and Section 2.4). GL positions **and VAF** obtained with uniformly refined meshes are also shown in Figure 5. For NSEP, GL position varies between 200 km and 520 km for meshes L0 (coarse mesh) and L3 (level of refinement equal to 3), respectively. For these same meshes, GL position varies between 620 km and 600 km for SEP1, and 550 km and 600 km for SEP2.

We note that AMR meshes with NeoPZ produces GL positions that are very similar to the ones produced with uniformly refined mesh. This holds for all sub-element parameterizations. AMR with Bamg is more sensitive to NSEP, for which GL positions depend on the element distance to the GL (R_{gl}) used, especially for the lower refinement level (level equal to 1). Despite this, GL positions from AMR with Bamg are in agreement with uniformly refined meshes for SEP1 and SEP2. **Similar behaviour is observed in the VAF amounts.**

4.1.2 MISMIP+ setup

The MISMIP+ bed topography (see Section 3.2 and Figure 4) is designed to introduce a strong buttressing on the ice stream from the confined ice shelf. It is therefore expected that the results are more sensitive to the mesh refinement compared to simpler bedrock descriptions (e.g., MISMIP3d), since refining the mesh also improves the resolution of the bedrock geometry (see Section 3.2).

Figure 6 presents the coarse mesh and 3 examples of adaptive meshes obtained with Bamg and NeoPZ and different criteria: element distance to the GL, R_{gl} ($= 5$ km, R5) and error estimator ZZ (see Table 1). The figure also shows the GL positions obtained with these meshes **and with the most refined uniform mesh (250 m resolution). Figure 6 provides an example of a case for which the GL position remains resolution-dependent and refinement criterion-dependent.** We can note that, using the same criterion based on the element distance the to GL (meshes R5), Bamg and NeoPZ produce different meshes, as

[1] **The ice volume above floatation is the ice volume that contributes to sea level (Bindschadler et al., 2013)**

expected. For Bamg, the transition zone between the lowest and highest resolution is smoother than NeoPZ's mesh, since the resolutions in NeoPZ are obtained stepwise by nested elements. **In Figure 6, at** ~~At~~ the center of the domain (y=40 km), the GL position varies by **12 and 13 km between the most refined uniform mesh and the adaptive meshes generated by Bamg and NeoPZ, respectively. Between the coarse mesh and the adaptive meshes, the GL position varies by about 10 km (for both Bamg and NeoPZ).** ~~10 km between the coarse mesh and the adaptive meshes (for both Bamg and NeoPZ).~~ When the ZZ criterion is used, the GL positions differ by **6 km (17 km)** ~~17 km~~ in comparison with the one obtained from the **most refined uniform mesh (coarse mesh).** ~~coarse mesh.~~

Figure 7 presents a set of results for the grounding line position **and the ice volume above floatation** as a function of mesh resolution. AMR mesh-dependency is clear in Figure 7. For AMR with NeoPZ, GL positions obtained with AMR R5 are below the ones produced by AMR R15 and AMR R30. Marginally AMR R15 and AMR R30 produce the same GL positions. For AMR with Bamg, AMR R5 and AMR R15 do not improve the position of the GL as the resolution increases. We can note the differences of GL positions from AMR (with both Bamg and NeoPZ) and from uniformly refined meshes are higher in comparison to **the** MISMIP3d experiment. **The same AMR mesh-dependency is observed in the VAF values.**

To investigate the possible causes of this AMR mesh-dependency, we perform the AMR using the ZZ error estimator calculated for the deviatoric stress tensor, τ (Table 1). The GL positions obtained with AMR ZZ is presented in Figure 7 ~~, for the mesh generator NeoPZ only~~ . We observe that GL positions with AMR ZZ are closer to the ones obtained with uniform meshes, for all mesh resolutions. To understand this AMR ZZ result, we plot the spatial distributions of the ZZ error estimator for the coarse and adaptive meshes (using NeoPZ), as illustrated in Figure 8 (see also the movies in the supporting information). The ZZ error values are normalized between 0 and 1. For the coarse mesh, we see in Figure 8 that the error estimators calculated for the deviatoric stress tensor and the ice thickness present high values around the GL. In particular, for the ice thickness, the estimator also presents high values in the grounded part of the marine ice sheet, following the high gradient in the side walls of the bed topography (see Figure 4). For AMR R5 meshes, there are high ZZ error values around the refined region. This is not observed when the refinement criterion used is the ZZ estimator (AMR ZZ, see Table 1), as expected. Using the ZZ criterion induces an equalization in the spatial distribution of the estimated errors, improving the solutions (e.g., GL position, see Figure 7). In terms of performance, AMR ZZ generates fewer elements than AMR R30. At the end of the experiment and for a level of refinement equal to 4 (resolution equal to 250 m), **using NeoPZ,** AMR R30 mesh has 464,712 elements, while AMR ZZ mesh has 24,428 elements (i.e., only $\sim$5% of the number of elements in AMR R30).

4.2 AMR time performance

To analyze the AMR performance in terms of computational time, we run the experiment Ice1r of MISMIP+ (Asay-Davis et al., 2016). The experiment starts from the steady state condition and runs forward in time for 100 years with a basal melt rate applied. The time step is equal to **0.2 yr (computed to fulfil the CFL condition for the highest resolution mesh).** ~~1 yr. Although the time step should be around ~0.2 yr for the highest resolution mesh (to fulfil the CFL condition), the simulations here do not present any numerical instabilities.~~ The non-linear SSA equations are solved using the Picard scheme and the Multifrontal Massively Parallel sparse direct Solver, MUMPS (Amestoy et al., 2001, 2006).

The purpose of the experiments described here is to assess the computational overhead when AMR is active. We initialize all the models using the steady state solution obtained with the same AMR mesh (level of refinement and criteria) used to carry out the experiment Ice1r. This procedure emulates a common modeling practice (e.g., Cornford et al., 2013; Lee et al., 2015): the initial conditions are self-consistent with the AMR mesh, avoiding numerical artifacts during the transient simulation. All the experiments are run in parallel (16 cores) in a 2x Intel Xeon E5-2630 v3 2.40 GHz with 64 GB of RAM.

~~We initialize the models using the steady state solution obtained with the coarse mesh. This procedure emulates a common modeling practice: a coarse mesh is initialized with observed fields and the AMR is carried out in the model during the forcing (experiment) scenarios. It is important to note that, in the sense of MISMIP+, both the steady state and the forcing experiments should be carried out using the same AMR mesh. The purpose of the experiments here is only to assess the processing time with AMR. All the experiments are run in parallel (16 cores) in a 2x Intel Xeon E5-2630 v3 2.40 GHz with 64 GB of RAM.~~

Table 3 presents GL positions obtained with different meshes at the end of experiment Ice1r, and the computational time and number of elements required for each mesh, as well as the criterion used. The levels of refinement are labeled as 'L#', e.g., L3 means level 3 (see Table 2). Considering the GL position obtained from the highest resolution mesh (L4 uniform) as a reference result, we compare the computational cost using uniform and AMR meshes to obtain the same result within a deviation of **1.5%** ~~1 km (i.e. 394 ± 1 km)~~ . In Table 3, only L3 **uniform, L3 AMR ZZ and L3 AMR R5+ZZ** meshes produce this required accuracy. L3 uniform mesh has at least ~~3.5~~ **4**× more elements than the AMR L30 meshes, which represents a computational time ~~2.5~~ **24%**× higher in comparison with the adaptive approach. In terms of refinement criteria, AMR ZZ generates ~~half~~ **one-fifth of** the number of elements in comparison to AMR R30, which means virtually at least ~~half of~~ **a quarter of** computational time. Comparing AMR ZZ and L3 uniform, the computational time using the adaptive mesh is at least ~~4~~ **4.5**× less. The performance of Bamg and NeoPZ is similar, once the ratio of computational time and number of elements is virtually equal for both packages **(not shown here)** .

Figure 9 shows the element counts and the solution time for the AMR meshes normalized against the values for the equivalent uniform meshes. In Figure 9, the solution time curve represents the relative savings due to AMR, while the gap between the two curves (solution time minus element counts) illustrates the overhead due to the AMR procedure. We note the AMR overhead decreases with the level of refinement and becomes reasonable for level 2 or higher.

5 Discussion

In this work, we describe the implementation of an adaptive mesh refinement approach in the Ice Sheet System Model (v4.14) as well as the performance of our implementation in terms of grounding line position and simulation time. We investigate the adaptive meshes performance **using a heuristic criterion based on the distance to the GL** ~~using a criterion commonly applied by the community~~ (Durand et al., 2009; Goldberg et al., 2009; Gudmundsson et al., 2012; Cornford et al., 2013), and we compare with an error estimator (ZZ, Zienkiewicz and Zhu, 1987) based on the a posteriori analysis of the transient solutions **(e.g., Goldberg et al., 2009; Gudmundsson et al., 2012; Cornford et al., 2013)** ~~(deviatoric stress tensor and ice thickness)~~ .

We rely on two different mesh generators, Bamg (Hecht, 2006) and NeoPZ (Devloo, 1997) that have different properties. It is therefore expected that their solutions are not identical. This explains the difference observed in GL positions **(and VAF)** compared to uniform meshes for the 3 sub-element parameterizations (e.g., **the** MISMIP3d setup, Figure 5).

NeoPZ generates nested meshes, which reduces errors in the interpolation step, ~~what~~ **which** is useful to assess AMR performance in comparison to uniformly refined mesh. Bamg's algorithm works differently: the fact that some vertices positions change produces at least two side effects: (1) induced errors in the interpolation process; (2) positive or negative impact on the convergence of the solutions. The weight of the first side effect can be reduced using higher element distance to the GL (R_{gl}), for which the highest resolution is applied, and increasing the length of the transition zone between fine and coarse elements. Higher-order interpolative ~~scheme~~ **schemes** can be also used, as pointed out by Goldberg et al. (2009), to avoid solution diffusion. In ISSM, the interpolation scheme is carried out by P0 and P1 Lagrange polynomials, and we suspect these are enough for our AMR procedure. The weight of the second side effect depends on the problem considered. We suspect that for GL dynamics this effect has overall a positive impact, once updating vertex positions is somewhat similar to the moving mesh technique, although the GL is not explicitly defined in our approach as in other studies (e.g., Vieli and Payne, 2005). ~~;Goldberg et al., 2009).~~ This argument is based on the results shown here, for both MISMIP3d and MISMIP+ setup**s**. Some mesh packages and finite element libraries related to NeoPZ are: Deal II (Bangerth et al., 2007), Hermes (Šolín et al., 2008), libMesh (Kirk et al., 2006) and HP90 (Demkowicz et al., 1998). Mesh generators related to Bamg are: MMG (Dapogny et al., 2014), Yams (Frey, 2001) and Gmsh (Geuzaine and Remacle, 2009). So, we expect that the results shown here in this work would be reproduced with these related packages.

The results from MISMIP3d suggest that independently of the sub-element parameterization and refinement level, refining elements within a 5 km region with highest resolution around the GL is enough to generate solutions similar to the ones produced by uniform meshes. This holds for Bamg and NeoPZ (Figure 5). Cornford et al. (2013) presented similar results for SSA equations through BISICLES, an AMR finite volume-based ice sheet simulator. They concluded that refining 4 cells on either sides of the GL was enough to achieve results similar to uniform meshes for all levels of refinement.

For MISMIP+, a minimal distance of 30 km for the highest resolution around the GL is necessary to accurately capture the GL position (Figure 7). Nevertheless, there is a residual between GL positions from AMR and uniform meshes. This AMR mesh-dependency can be explained by the bed topography of MISMIP+ (Figure 4): the high gradient in the side walls induces numerical errors on the gradients of the velocity field (deviatoric stress tensor, near the GL) and ice thickness (on grounded ice), as illustrated by the spatial distribution of the a posteriori error estimator used here (Figure 8). For **the** MISMIP3d setup, the highest values of the error estimate concentrate only around the GL (not shown here), which explains why a few kilometers of high resolution near the GL improves the GL positions.

Figures 5 and 7 present a picture of the impact of mesh resolution in integrated quantities like VAF. The VAF curves follow the GL position behaviour, presenting the same AMR mesh-dependency in the MISMIP+ setup. Therefore, the accuracy of VAF depends on the accuracy of the GL dynamics. Since VAF changes represent potential sea level rise, we highlight that the GL movement should be accurately tracked in ice sheet models.

Since numerical errors are not only concentrated near the GL for the MISMIP+ setup, an error estimator ~~may be~~ **is likely** more appropriate **to understand the error structure of the problem,** to guide the refinement and to reduce the error estimates along the domain, improving AMR performance. This explains why a simple test with the AMR ZZ produces better convergence with much less elements than AMR based on the heuristic criterion (element distance to the GL, Figure 7). Related works have used proxies of error estimators: Goldberg et al. (2009) used the jumps in strain rate between adjacent cells; Gudmundsson et al. (2012) used the second derivative of ice thickness; Cornford et al. (2013) used the Laplacian of the velocity field and Gillet-Chaulet et al. (2017) used the estimator proposed by Frey and Alauzet (2005), whose metric is based on a priori interpolation error calculated by the field's Hessian matrix (second derivative). The ZZ used here is a true a posteriori error estimator based on the recovered gradient (Ainsworth and Oden, 2000, p. 3), widely used in the finite element community (Ainsworth et al., 1989; Grätsch and Bathe, 2005) and suitable to be implemented in ice sheet models, or the ones based on finite volumes or finite differences. As the MISMIP+ bed geometry is more realistic than MISMIP3d, we can expect a similar result for real glaciers, i.e., high numerical errors present in regions not necessarily adjacent to the GL.

Further analysis with ZZ or another error estimator should be developed to improve the AMR criterion used in ice sheet modeling. An important issue to be investigated is the interpolation of real bed topography directly from a dataset every time AMR is carried out. This interpolation increases bed resolution according to mesh adaptation, which reduces the smoothness of the bed in the model (since real beds are not necessarily smooth). The reduction of the bed smoothness induces some numerical errors and counterbalances the effect of mesh adaptation, increasing AMR mesh-dependency. Real bed topographies should be analyzed in benchmark models as well as in real ice sheet domains. Our current AMR implementation interpolates the bed elevation from the coarse (initial) mesh, except for the MISMIP+ experiment, for which we hard-coded the calculation of the bed topography directly in the code (in this case, AMR reduces the smoothness of the bed in the model, but as there is no noise, the numerical error based on the ZZ error estimator for the ice thickness is reduced). The interpolation from a dataset will be implemented in ISSM in the future. Based on this discussion and the results shown in this study, we recommend AMR with the combination of the heuristic criterion (using a minimal distance, e.g., 5 km) with an associated error estimator. **Our recommendation is based on the following: we know a priori that applying high resolution around the GL would reduce the error caused by the basal friction discretization within the elements. In fact, applying only an error estimator does not guarantee that the elements around the GL are refined until the highest (desired) resolution. We noted this for the MISMIP+ setup (see the last mesh in Figure 6). Otherwise,** ~~In other words,~~ only imposing fine mesh resolution near the GL does not ensure that the GL position is correctly captured **because the extension of the region (around the GL) where the velocity field changes significantly (where the deviatoric stress dominates the stress balance in the ice sheet-shelf transition; e.g., Figure 11 in Schoof (2007b)) depends on the physical parameters of the ice sheet. Interestingly, for the MISMIP+ setup, the combination of the heuristic criterion with the ZZ error estimator (AMR R5+ZZ) and the AMR ZZ produce similar results (as shown in Table 4), which does not mean that it would be the case for real ice sheets. Therefore, for real ice sheets, we suspect that using both criteria (R5+ZZ) should work properly.** Tests varying AMR parameters (distance to the GL, maximum thresholds for the error estimator, level of refinement, etc.) should be carried before any ice sheet simulation to optimize AMR performance in terms of both solutions and computational time.

The grounding line zone is not the only place where AMR can be applied. Ice front and calving dynamics (Todd et al., 2018) as well as shear margins in ice streams (Haseloff et al., 2015) are examples for which adaptive meshes can improve numerical solutions with reduced computational efforts. In ISSM, the AMR can be applied to these regions through extension of Algorithm 2. Other experiments (not shown here) testing the AMR to refine the ice front region show promising results (Santos et al., 2018).

Our AMR performance analysis shows that the computational time in AMR simulations reaches up to one order of magnitude less in comparison to models based on uniform meshes. Computational time and solution accuracy of AMR depend on **the physical problem and** the refinement criterion used **. In this work,** ~~, and~~ even with ~~a hundred~~ **hundreds** of elements generated (e.g., meshes AMR R30), the computational time is satisfactory. This is observed for both NeoPZ and Bamg. Further analysis should be carried out to check the performance **in real ice sheets and** in higher computational scale (thousand of elements), but the results presented in this study suggest that our AMR implementation strategy is adapted to the modeling questions being investigated. Our AMR computation time compares to Cornford et al. (2013), in which AMR simulations spend $\sim$1/3 of CPU time needed in simulations performed by uniform meshes.

6 Conclusions

We implemented ~~here~~ dynamic AMR into ISSM and tested its performance on two different experiments with different refinement criteria. The comparison between Bamg and NeoPZ shows that they present similar performance, and the choice of which to be used is up to the user. Moreover, users using Bamg (or similar mesh generator) should pay attention in the minimal extension of the transition zone to reduce numerical errors (e.g., in the interpolation step). NeoPZ is more suitable with error estimators, as well as in AMR performance comparison. Based on the AMR mesh-sensitivity observed here, we conclude that AMR without an error estimator should be avoided, mainly in setups where bedrock induces **complex stress distributions and/or** strong buttressing. In real bedrock topographies, where small scale features may play an important role, an error estimator is suitable to guide the AMR. Further research should be carried out in order to evaluate AMR performance in real bed geometries. Our recommendation to improve the AMR performance while minimizing computational effort is the combination of the heuristic criteria, applying a minimal distance around the GL (e.g., 5 km), with an error estimator. The simple tests with the ZZ error estimator show a significant potential, mostly due to its simple implementation and performance. The AMR technique in ISSM can be extended to others physical processes such that the evolution of ice sheets and, consequently the sea level rise, can be accurately modeled and projected.

Code availability. The adaptive mesh refinement are currently implemented in the ISSM code for triangular elements. The code can be download, compiled and executed following the instructions avaiable on the ISSM website: https://issm.jpl.nasa.gov/download.

Competing interests. Authors declare no ~~compenting~~ **competing** interests.

Acknowledgements. This work was performed at the University of Campinas (UNICAMP) and Federal University of Rio Grande do Sul (UFRGS) with financial support from CNPq - Conselho Nacional de Desenvolvimento Científico e Tecnológico, Brasil, PhD scholarship N^o 140186/2015-8 - and at the University of California Irvine (UCI) under a contract with the National Aeronautics and Space Administration (NASA), Cryospheric Sciences Program (N^o NNX14AN03G).

References

Ainsworth, M. and Oden, J. T.: A Posterori Error Estimation in Finite Element Analysis, Pure and Applied Mathematics: A Wiley Series of Texts, Monographs and Tracts, Wiley-Interscience, New York, NY, USA, 1st edn., 2000.

Ainsworth, M., Zhu, J. Z., Craig, A. W., and Zienkiewicz, O. C.: Analysis of the Zienkiewicz–Zhu a-posteriori error estimator in the finite element method, International Journal for Numerical Methods in Engineering, 28, 2161–2174, https://doi.org/10.1002/nme.1620280912, https://onlinelibrary.wiley.com/doi/abs/10.1002/nme.1620280912, 1989.

Amestoy, P. R., Duff, I. S., L'Excellent, J.-Y., and Koster, J.: A Fully Asynchronous Multifrontal Solver Using Distributed Dynamic Scheduling, SIAM Journal on Matrix Analysis and Applications, 23, 15–41, https://doi.org/10.1137/S0895479899358194, 2001.

Amestoy, P. R., Guermouche, A., L'Excellent, J.-Y., and Pralet, S.: Hybrid scheduling for the parallel solution of linear systems, Parallel Computing, 32, 136–156, https://doi.org/https://doi.org/10.1016/j.parco.2005.07.004, http://www.sciencedirect.com/science/article/pii/S0167819105001328, parallel Matrix Algorithms and Applications (PMAA'04), 2006.

Anderson, D. A., Tannehill, J. C., and Pletcher, R. H.: Computational Fluid Mechanics and Heat Transfer, Series in computational methods in mechanics and thermal sciences, McGraw-Hill Book Company, USA, 1984.

Asay-Davis, X. S., Cornford, S. L., Durand, G., Galton-Fenzi, B. K., Gladstone, R. M., Gudmundsson, G. H., Hattermann, T., Holland, D. M., Holland, D., Holland, P. R., Martin, D. F., Mathiot, P., Pattyn, F., and Seroussi, H.: Experimental design for three interrelated marine ice sheet and ocean model intercomparison projects: MISMIP v. 3 (MISMIP+), ISOMIP v. 2 (ISOMIP+) and MISOMIP v. 1 (MISOMIP1), Geoscientific Model Development, 9, 2471–2497, https://doi.org/10.5194/gmd-9-2471-2016, https://www.geosci-model-dev.net/9/2471/2016/, 2016.

Bangerth, W., Hartmann, R., and Kanschat, G.: Deal.II&Mdash;A General-purpose Object-oriented Finite Element Library, ACM Trans. Math. Softw., 33, https://doi.org/10.1145/1268776.1268779, http://doi.acm.org/10.1145/1268776.1268779, 2007.

Berger, M. and Colella, P.: Local adaptive mesh refinement for shock hydrodynamics, Journal of Computational Physics, 82, 64–84, https://doi.org/https://doi.org/10.1016/0021-9991(89)90035-1, http://www.sciencedirect.com/science/article/pii/0021999189900351, 1989.

Bindschadler, R. A., Nowicki, S., Abe-Ouchi, A., Aschwanden, A., Choi, H., Fastook, J., Granzow, G., Greve, R., Gutowski, G., Herzfeld, U., and et al.: Ice-sheet model sensitivities to environmental forcing and their use in projecting future sea level (the SeaRISE project), Journal of Glaciology, 59, 195–224, https://doi.org/10.3189/2013JoG12J125, 2013.

Calle, J. L. D., Devloo, P. R., and Gomes, S. M.: Implementation of continuous hp-adaptive finite element spaces without limitations on hanging sides and distribution of approximation orders, Computers & Mathematics with Applications, 70, 1051–1069, https://doi.org/https://doi.org/10.1016/j.camwa.2015.06.033, http://www.sciencedirect.com/science/article/pii/S0898122115003193, 2015.

Christie, F. D. W., Bingham, R. G., Gourmelen, N., Tett, S. F. B., and Muto, A.: Four-decade record of pervasive grounding line retreat along the Bellingshausen margin of West Antarctica, Geophysical Research Letters, 43, 5741–5749, https://doi.org/10.1002/2016GL068972, https://agupubs.onlinelibrary.wiley.com/doi/abs/10.1002/2016GL068972, 2016.

Church, J., Clark, P., Cazenave, A., Gregory, J., Jevrejeva, S., Levermann, A., Merrifield, M., Milne, G., Nerem, R., Nunn, P., Payne, A., Pfeffer, W., Stammer, D., and Unnikrishnan, A.: Sea Level Change, in: Climate Change 2013: The Physical Science Basis. Contribution of Working Group I to the Fifth Assessment Report of the Intergovernmental Panel on Climate Change, edited by Stocker, T., Qin, D., Plattner, G.-K., Tignor, M., Allen, S., Boschung, J., Nauels, A., Xia, Y., Bex, V., and Midgley, P., pp. 1137–1216, Cambridge University

Press, Cambridge, United Kingdom and New York, NY, USA, http://www.ipcc.ch/pdf/assessment-report/ar5/wg1/WG1AR5_Chapter13_FINAL.pdf, 2013.

Cornford, S. L., Martin, D. F., Graves, D. T., Ranken, D. F., Brocq, A. M. L., Gladstone, R. M., Payne, A. J., Ng, E. G., and Lipscomb, W. H.: Adaptive mesh, finite volume modeling of marine ice sheets, Journal of Computational Physics, 232, 529 – 549, https://doi.org/https://doi.org/10.1016/j.jcp.2012.08.037, http://www.sciencedirect.com/science/article/pii/S0021999112005050, 2013.

Cuffey, K. and Paterson, W. S. B.: The Physics of Glaciers, Elsevier, Oxford, 4th edn., 2010.

Dapogny, C., Dobrzynski, C., and Frey, P.: Three-dimensional adaptive domain remeshing, implicit domain meshing, and applications to free and moving boundary problems, Journal of Computational Physics, 262, 358–378, https://doi.org/https://doi.org/10.1016/j.jcp.2014.01.005, http://www.sciencedirect.com/science/article/pii/S0021999114000266, 2014.

DeConto, R. and Pollard, D.: Contribution of Antarctica to past and future sea-level rise, Nature, 531, 591–597, https://doi.org/10.1038/nature17145, http://dx.doi.org/10.1038/nature17145, 2016.

Demkowicz, L., Gerdes, K., Schwab, C., Bajer, A., and Walsh, T.: HP90: A general and flexible Fortran 90 hp-FE code, Computing and Visualization in Science, 1, 145–163, https://doi.org/10.1007/s007910050014, https://doi.org/10.1007/s007910050014, 1998.

Devloo, P., Oden, J., and Strouboulis, T.: Implementation of an adaptive refinement technique for the SUPG algorithm, Computer Methods in Applied Mechanics and Engineering, 61, 339–358, https://doi.org/https://doi.org/10.1016/0045-7825(87)90099-5, http://www.sciencedirect.com/science/article/pii/0045782587900995, 1987.

Devloo, P. R. B.: PZ: An object oriented environment for scientific programming, Computer Methods in Applied Mechanics and Engineering, 150, 133–153, https://doi.org/https://doi.org/10.1016/S0045-7825(97)00097-2, http://www.sciencedirect.com/science/article/pii/S0045782597000972, symposium on Advances in Computational Mechanics, 1997.

Durand, G., Gagliardini, O., Zwinger, T., Meur, E. L., and Hindmarsh, R. C.: Full Stokes modeling of marine ice sheets: influence of the grid size, Annals of Glaciology, 50, 109–114, https://doi.org/10.3189/172756409789624283, 2009.

Dutrieux, P., De Rydt, J., Jenkins, A., Holland, P. R., Ha, H. K., Lee, S. H., Steig, E. J., Ding, Q., Abrahamsen, E. P., and Schröder, M.: Strong Sensitivity of Pine Island Ice-Shelf Melting to Climatic Variability, Science, 343, 174–178, https://doi.org/10.1126/science.1244341, http://science.sciencemag.org/content/343/6167/174, 2014.

Favier, L., Durand, G., Cornford, S. L., Gudmundsson, G. H., Gagliardini, O., Gillet-Chaulet, F., Zwinger, T., Payne, A. J., and Le Brocq, A. M.: Retreat of Pine Island Glacier controlled by marine ice-sheet instability, Nature Climate Change, 4, 117–121, https://doi.org/10.1038/nclimate2094, https://www.nature.com/articles/nclimate2094#supplementary-information, 2014.

Feldmann, J., Albrecht, T., Khroulev, C., Pattyn, F., and Levermann, A.: Resolution-dependent performance of grounding line motion in a shallow model compared with a full-Stokes model according to the MISMIP3d intercomparison, Journal of Glaciology, 60, 353–360, https://doi.org/10.3189/2014JoG13J093, 2014.

Fretwell, P., Pritchard, H. D., Vaughan, D. G., Bamber, J. L., Barrand, N. E., Bell, R., Bianchi, C., Bingham, R. G., Blankenship, D. D., Casassa, G., Catania, G., Callens, D., Conway, H., Cook, A. J., Corr, H. F. J., Damaske, D., Damm, V., Ferraccioli, F., Forsberg, R., Fujita, S., Gim, Y., Gogineni, P., Griggs, J. A., Hindmarsh, R. C. A., Holmlund, P., Holt, J. W., Jacobel, R. W., Jenkins, A., Jokat, W., Jordan, T., King, E. C., Kohler, J., Krabill, W., Riger-Kusk, M., Langley, K. A., Leitchenkov, G., Leuschen, C., Luyendyk, B. P., Matsuoka, K., Mouginot, J., Nitsche, F. O., Nogi, Y., Nost, O. A., Popov, S. V., Rignot, E., Rippin, D. M., Rivera, A., Roberts, J., Ross, N., Siegert, M. J., Smith, A. M., Steinhage, D., Studinger, M., Sun, B., Tinto, B. K., Welch, B. C., Wilson, D., Young, D. A., Xiangbin, C., and Zirizzotti, A.: Bedmap2: improved ice bed, surface and thickness datasets for Antarctica, The Cryosphere, 7, 375–393, https://doi.org/10.5194/tc-7-375-2013, https://www.the-cryosphere.net/7/375/2013/, 2013.

Frey, P.: YAMS A fully Automatic Adaptive Isotropic Surface Remeshing Procedure, Tech. rep., INRIA, 2001.

Frey, P. and Alauzet, F.: Anisotropic mesh adaptation for CFD computations, Computer Methods in Applied Mechanics and Engineering, 194, 5068–5082, https://doi.org/https://doi.org/10.1016/j.cma.2004.11.025, http://www.sciencedirect.com/science/article/pii/S0045782505000794, unstructured Mesh Generation, 2005.

Gagliardini, O., Zwinger, T., Gillet-Chaulet, F., Durand, G., Favier, L., de Fleurian, B., Greve, R., Malinen, M., Martín, C., Råback, P., Ruokolainen, J., Sacchettini, M., Schäfer, M., Seddik, H., and Thies, J.: Capabilities and performance of Elmer/Ice, a new-generation ice sheet model, Geoscientific Model Development, 6, 1299–1318, https://doi.org/10.5194/gmd-6-1299-2013, https://www.geosci-model-dev.net/6/1299/2013/, 2013.

Geuzaine, C. and Remacle, J.-F.: Gmsh: A 3-D finite element mesh generator with built-in pre- and post-processing facilities, International Journal for Numerical Methods in Engineering, 79, 1309–1331, https://doi.org/10.1002/nme.2579, https://onlinelibrary.wiley.com/doi/abs/10.1002/nme.2579, 2009.

Gillet-Chaulet, F., Tavard, L., Merino, N., Peyaud, V., Brondex, J., Durand, G., and Gagliardini, O.: Anisotropic mesh adaptation for marine ice-sheet modelling, in: EGU General Assembly 2017, vol. 19, Geophysical Research Abstracts, Vienna, Austria, https://meetingorganizer.copernicus.org/EGU2017/EGU2017-2048.pdf, 2017.

Gladstone, R. M., Lee, V., Vieli, A., and Payne, A. J.: Grounding line migration in an adaptive mesh ice sheet model, Journal of Geophysical Research: Earth Surface, 115, https://doi.org/10.1029/2009JF001615, https://agupubs.onlinelibrary.wiley.com/doi/abs/10.1029/2009JF001615, 2010.

Goldberg, D., Holland, D. M., and Schoof, C.: Grounding line movement and ice shelf buttressing in marine ice sheets, Journal of Geophysical Research: Earth Surface, 114, https://doi.org/10.1029/2008JF001227, https://agupubs.onlinelibrary.wiley.com/doi/abs/10.1029/2008JF001227, 2009.

Grätsch, T. and Bathe, K.-J.: A posteriori error estimation techniques in practical finite element analysis, Computers & Structures, 83, 235–265, https://doi.org/https://doi.org/10.1016/j.compstruc.2004.08.011, http://www.sciencedirect.com/science/article/pii/S0045794904003165, 2005.

Gudmundsson, G. H., Krug, J., Durand, G., Favier, L., and Gagliardini, O.: The stability of grounding lines on retrograde slopes, The Cryosphere, 6, 1497–1505, https://doi.org/10.5194/tc-6-1497-2012, https://www.the-cryosphere.net/6/1497/2012/, 2012.

Haseloff, M., Schoof, C., and Gagliardini, O.: A boundary layer model for ice stream margins, Journal of Fluid Mechanics, 781, 353–387, https://doi.org/10.1017/jfm.2015.503, 2015.

Hecht, F.: A few snags in mesh adaptation loops, in: Proceedings of the 14th International Meshing Roundtable, edited by Hanks, B. W., pp. 301–311, Springer-Verlag Berlin Heidelberg, Germany, 2005.

Hecht, F.: BAMG: Bidimensional Anisotropic Mesh Generator, Tech. rep., FreeFem++, 2006.

Jacobs, S. S., Jenkins, A., Giulivi, C. F., and Dutrieux, P.: Stronger ocean circulation and increased melting under Pine Island Glacier ice shelf, Nature Geoscience, 4, 519–523, https://doi.org/10.1038/ngeo1188, 2011.

Jevrejeva, S., Grinsted, A., and Moore, J. C.: Upper limit for sea level projections by 2100, Environmental Research Letters, 9, 104 008, http://stacks.iop.org/1748-9326/9/i=10/a=104008, 2014.

Jouvet, G. and Gräser, C.: An adaptive Newton multigrid method for a model of marine ice sheets, Journal of Computational Physics, 252, 419 – 437, https://doi.org/https://doi.org/10.1016/j.jcp.2013.06.032, http://www.sciencedirect.com/science/article/pii/S0021999113004622, 2013.

Katz, R. F. and Worster, M. G.: Stability of ice-sheet grounding lines, Proceedings of the Royal Society of London A: Mathematical, Physical and Engineering Sciences, 466, 1597–1620, https://doi.org/10.1098/rspa.2009.0434, http://rspa.royalsocietypublishing.org/content/466/2118/1597, 2010.

Kimura, S., Jenkins, A., Dutrieux, P., Forryan, A., Naveira Garabato, A. C., and Firing, Y.: Ocean mixing beneath Pine Island Glacier ice shelf, West Antarctica, Journal of Geophysical Research: Oceans, 121, 8496–8510, https://doi.org/10.1002/2016JC012149, https://agupubs.onlinelibrary.wiley.com/doi/abs/10.1002/2016JC012149, 2016.

Kirk, B. S., Peterson, J. W., Stogner, R. H., and Carey, G. F.: libMesh : a C++ library for parallel adaptive mesh refinement/coarsening simulations, Engineering with Computers, 22, 237–254, https://doi.org/10.1007/s00366-006-0049-3, https://doi.org/10.1007/s00366-006-0049-3, 2006.

Larour, E., Seroussi, H., Morlighem, M., and Rignot, E.: Continental scale, high order, high spatial resolution, ice sheet modeling using the Ice Sheet System Model (ISSM), Journal of Geophysical Research: Earth Surface, 117, https://doi.org/10.1029/2011JF002140, https://agupubs.onlinelibrary.wiley.com/doi/abs/10.1029/2011JF002140, 2012.

Lee, V., Cornford, S. L., and Payne, A. J.: Initialization of an ice-sheet model for present-day Greenland, Annals of Glaciology, 56, 129–140, https://doi.org/10.3189/2015AoG70A121, 2015.

Leguy, G. R., Asay-Davis, X. S., and Lipscomb, W. H.: Parameterization of basal friction near grounding lines in a one-dimensional ice sheet model, The Cryosphere, 8, 1239–1259, https://doi.org/10.5194/tc-8-1239-2014, https://www.the-cryosphere.net/8/1239/2014/, 2014.

MacAyeal, D.: Large-scale ice flow over a viscous basal sediment: Theory and application to ice stream B, Antarctica, Journal of Geophysical Research: Solid Earth, 94, 4071–4087, https://doi.org/10.1029/JB094iB04p04071, https://agupubs.onlinelibrary.wiley.com/doi/abs/10.1029/JB094iB04p04071, 1989.

Mercer, J. H.: West Antarctic ice sheet and CO2 greenhouse effect: a threat of disaster, Nature, 271, 321–325, https://doi.org/10.1038/271321a0, 1978.

Morland, L. W.: Unconfined ice shelf flow, in: Dynamics of the West Antarctic Ice Sheet, edited by Van der Veen, C. and Oerlemans, J., vol. 4 of Glaciology and Quaternary Geology, pp. 99–116, Springer, Dordrecht, The Netherlands, 1987.

Morlighem, M., Rignot, E., Seroussi, H., Larour, E., Ben Dhia, H., and Aubry, D.: Spatial patterns of basal drag inferred using control methods from a full-Stokes and simpler models for Pine Island Glacier, West Antarctica, Geophysical Research Letters, 37, https://doi.org/10.1029/2010GL043853, https://agupubs.onlinelibrary.wiley.com/doi/abs/10.1029/2010GL043853, 2010.

Oden, J., Strouboulis, T., and Devloo, P.: Adaptive finite element methods for the analysis of inviscid compressible flow: Part I. Fast refinement/unrefinement and moving mesh methods for unstructured meshes, Computer Methods in Applied Mechanics and Engineering, 59, 327–362, https://doi.org/https://doi.org/10.1016/0045-7825(86)90004-6, http://www.sciencedirect.com/science/article/pii/0045782586900046, 1986.

Pattyn, F.: A new three-dimensional higher-order thermomechanical ice sheet model: Basic sensitivity, ice stream development, and ice flow across subglacial lakes, Journal of Geophysical Research, 108, 1–15, 2003.

Pattyn, F.: Sea-level response to melting of Antarctic ice shelves on multi-centennial timescales with the fast Elementary Thermomechanical Ice Sheet model (f.ETISh v1.0), The Cryosphere, 11, 1851–1878, https://doi.org/10.5194/tc-11-1851-2017, https://www.the-cryosphere.net/11/1851/2017/, 2017.

Pattyn, F., Schoof, C., Perichon, L., Hindmarsh, R. C. A., Bueler, E., de Fleurian, B., Durand, G., Gagliardini, O., Gladstone, R., Goldberg, D., Gudmundsson, G. H., Huybrechts, P., Lee, V., Nick, F. M., Payne, A. J., Pollard, D., Rybak, O., Saito, F., and Vieli, A.: Results

of the Marine Ice Sheet Model Intercomparison Project, MISMIP, The Cryosphere, 6, 573–588, https://doi.org/10.5194/tc-6-573-2012, https://www.the-cryosphere.net/6/573/2012/, 2012.

Pattyn, F., Perichon, L., Durand, G., Favier, L., Gagliardini, O., Hindmarsh, R. C., Zwinger, T., Albrecht, T., Cornford, S., Docquier, D., and et al.: Grounding-line migration in plan-view marine ice-sheet models: results of the ice2sea MISMIP3d intercomparison, Journal of Glaciology, 59, 410–422, https://doi.org/10.3189/2013JoG12J129, 2013.

Pollard, D. and DeConto, R. M.: Modelling West Antarctic ice sheet growth and collapse through the past five million years, Nature, 458, 329–332, https://doi.org/10.1038/nature07809, https://www.nature.com/articles/nature07809#supplementary-information, 2009.

Pollard, D. and DeConto, R. M.: Description of a hybrid ice sheet-shelf model, and application to Antarctica, Geoscientific Model Development, 5, 1273–1295, https://doi.org/10.5194/gmd-5-1273-2012, https://www.geosci-model-dev.net/5/1273/2012/, 2012.

Reinders, J. and Jeffers, J.: High Performance Parallelism Pearls, vol. 2, Morgan Kaufmann, Waltham, MA, USA, 2015.

Rignot, E., Mouginot, J., Morlighem, M., Seroussi, H., and Scheuchl, B.: Widespread, rapid grounding line retreat of Pine Island, Thwaites, Smith, and Kohler glaciers, West Antarctica, from 1992 to 2011, Geophysical Research Letters, 41, 3502–3509, https://doi.org/10.1002/2014GL060140, https://agupubs.onlinelibrary.wiley.com/doi/abs/10.1002/2014GL060140, 2014.

Ritz, C., Edwards, T., Durand, G., Payne, A., Peyaud, V., and Hindmarsh, R.: Potential sea-level rise from Antarctic ice-sheet instability constrained by observations, Nature, 528, 115–118, https://doi.org/10.1038/nature16147, http://dx.doi.org/10.1038/nature16147, 2015.

Santos, T. D., Devloo, P. R. B., Simões, J. C., Morlighem, M., and Seroussi, H.: Adaptive Mesh Refinement Applied to Grounding Line and Ice Front Dynamics, in: EGU General Assembly 2018, vol. 20, Geophysical Research Abstracts, Vienna, Austria, https://meetingorganizer.copernicus.org/EGU2018/EGU2018-1886.pdf, 2018.

Schoof, C.: Marine ice-sheet dynamics. Part 1. The case of rapid sliding, Journal of Fluid Mechanics, 573, 27–55, https://doi.org/10.1017/S0022112006003570, 2007a.

Schoof, C.: Ice sheet grounding line dynamics: Steady states, stability, and hysteresis, Journal of Geophysical Research: Earth Surface, 112, https://doi.org/10.1029/2006JF000664, https://agupubs.onlinelibrary.wiley.com/doi/abs/10.1029/2006JF000664, 2007b.

Seroussi, H., Morlighem, M., Larour, E., Rignot, E., and Khazendar, A.: Hydrostatic grounding line parameterization in ice sheet models, The Cryosphere, 8, 2075–2087, https://doi.org/10.5194/tc-8-2075-2014, https://www.the-cryosphere.net/8/2075/2014/, 2014a.

Seroussi, H., Morlighem, M., Rignot, E., Mouginot, J., Larour, E., Schodlok, M., and Khazendar, A.: Sensitivity of the dynamics of Pine Island Glacier, West Antarctica, to climate forcing for the next 50 years, The Cryosphere, 8, 1699–1710, https://doi.org/10.5194/tc-8-1699-2014, https://www.the-cryosphere.net/8/1699/2014/, 2014b.

Seroussi, H., Nakayama, Y., Larour, E., Menemenlis, D., Morlighem, M., Rignot, E., and Khazendar, A.: Continued retreat of Thwaites Glacier, West Antarctica, controlled by bed topography and ocean circulation, Geophysical Research Letters, 44, 6191–6199, https://doi.org/10.1002/2017GL072910, https://agupubs.onlinelibrary.wiley.com/doi/abs/10.1002/2017GL072910, 2017.

Szabó, B. and Babuška, I.: Finite Element Analysis, John Wiley & Sons, USA, 1991.

Thomas, R.: The Dynamics of Marine Ice Sheet, Journal of Glaciology, 24, 167–177, https://doi.org/10.3189/S0022143000014726, 1979.

Todd, J., Christoffersen, P., Zwinger, T., Råback, P., Chauché, N., Benn, D., Luckman, A., Ryan, J., Toberg, N., Slater, D., and Hubbard, A.: A Full-Stokes 3-D Calving Model Applied to a Large Greenlandic Glacier, Journal of Geophysical Research: Earth Surface, 123, 410–432, https://doi.org/10.1002/2017JF004349, https://agupubs.onlinelibrary.wiley.com/doi/abs/10.1002/2017JF004349, 2018.

Vieli, A. and Payne, A. J.: Assessing the ability of numerical ice sheet models to simulate grounding line migration, Journal of Geophysical Research: Earth Surface, 110, https://doi.org/10.1029/2004JF000202, https://agupubs.onlinelibrary.wiley.com/doi/abs/10.1029/2004JF000202, 2005.

Šolín, P., Červený, J., and Doležel, I.: Arbitrary-level hanging nodes and automatic adaptivity in the hp-FEM, Mathematics and Computers in Simulation, 77, 117–132, https://doi.org/https://doi.org/10.1016/j.matcom.2007.02.011, http://www.sciencedirect.com/science/article/pii/S0378475407001504, 2008.

Weertman, J.: Stability of the junction of an ice sheet and an ice shelf, Journal of Glaciology, 13, 3–11, https://doi.org/10.3189/S0022143000023327, 1974.

Zienkiewicz, O. C. and Zhu, J. Z.: A simple error estimator and adaptive procedure for practical engineerng analysis, International Journal for Numerical Methods in Engineering, 24, 337–357, https://doi.org/10.1002/nme.1620240206, https://onlinelibrary.wiley.com/doi/abs/10.1002/nme.1620240206, 1987.

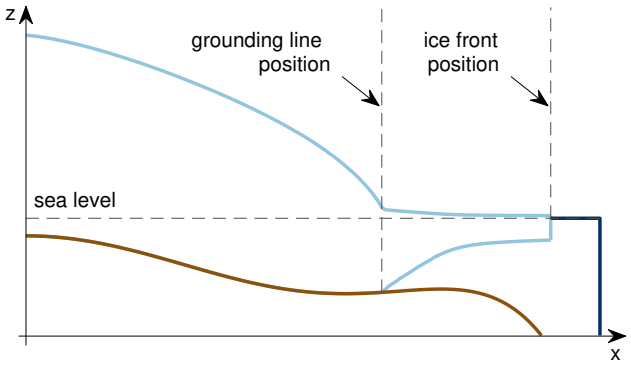

Figure 1. Vertical ~~plane view~~ **cross-section** of a marine ice sheet: **marine ice sheet**, **ocean** and **bed**. The position of the grounding line is implicitly defined by the level set function, ϕ_{gl}, based on a hydrostatic floatation criterion (Seroussi et al., 2014a).

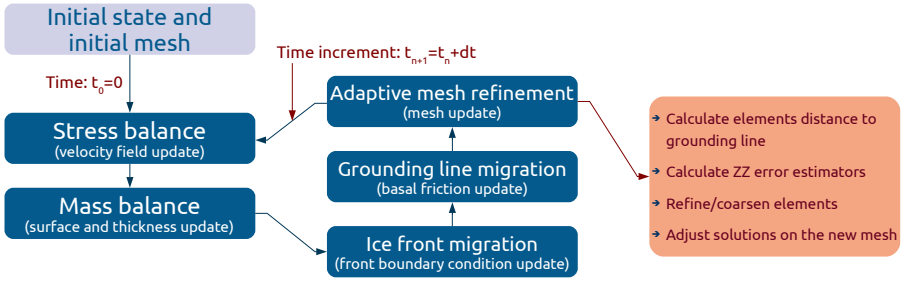

Figure 2. Solution sequence for ice sheet transient simulation with adaptive mesh refinement.

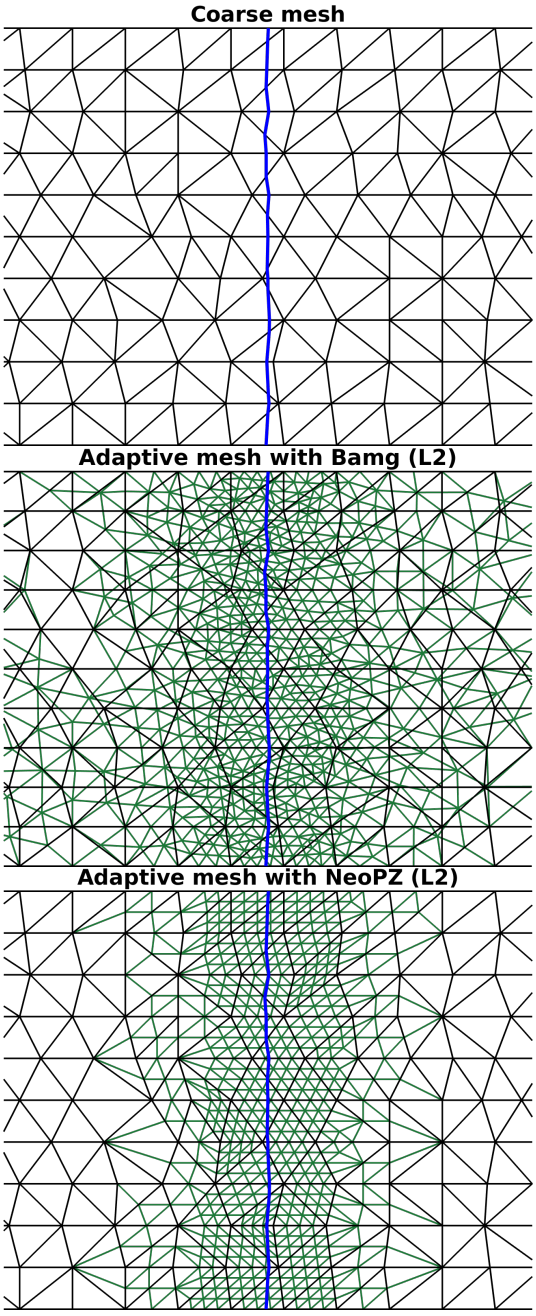

Figure 3. Examples of adaptive meshes using Bamg and NeoPZ. **Blue line**: grounding line position. **Black lines**: coarse mesh, common for Bamg and NeoPZ. **Green lines**: adaptive meshes with level of refinement equal to 2 (L2). Bamg keeps vertices and connectivities unchanged as much as possible compared to the coarse mesh. NeoPZ generates nested meshes: vertices and connectivities of the coarse mesh are kept unchanged.

Algorithm 1 Transient simulation with AMR

1. set initial solution state and initial ~~coarse~~ mesh[2]
2. while $t_n \leq t_{max}$ do:
    a. call stress balance core (diagnostic)
    b. call thickness balance core (prognostic)
    c. call ice front migration core (level set adjustment)
    d. call grounding line migration core (hydrostatic adjustment)
    e. call remesh core (AMR)
        e.1. call AMR core (refine/coarsen mesh, Bamg or NeoPZ, serial in CPU #0)
        e.2. call mesh partitioning (over all CPU's, serial)
        e.3. build new data structures (all CPU's, parallel)
        e.4. interpolate solutions (all CPU's, parallel)
        e.5. call geometry adjustment core (all CPU's, parallel)
    f. time increment $t_{n+1} = t_n + dt$
3. post processing

[2] **The setup of the inital solution into the initial mesh is important to reduce numerical artifacts in the first time steps. Therefore, the initial mesh should be defined using AMR with the same level of refinement chosen in Algorithm 1 (e.g., see Cornford et al., 2013; Lee et al., 2015).**

Algorithm 2 AMR core: refinement criteria calculation, refinement and coarsening processes. e = element. g = group of elements that are nested and derived from a refined element. $L(e)$ = level of refinement of the element e. L^{max} = maximum level of refinement. R^{max} = maximum threshold for element/group distance to the grounding line. ϵ^{max} = maximum threshold for element/group error estimator (thickness/deviatoric stress). θ = binary flags that define the **criteria** ~~criterion to use~~.

1. if $\theta_{gl} = 1$, then **compute** the element and group distances to the grounding line, $R_{gl}(e)$ and $R_{gl}(g)$.
2. if $\theta_{\tau} = 1$, then **compute** the element and group deviatoric stress error estimators, $\epsilon_{\tau}(e)$ and $\epsilon_{\tau}(g)$.
3. if $\theta_{H} = 1$, then **compute** the element and group thickness error estimators, $\epsilon_{H}(e)$ and $\epsilon_{H}(g)$.
4. for each element e such that $L(e) < L^{max}$, do:
   if $\left[R_{gl}(e) < \theta_{gl} \cdot R_{gl,e}^{max}\right]$ or if $\left[\theta_{\tau} \cdot \epsilon_{\tau}(e) > \epsilon_{\tau,e}^{max}\right]$ or if $\left[\theta_{H} \cdot \epsilon_{H}(e) > \epsilon_{H,e}^{max}\right]$,
   then **refine** e.
5. for each group g, do:
   if $\left[R_{gl}(g) > \theta_{gl} \cdot R_{gl,g}^{max}\right]$ and if $\left[\theta_{\tau} \cdot \epsilon_{\tau}(g) < \epsilon_{\tau,g}^{max}\right]$ and if $\left[\theta_{H} \cdot \epsilon_{H}(g) < \epsilon_{H,g}^{max}\right]$,
   then **coarsen** g.

Table 1. Refinement criteria for the adaptive mesh refinement (AMR) simulations.

Experiment	Label	Criterion
MISMIP3d	AMR R5	distance of 5 km to the GL
MISMIP3d	AMR R10	distance of 10 km to the GL
MISMIP3d	AMR R15	distance of 15 km to the GL
MISMIP+	AMR R5	distance of 5 km to the GL
MISMIP+	AMR R15	distance of 15 km to the GL
MISMIP+	AMR R30	distance of 30 km to the GL
MISMIP+	AMR ZZ	ZZ error estimator for τ

GL = grounding line. τ = deviatoric stress tensor. The distance to the GL refers to the region with the highest level of refinement. For example, AMR R5 means that 5 km on both sides of the GL (upstream and downstream) are refined with the highest level.

Table 2. Levels of refinement tested in the experiments.

Experiment	Level	Label	Resolution
MISMIP3d	0 (CM)	L0	5 km
MISMIP3d	1	L1	2.5 km
MISMIP3d	2	L2	1.25 km
MISMIP3d	3	L3	625 m
MISMIP+	0 (CM)	L0	4 km
MISMIP+	1	L1	2 km
MISMIP+	2	L2	1 km
MISMIP+	3	L3	500 m
MISMIP+	4	L4	250 m

CM = coarse mesh, common for Bamg and NeoPZ.

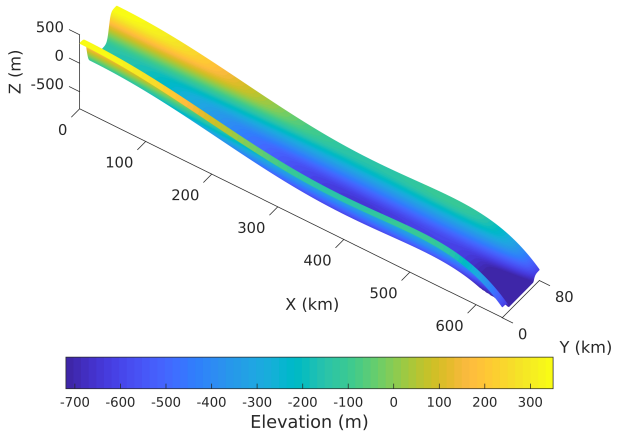

Figure 4. The bedrock topography for the MISMIP+ experiment (Asay-Davis et al., 2016).

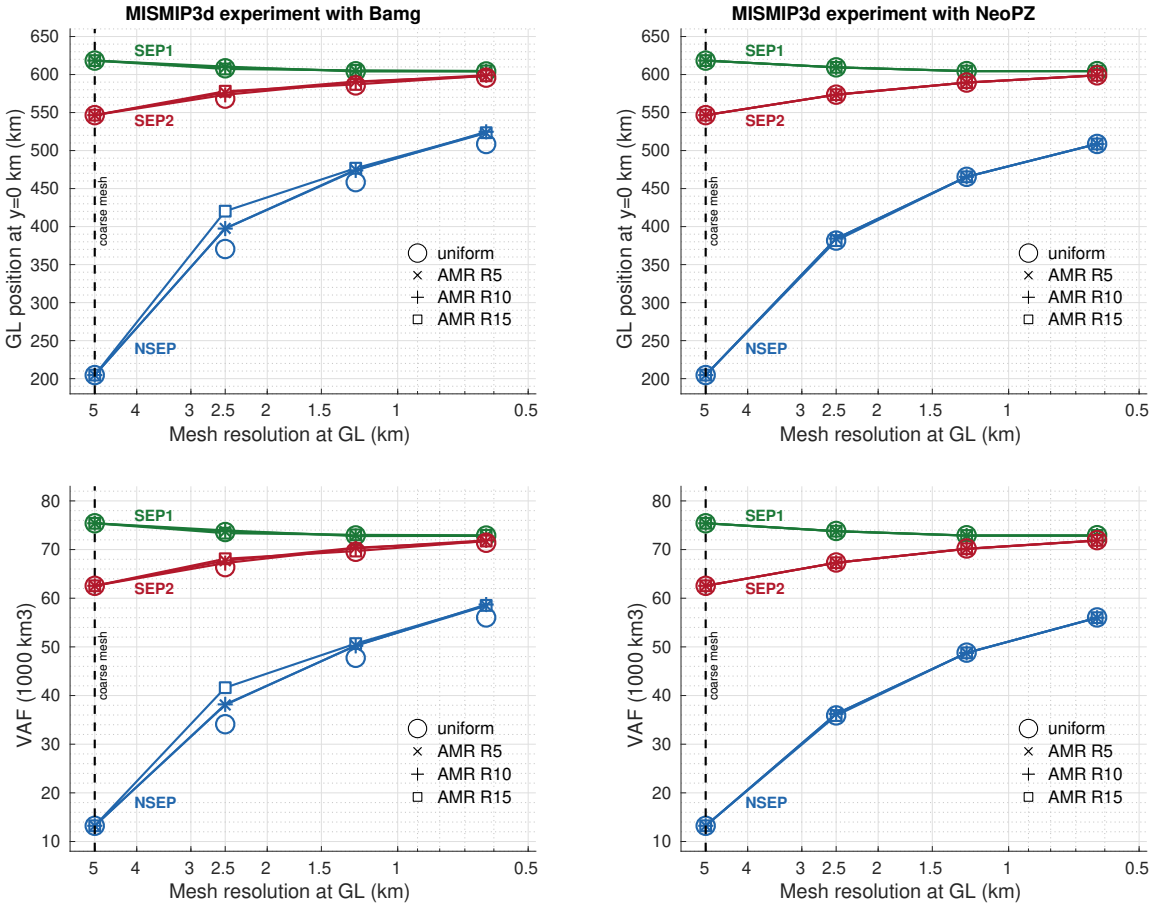

Figure 5. Grounding line (GL) positions **and ice volume above floatation (VAF)** at steady state obtained from the coarse mesh and from adaptive mesh refinement (AMR) using the refinement criterion based on the element distance to the GL, R_{gl}. Three element distances are used and compared: $R_{gl} = 5$, $= 10$ and $= 15$ km. The meshes generated with these distances are labeled as AMR R5, AMR R10 and AMR R15, respectively (see Tables 1 and 2). Results from uniformly refined meshes (labeled as uniform) are also shown. The simulations are carried out through the mesh generators Bamg (left) and NeoPZ (right) using 3 sub-element parameterizations: NSEP, SEP1 and SEP2.

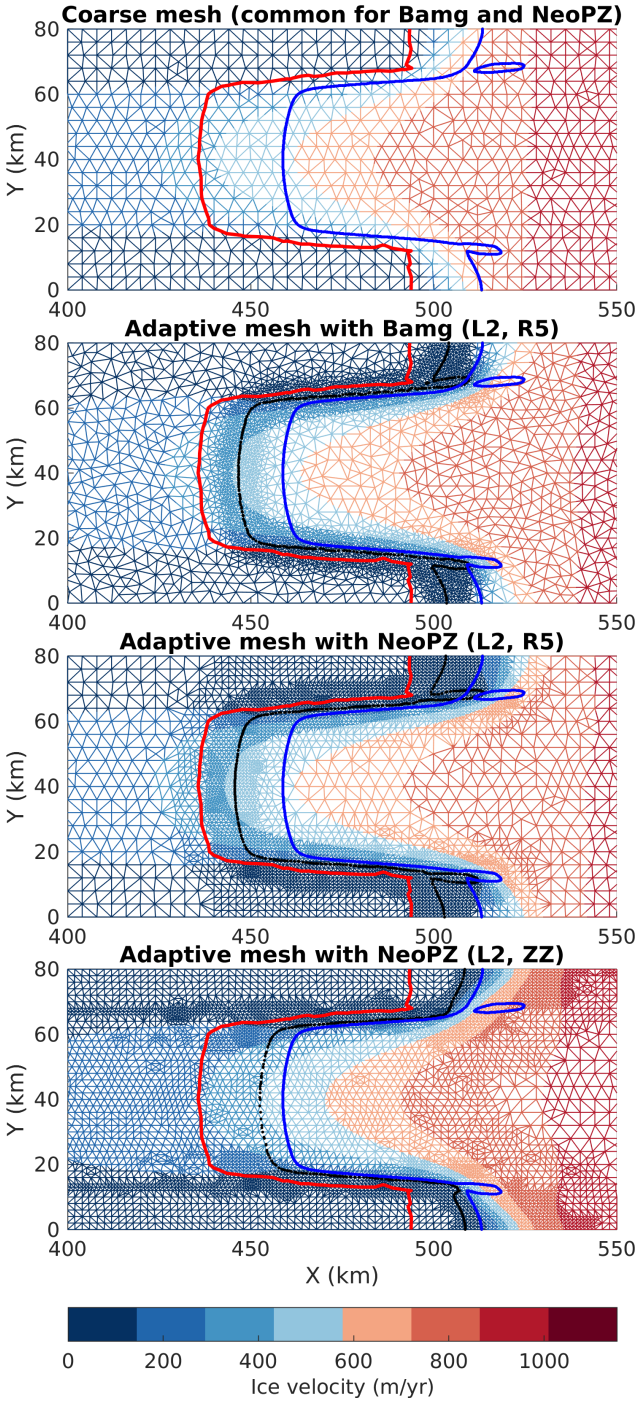

Figure 6. Examples of adaptive meshes for **the** MISMIP+ experiment using different refinement criteria and mesh generators (see Tables 1 and 2). **Red line**: grounding line position at steady state obtained with the coarse mesh. **Black dots**: grounding line position at steady state obtained with each adaptive mesh. **Blue line: grounding line position at steady state obtained with the most refined mesh (L4, uniform). The thresholds used in the ZZ crterion are described in the legend of Figure 7.**

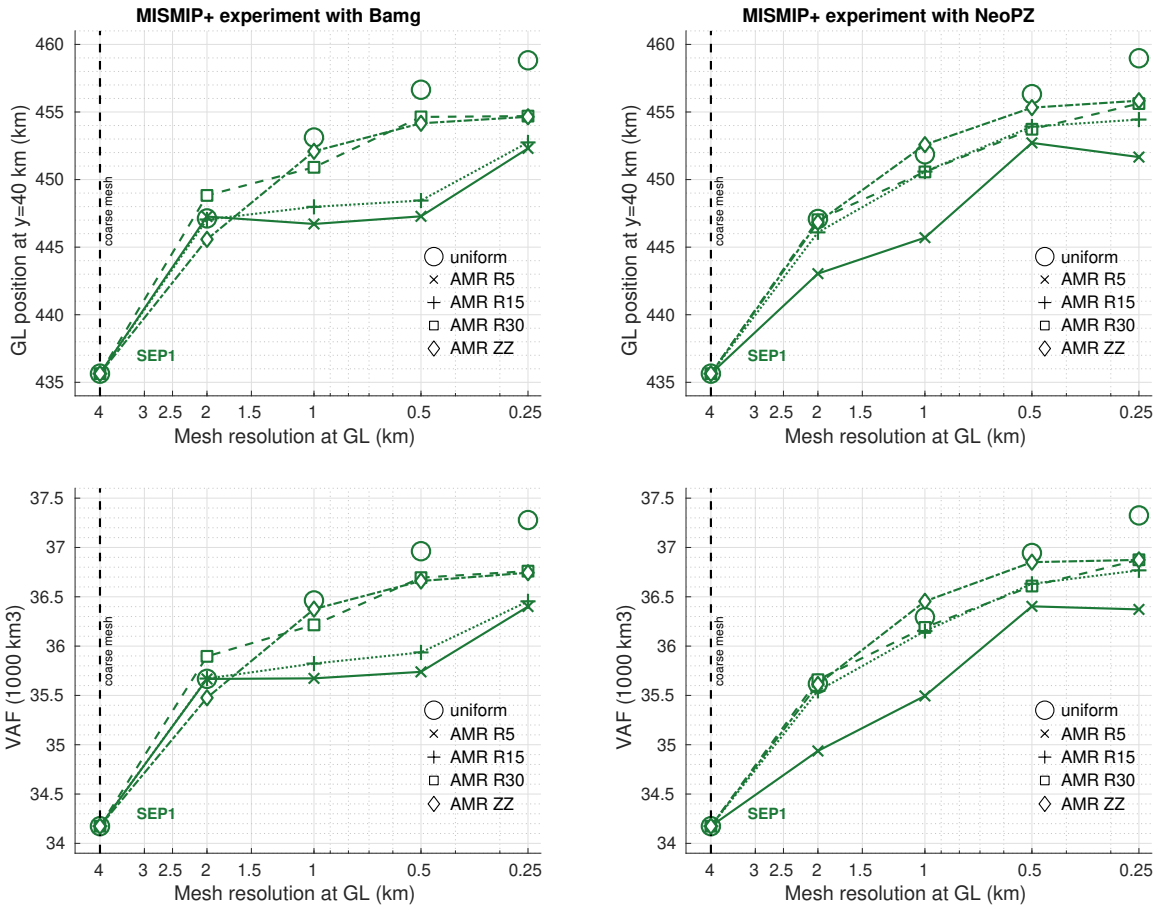

Figure 7. Grounding line (GL) positions **and ice volume above floatation (VAF)** at steady state obtained from the coarse mesh and from adaptive mesh refinement (AMR) for 4 refinement criteria: R5, R15, R30 and ZZ (see Tables 1 and 2). Results from uniformly refined meshes (uniform) are also shown. The simulations are carried out through the mesh generators Bamg (left) and NeoPZ (right) using sub-element parameterization type 1 (SEP1). **The thresholds for element/group used in the ZZ criterion are, respectively,** $\epsilon_{\tau,e}^{max} = 0.08\epsilon_{\tau}^{max}$ **(for both Bamg and NeoPZ) and** $\epsilon_{\tau,g}^{max} = 0.04\epsilon_{\tau}^{max}$ **for NeoPZ and** $\epsilon_{\tau,g}^{max} = 0.008\epsilon_{\tau}^{max}$ **for Bamg, where** ϵ_{τ}^{max} **is the maximum error value observed in the coarse mesh.**

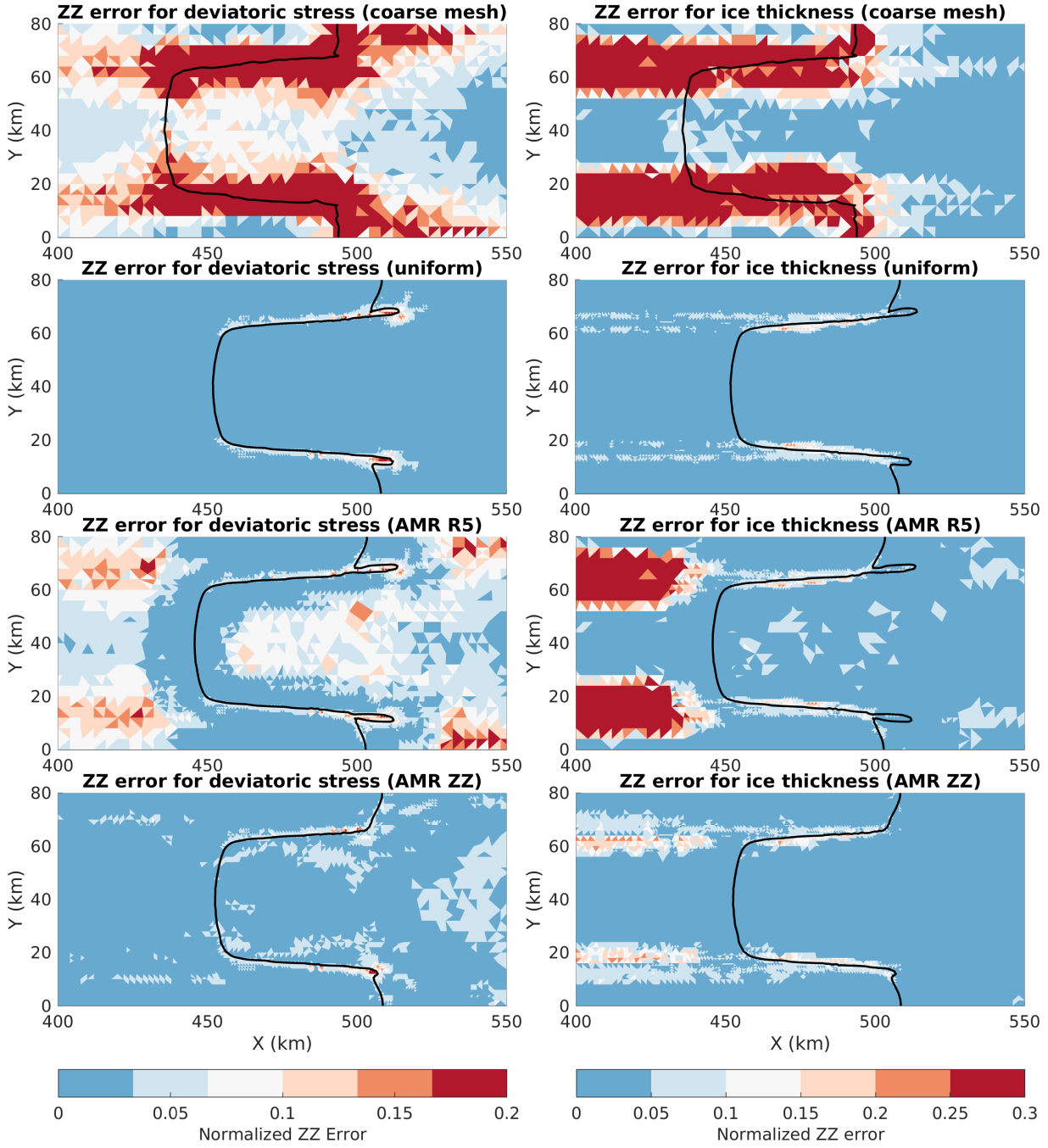

Figure 8. Spatial distribution of the ZZ error estimator in the coarse and **refined meshes (uniform and AMR)** ~~adaptive meshes (AMR)~~ used in the MISMIP+ experiments. The ZZ error values are normalized between 0 and 1 **using the maximum error value observed in the coarse mesh.** **Black lines** are the grounding line positions at steady state obtained with the respective meshes. The **refined meshes (uniform and AMR)** ~~and adaptive meshes shown here~~ are generated by NeoPZ **considering level of refinement equal to 2 (L2, see Table 2),** and the criteria used (R5 and ZZ) are summarized in Table 1. **The thresholds used in the AMR ZZ are described in the legend of Figure 7.**

Table 3. AMR time performance comparison for the experiment Ice1r, MISMIP+.

Level	CPU time (s)	Nb elem.	GL pos. (km)
L0 uniform	40	6,780	396.5
L1 uniform	188	27,706	407.0
L2 uniform	857	107,722	411.9
L3 uniform	1,705	473,446	416.0
L4 uniform	9,035	1,780,012	419.0
L3 AMR R5	498	33,794	405.2
L3 AMR R30	1,376	110,332	413.7
L3 AMR ZZ	369	21,088	415.7
L3 AMR R5+ZZ	807	56,267	413.7

Level = level of refinement. Nb elem. = number of elements. GL pos. = grounding line position at the end of the experiment Ice1r, MISMIP+. AMR R5+ZZ = combination of the criteria ZZ error estimator (deviatoric stress tensor) and element distance to the GL ($R_{gl} = 5$ km, R5). Mesher used: Bamg. The thresholds for element/group used in the ZZ criterion are, respectively, $\epsilon^{max}_{\tau,e} = 0.16\epsilon^{max}_{\tau}$ and $\epsilon^{max}_{\tau,g} = 0.016\epsilon^{max}_{\tau}$ for AMR ZZ, and $\epsilon^{max}_{\tau,e} = 0.48\epsilon^{max}_{\tau}$ and $\epsilon^{max}_{\tau,g} = 0.08\epsilon^{max}_{\tau}$ for AMR R5+ZZ, where ϵ^{max}_{τ} is the maximum error value observed in the coarse mesh.

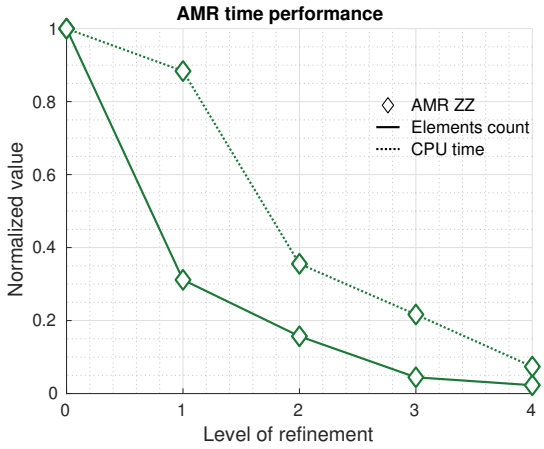

Figure 9. **Number of elements and CPU time for AMR meshes using the ZZ error estimator (AMR ZZ). The number of elements and CPU time are normalized by the respective values of the uniformly refined meshes. The normalized CPU time curve represents the AMR savings, while the difference between the two curves represents the adaptive mesh procedure cost. Mesher used: Bamg. The thresholds for element/group used in the AMR ZZ are, respectively,** $\epsilon_{\tau,e}^{max} = 0.64\epsilon_{\tau}^{max}$ **and** $\epsilon_{\tau,g}^{max} = 0.32\epsilon_{\tau}^{max}$ **for L1,** $\epsilon_{\tau,e}^{max} = 0.24\epsilon_{\tau}^{max}$ **and** $\epsilon_{\tau,g}^{max} = 0.08\epsilon_{\tau}^{max}$ **for L2,** $\epsilon_{\tau,e}^{max} = 0.16\epsilon_{\tau}^{max}$ **and** $\epsilon_{\tau,g}^{max} = 0.016\epsilon_{\tau}^{max}$ **for L3,** $\epsilon_{\tau,e}^{max} = 0.048\epsilon_{\tau}^{max}$ **and** $\epsilon_{\tau,g}^{max} = 0.0064\epsilon_{\tau}^{max}$ **for L4, where** ϵ_{τ}^{max} **is the maximum error value observed in the coarse mesh.**

Table 4. AMR criteria comparison for the experiment MISMIP+.

Level	Criteria	GL pos. (km)	Nb elem.
L0	(coarse mesh)	435.6	6,780
L1	AMR ZZ	446.8	15,864
L1	AMR R5+ZZ	446.7	15,976
L1	Uniform	447.0	27,120
L2	AMR ZZ	452.6	20,891
L2	AMR R5+ZZ	452.2	22,692
L2	Uniform	451.9	108,480
L3	AMR ZZ	455.3	21,936
L3	AMR R5+ZZ	455.6	42,617
L3	Uniform	456.3	433,920
L4	AMR ZZ	455.8	24,428
L4	AMR R5+ZZ	455.4	192,149
L4	Uniform	459.0	1,735,680

Level = level of refinement. GL pos. = grounding line position at the end of the experiment. Nb elem. = number of elements. AMR R5+ZZ = combination of the criteria ZZ error estimator (deviatoric stress tensor) and element distance to the GL ($R_{gl} = 5$ km, R5). Mesher used: NeoPZ. The thresholds used in the ZZ crterion are described in the legend of Figure 7.

Author's responses for the paper "Implementation and Performance of Adaptive Mesh Refinement in the Ice Sheet System Model (ISSM v4.14)"

Thiago Dias dos Santos, Mathieu Morlighem, Hélène Seroussi, Philippe Remy Bernard Devloo and Jefferson Cardia Simões

December 10th

Response notes

We appreciate the comments and the suggestions given by the Topical Editor, A. Robel. We reproduced below all his comments. **The author's responses are in blue and bold**.

Below is the diff version of the manuscript, highlighting the modification. The figures were removed to avoid large files.
(Page numbers and lines from the diff version)

---

1) Response to A. Robel, Topical Editor

Comments to the Author:
Thank you for submitting a thorough response to the reviewers and a suitable revised manuscript. As you have adequately responded to all reviewer comments, your manuscript is accepted pending some technical corrections, primarily related to readability. These correction are detailed below.

Best,
Alex Robel

Topical Editor
Geoscientific Model Development
Assistant Professor
Georgia Institute of Technology

_____

Technical corrections required before final acceptance:
(Page numbers and lines from diff'ed version)

Page 1:
Ln 1: resolution in ice sheet models
Done. **Ln 2.**
Ln 9-13: delete sentences starting from "We find…" to "…the complex bedrock topography of MISMIP+" These are quite specific results, and the abstract does not necessarily need them.
Done. Ln 9-13.
Ln 15: The ZZ estimator helps
Done. **Ln 15.**

Page 2:
Ln 9: Recently, WAIS has
Done. **Ln 9.**
Ln 10-11: under ice shelves, reduced the buttressing they provide to inland ice, and trigged the retreat of grounding lines around WAIS observed
Done. Ln 10-11.

Ln 14: accuracy of the result is
Done. Ln 14.

Ln 18: identify which intercomparison projects
Done. Ln 18-19.

Ln 27: as is the case for GL dynamics as defined in Schoof (2007)
(From the editor: To be clear, it is not necessarily the case that the step function in basal friction at the grounding line is necessarily the "right" way to described grounding line dynamics, it just the way that Schoof did it, and so is now commonly done in the field. Do note, however, that when the basal friction transition is smooth, as in Gladstone et al. 2017 in The Cryosphere, the resolution requirements at the grounding line are less stringent. Some have suggested this is a more realistic representation of reality.)
Done. We aggree with the Topical Editor that the model Schoof (2007) applied (Weertman's model) is not necessarily the "right" way; a Coulomb's model may be a more realistic, for example. But in terms for numerical representation, both models represent a "discontinuity" within the elements (in Coulomb's model it is smoother, wich may reduce the high mesh resolution requirement).
Ln 27.

Page 3:
Ln 17: make it clear here that one or the other mesh generator is used, not both simultaneously
Done. Ln 18.

Page 4:
Ln 13: in many cores
Done. Ln 13.
Ln 17: of the mesh generators BamG
Done. Ln 17.
Ln 25: is the transition zone length specified by the user?
Actually the "transition zone" here is a "mesh transition zone" (where the elements size changes gradually). This is not the "transition zone" in the context of Pattyn et al. (2006, JGR). Then, to avoid any misunderstanding, we change "transition zone" to "mesh transition zone" everywhere.
We also added "by the user". Ln 25.

Page 5:
Ln 2: of an adapted mesh
Done. (also changed to "adaptive mesh"). Ln 2.
Ln 6: transient ISSM simulations
Done. Ln 6.
Ln 29: Grounding line dynamics are implemented
Done. Ln 28.

Page 6:
Ln 1: flotation height
Done. Page 5, Ln 31.

Page 7:
Ln 18: for an explanation of how these
Done. Ln 14.

Page 8:
Ln 7: n=3, a commonly used value for the exponent in Glen's flow law
Done. Ln 4.
Ln 13: does accumulation rate have to be specified in order to reach a steady state? (I would think yes if there is ice outflow from the domain and it reaches a steady-state)
Good point. We didn't write the values of the accumulation rate. We apologize for this. Page 8 Ln 10-11, and Page 9, Ln 18-19.
Ln 19: What about the reviewer comments regarding use of coarse mesh for initialization? Does this present a problem for these simulations?
Good point. This is not a problem in these experiments because we are running until the steady state. We added a footnote to make it clearer to the reader.
Page 8, Ln 18 (and the footnote on Page 8), and Page 9, Ln 23 (and the footnote on Page 9).
Ln 31: SPE2?
Corrected. Ln 30.

Page 10:
Ln 7: the uniformly refined mesh
Done. Ln 7.

Page 11:
Ln 3: position differs
Done. Ln 3.
Ln 4: position differs
Done. Ln 4.
Ln 9: below in what sense?
Changed to "differ from". Ln 8-9.
Ln 10: not sure what marginally means here
Changed to "virtually". Ln 9.
Ln 25: terms of efficiency
Done. Ln 24.

Page 12:
Ln 17-20: you use inconsistent types of numbers to indicate the difference in computational times between these sentences (a % first, then a fraction of, then a factor less than). Perhaps switch to one common way to describe these, like a % of the benchmark non-AMR computational time.
Done. We switched to %. Ln 9-14.
Ln 17: L30?
Corrected (R30). Ln 9.
Ln 21: is similar, and the ratio
Done. Ln 15.
Ln 29: terms of accuracy of the simulated grounding line
Done. Ln 23.

Page 13:
Ln 4: step, and is useful
Done. Page 12, Ln 31.
Ln 22: ice sheet model
Done. Ln 16.

Ln 23: it is the case that these specific results depend on the particular topography and assumptions regarding basal friction across the grounding line.
Yes, we agree. We changed that sentence specifying the results were valid for MISMIP3d. Ln 16-17.

Page 14:
Ln 10: implemented in ice sheet models, including those based on
Done. Ln 4-5.
Ln 21: there is no small-scale bed topography, the numerical error
Done. Ln 15.
Ln 28-29: the extension of the grounding zone (where…
Done. Ln 22-23.

Page 15:
Ln 1: The grounding zone is not
Done. Page 14, Ln 30.
Ln 18: the grounding zone to reduce
Actually the "transition zone" here refers to the "mesh transition zone" (zone between the lowest and highest mesh resolution), not to the "grounding zone".
To avoid any misunderstanding, we decide to change "transition zone" to "mesh transition zone" along the whole manuscript.
Page 15, Ln 13 (and elsewhere).

Implementation and Performance of Adaptive Mesh Refinement in the Ice Sheet System Model (ISSM v4.14)

Thiago Dias dos Santos[1], Mathieu Morlighem[2], Hélène Seroussi[3], Philippe Remy Bernard Devloo[1], and Jefferson Cardia Simões[4]

[1]Department of Structures, School of Civil Engineering, Architecture and Urban Design, University of Campinas (UNICAMP), Campinas, SP, Brazil
[2]Department of Earth System Science, University of California, Irvine, CA, USA
[3]Jet Propulsion Laboratory, California Institute of Technology, Pasadena, CA, USA
[4]Polar and Climate Center, Geosciences Institute, Federal University of Rio Grande do Sul (UFRGS), Porto Alegre, RS, Brazil

Correspondence: Thiago Dias dos Santos (santos.td@gmail.com)

Abstract. Accurate projections of the evolution of ice sheets in a changing climate require a fine mesh/grid resolution in ice sheet models to correctly capture fundamental physical processes, such as the evolution of the grounding line, the region where grounded ice starts to float. The evolution of the grounding line indeed plays a major role in ice sheet dynamics, as it is a fundamental control on marine ice sheet stability. Numerical modeling of a grounding line requires significant computational resources since the accuracy of its position depends on grid or mesh resolution. A technique that improves accuracy with reduced computational cost is the adaptive mesh refinement (AMR) approach. We present here the implementation of the AMR technique in the finite element Ice Sheet System Model (ISSM) to simulate grounding line dynamics under two different benchmarks, MISMIP3d and MISMIP+. We test different refinement criteria: (a) distance around the grounding line, (b) a posteriori error estimator, the Zienkiewicz-Zhu (ZZ) error estimator, and (c) different combinations of (a) and (b). ~~We find that for the MISMIP3d setup, refining 5 km around the grounding line, both on grounded and floating ice, is sufficient to produce AMR results similar to the ones obtained with uniformly refined meshes. However, for the MISMIP+ setup, we note that there is a minimum distance of 30 km around the grounding line required to produce accurate results. We find this AMR mesh-dependency is linked to the complex bedrock topography of MISMIP+.~~ In both benchmarks, the ZZ error estimator presents high values around the grounding line. Particularly for the MISMIP+ setup, the estimator also presents high values in the grounded part of the ice sheet, following the complex shape of the bedrock geometry. ~~This~~ The ZZ estimator helps guide the refinement procedure such that AMR performance is improved. Our results show that computational time with AMR depends on the required accuracy, but in all cases, it is significantly shorter than for uniformly refined meshes. We conclude that AMR without an associated error estimator should be avoided, especially for real glaciers that have a complex bed geometry.

1 Introduction

The uncertainty in projections of ice sheet contribution to sea level rise in the next century remains large, primarily due to the potential collapse of the West Antarctic Ice Sheet, WAIS (Church et al., 2013; Jevrejeva et al., 2014; Ritz et al., 2015; DeConto

and Pollard, 2016). Projections of the collapse of WAIS are based on the Marine Ice Sheet Instability (MISI) hypothesis (Weertman, 1974; Mercer, 1978; Thomas, 1979). This hypothesis refers to ice sheets grounded below sea level on retrograde bedrock slopes (as seen in Figure 1), as is the case for many glaciers in WAIS (Fretwell et al., 2013). MISI states that the grounding line (GL), the region where the ice sheet starts to float (see Figure 1), cannot remain stable on such bedrock slopes (Schoof, 2007b; Katz and Worster, 2010; Gudmundsson et al., 2012). Accordingly, the GL retreat on retrograde bedrock slopes causes increased ice discharge, which in turn leads to further GL retreat, resulting in a non-linear positive feedback. This self-sustaining GL retreat persists until a prograde bedrock slope is reached. Therefore, a change in climate or ocean can potentially force a large-scale fast migration of the GL inland (Schoof, 2007a; Favier et al., 2014; Seroussi et al., 2014b). Recently, ~~the region of~~ WAIS has experienced an increase in the intrusion of ocean warm deep water (Jacobs et al., 2011; Dutrieux et al., 2014) that likely increased the ocean induced melt under ~~the~~ ice shelves, reduced the buttressing they provide to ~~the~~ inland ice, and triggered the retreat of ~~the GL~~ grounding lines around WAIS observed over the last decades (Rignot et al., 2014; Christie et al., 2016; Kimura et al., 2016; Seroussi et al., 2017).

Modeling this positive feedback requires the coupling of different physical processes (ice sheet and ice shelf evolutions, GL migration, basal friction, etc.), and the accuracy of the ~~results~~ result is highly dependent on the GL parameterization and the spatial discretization of the domain. Vieli and Payne (2005) compared the results of different ice sheet numerical models in terms of GL migration, and found that the numerical results have a strong dependency on horizontal grid size. Analyzing the stability and dynamics of the GL on reverse bed slopes, Schoof (2007b) pointed out that sufficiently high grid resolution in the GL zone is a critical element to obtain reliable numerical results. Two ice sheet model intercomparison projects (MISMIP and MISMIP3d) later confirmed the GL dynamics dependency on spatial resolutions (Pattyn et al., 2012, 2013).

Several marine ice sheet models have employed different numerical schemes to overcome this mesh resolution requirement at the GL with reduced computational cost: by imposing a flux condition at the GL position (Pollard and DeConto, 2009, 2012; Pattyn, 2017), by treating the GL and basal friction with sub-grid or sub-element schemes (Feldmann et al., 2014; Leguy et al., 2014; Seroussi et al., 2014a) or by applying high spatial resolution only in the GL region with adaptive grid refinement (Durand et al., 2009; Goldberg et al., 2009; Gladstone et al., 2010; Gudmundsson et al., 2012; Cornford et al., 2013).

The grid or mesh adaptation technique allows resources to be applied only where they are required, which is very useful in transient simulations that include some discontinuity in the time-dependent solution (Devloo et al., 1987; Berger and Colella, 1989), as is the case for GL dynamics as defined in Schoof (2007b) (the basal friction is only applied to grounded ice). This technique can be performed with two different methods: *r*-adaptivity and *h*-adaptivity methods (Oden et al., 1986). The *r*-adaptivity, also known as moving mesh method, moves progressively a fixed number of vertices in a given direction or region (Anderson et al., 1984, p. 533), while the *h*-adaptivity method, named in this work as adaptive mesh refinement (AMR), splits edges and/or elements, inserting new vertices into the mesh where high resolution is required (Devloo et al., 1987; Berger and Colella, 1989). The performance of each of these methods depends on the problem for which they are applied. Vieli and Payne (2005) showed that models applying moving grid to track the GL movement perform better than fixed grid models. Since the position of the GL is explicitly defined in moving grids, Vieli and Payne (2005) noticed for this method a weak grid resolution dependency in comparison to fixed grid method, for which the GL position falls between grid points. Goldberg et al. (2009)

obtained accurate solutions with fewer resources solving the time-dependent Shelfy-Stream equations with the two different mesh adaptation techniques mentioned above, moving mesh and AMR. Using a one-dimensional Shelfy-Stream model based on finite difference scheme, Gladstone et al. (2010) demonstrated that AMR and sub-grid parameterization for GL position could produce robust predictions of GL migration. Pattyn et al. (2012) found that moving grid methods tend to be the most accurate and AMR can further improve accuracy compared to models based on fixed grid. Cornford et al. (2013) implemented a block-structured AMR in BISICLES, a $2^1/_2$D ice sheet model based on the finite volume method. They demonstrated that simulations with AMR are computationally cheaper and more efficient, even as the grounding line moves over significant distances. Jouvet and Gräser (2013) combined the Shallow Ice Approximation and the Shallow Shelf Approximation in an AMR numerical scheme involving a truncated Newton multigrid and finite volume method. Through MISMIP3d experiments (Pattyn et al., 2013), they highlighted the relevance and efficiency of AMR in terms of computational cost when high resolution ($\sim$100 m) is necessary to reproduce GL reversibility. Recently, Gillet-Chaulet et al. (2017) implemented an anisotropic mesh adaptation in the finite element ice flow model Elmer/Ice (Gagliardini et al., 2013). Based on the MISMIP+ experiment (Asay-Davis et al., 2016), they showed that combining various variables (ice thickness, basal drag, velocity, etc.) in an estimator allowed to reduce the number of mesh vertices by more than one order of magnitude compared to uniformly refined meshes, for the same level of numerical accuracy.

Here, we implement the AMR technique for unstructured meshes in the parallel finite element Ice Sheet System Model (ISSM v4.14, Larour et al., 2012). The AMR capability in ISSM relies on two different and independent mesh generators (one or the other mesh generator is used according to the user's choice): Bamg, a bidimensional anisotropic mesh generator developed by Hecht (2006), and NeoPZ, a finite element library developed by Devloo (1997). ISSM's architecture is based on the Message Passing Interface (MPI), where models are run in a distributed memory scheme. Our AMR implementation minimizes MPI communications, avoiding overheads and latencies. Since refinement criteria are crucial to AMR performance (Devloo et al., 1987), we implement different criteria based on: (a) the distance to the grounding line, (b) the ZZ error estimator (Zienkiewicz and Zhu, 1987), and (c) different combinations of (a) and (b). To analyze the performance of AMR, we run two benchmark experiments: MISMIP3d (Pattyn et al., 2013) and MISMIP+ (Asay-Davis et al., 2016). We compare AMR results from both Bamg and NeoPZ with uniformly refined meshes in terms of GL position and computational time.

This paper is organized as follows: in Section 2, we summarize the main features of ISSM's architecture, and the strategies used to implement an efficient AMR technique for transient simulations. In Section 3, we describe both MIMISP3d and MISMIP+ experiments used to analyze the AMR performance, and in Section 4 we present the results in terms of GL position and processing time. We finish this paper with a discussion of the results and conclusions in Sections 5 and 6, respectively.

2 AMR implementation

2.1 ISSM architecture

Our AMR implementation is strongly based on the architecture of ISSM. We describe here the main ISSM features necessary to understand the AMR strategy. We refer to Larour et al. (2012) for a more detailed description of ISSM.

Several stress balance approximations are implemented in ISSM, including higher-order models (e.g., Blatter-Pattyn, Pattyn, 2003, full-Stokes). The current AMR capability is supported for the 2-D vertically integrated Shallow-Shelf or Shelfy-Stream Approximation (SSA, Morland, 1987; MacAyeal, 1989). The SSA is employed for both grounded and floating ice, so membrane stress terms (which are required to correctly model the GL dynamics, Schoof, 2007b) are included but all vertical shearing is neglected (Seroussi et al., 2014a). Here, the mesh used for the SSA equations is unstructured and relies on a Delaunay triangulation.

ISSM is designed to run in parallel in a distributed memory fashion by Message Passing Interface (MPI). When a model is launched, the entire mesh is spatially partitioned over processing units or cores (CPU's), and data structures related to finite element method are built in each partition. All physical entities that vary in space (ice viscosity, ice thickness, surface, velocities, etc.) are kept within the elements.

MPI communications between the partitions (CPU's) are performed to assemble the global stiffness matrix and load vector, as well as during the solution update in the elements once the system of equations is solved. The advantage of MPI is its ability to handle larger models (i.e. for continental scale simulations) in ~~several~~ many cores and nodes on a cluster. Its disadvantage is the cost in the communications between the partitions.

2.2 Bamg and NeoPZ

The AMR technique in ISSM is implemented for unstructured meshes and triangular elements. Here are some short descriptions of the ~~meshers~~ mesh generators Bamg and NeoPZ.

Bamg (Hecht, 2006) is a bidimensional mesh generator based on Delaunay-like method (Hecht, 2005). This mesh generator is embedded in ISSM for static anisotropic mesh adaptation (Morlighem et al., 2010). Here, we extend Bamg capabilities for dynamic adaptation (AMR). The refinement in Bamg is carried out by specifying the desired resolution on the vertices. To reach the desired resolution, Bamg's algorithm splits triangle edges and inserts new vertices in the mesh (Hecht, 2006). The algorithm keeps new vertices and connectivities unchanged as much as possible compared to the previous mesh (Hecht, 2005). This procedure reduces the numerical errors introduced by the AMR when the solutions are interpolated into the new mesh (see Section 2.3). Regions of different resolutions are linked by a mesh transition zone, where the element sizes are changed gradually. The spatial extent of this mesh transition zone is also specified by the user in the Bamg's algorithm. An example of adaptive mesh using Bamg is shown in Figure 3.

NeoPZ (Devloo, 1997) is a finite element library dedicated to highly adaptive techniques (Calle et al., 2015). In NeoPZ's data structure, each element is refined into 4 topologically similar elements, whose resolutions are half of the refined element. To avoid hanging vertices (Calle et al., 2015), some elements are divided in specific ways such that any two elements in the mesh may have a vertex or an entire edge in common, or no vertices in common (Szabó and Babuška, 1991, p. 81). In this sense, all meshes refined by NeoPZ are nested, i.e., vertices and connectivities from the coarse mesh are kept fixed during all simulation time. This characteristic does not introduce any numerical error induced by the AMR during the interpolation process (see Section 2.3). The AMR with NeoPZ is given by specifying the level of refinement, i.e., how often elements

are refined. Therefore, the mesh transition zone, which links regions of different resolutions, is generated stepwise through resolutions dictated by levels of refinement. Figure 3 shows an example of an adaptive mesh using NeoPZ.

Here, we describe the algorithm to couple ISSM to Bamg and NeoPZ as well as the refinement criteria usage (Sections 2.3 and 2.4).

2.3 Parallel strategy

The solution sequence for transient ISSM simulations with AMR is summarized in Figure 2. Details of AMR processes are itemized in Algorithm 1. In Figure 2, the AMR is the last step to be executed for a given time step. This is an explicit approach, where a new adapted mesh is built for a given solution. In Algorithm 1, all processes involved to perform the AMR in ISSM are executed in the step 'e', the remeshing core. Step 'e.1' executes the mesh adaptation (refinement or coarsening of elements) and the other steps ('e.2' to 'e.5') prepare the adapted mesh, data structures and solutions for the next simulation time step.

Bamg and NeoPZ perform the AMR (step 'e.1', Algorithm 1) in serial, considering the entire mesh. In our implementation, only one partition (which CPU rank is #0) keeps the Bamg or NeoPZ entire mesh, and is responsible to execute the AMR process.

Our AMR implementation keeps the number of partitions constant during all simulation time. The number and distribution of elements into the partitions varies every time AMR is called, since the mesh partitioning process (step 'e.2', Algorithm 1) generates partitions with similar number of elements. This process avoids memory imbalance among the CPU's and overheads during the solver phase (Larour et al., 2012).

Each time remeshing is performed, the solutions and all data fields are interpolated from the old mesh onto the new mesh. This step is executed in parallel, where each CPU interpolates the solutions just on its own partition (step 'e.4', Algorithm 1). The construction of new data structures and the adjustment of solutions (steps 'e.3' and 'e.5', respectively, Algorithm 1) are also executed in parallel, as is the computation of the refinement criteria (see Section 2.4).

All MPI communications in the remesh core (step 'e', Algorithm 1) are minimized to avoid overheads when large models are run. In order to minimize MPI calls, we perform a single communication of a large array that includes all data structures. In the interpolation process, for example, all relevant fields are collected by CPU #0 in one single vector structure in such a way that only one MPI broadcast is called. This approach is based on the fact that, in general, it is more efficient to perform few large MPI messages instead of carrying out many smaller ones (Reinders and Jeffers, 2015, p. 327).

2.4 Refinement criteria

~~The grounding line dynamics is~~ Grounding line dynamics are implemented in ISSM through an implicit level set function, ϕ_{gl}, based on a hydrostatic floatation criterion (Seroussi et al., 2014a):

$$\phi_{gl} = H - H_f, \tag{1}$$

where H is the ice thickness and $H_f = -b(\rho_w/\rho_i)$ is the ~~floating~~ flotation height, with ρ_i the ice density, ρ_w the ocean density and b the bedrock elevation (negative if below sea level). Figure 1 illustrates the GL position in a vertical cross-section of a

marine ice sheet. The position of the GL is defined as:

$$\begin{cases} \phi_{gl} < 0: & \text{ice is floating} \\ \phi_{gl} > 0: & \text{ice is grounded} \\ \phi_{gl} = 0: & \text{grounding line position} \end{cases} . \tag{2}$$

The performance of AMR depends on the refinement criterion (Devloo et al., 1987). We implement the three following criteria:

(a) Element distance to the GL, R_{gl};

(b) ZZ error estimator for deviatoric stress tensor, τ, and ice thickness, H;

(c) Different combinations of (a) and (b).

The criterion (a) is based on a heuristic approach commonly applied (Goldberg et al., 2009; Gudmundsson et al., 2012; Cornford et al., 2013). The second criterion, (b), is based on the fact that high changes in the gradients in the velocity field (therefore, in the deviatoric stress tensor, τ) and ice thickness, H, are expected to be present near the grounding line. Criterion (c) extends and merges the features of the other two previous criteria. We define the AMR criterion used based on binary flags θ ($= 0$ or 1) such that:

$$\begin{cases} \theta_{gl} = 1: & \text{use element distance to the GL} \\ \theta_{\tau} = 1: & \text{use ZZ error estimator for } \tau \\ \theta_{H} = 1: & \text{use ZZ error estimator for } H \end{cases} . \tag{3}$$

We propose Algorithm 2, inspired by Devloo et al. (1987), to execute the refinement and coarsening processes under different criteria (AMR core, step 'e.2' in Algorithm 1). The first 3 steps in Algorithm 2 compute the criterion according to the binary flags, θ, defined above. These steps are performed in parallel. Step '4' verifies, for each element in the mesh, if it should be refined: its distance to the GL and its ZZ errors are compared with prescribed limits (thresholds). The element is refined if at least one of the thresholds is exceeded, so long as its level of refinement is less than the maximum level chosen. This logical operation is performed by the operator "or" in the statement "if" in step '4'. Once an element is refined, it is identified as a group. Step '5' verifies for each group if it should be coarsened. To be coarsened, a group should meet all thresholds; the logical operator used in this case is "and" (statement "if" in step '5'). Algorithm 2 has two sets of thresholds (shown with max), for elements and for groups of elements. For the algorithm to work properly, these sets of thresholds should be different, following Devloo et al. (1987).

2.5 ZZ error estimator

The generic form of the ZZ (Zienkiewicz and Zhu, 1987) error estimator $\epsilon(e)$ for a given element e is:

$$\epsilon(e) = \left[\int_{\Omega_e} (\nabla u^* - \nabla u)^2 \, d\Omega_e \right]^{1/2} , \tag{4}$$

where Ω_e is the domain of the element e, ∇u is the gradient of the finite element solution u and ∇u^* is the smoothed reconstructed gradient, calculated on the element e as:

$$\nabla u^* = \sum_{i=1}^{s} \psi_i \nabla u_i^*, \tag{5}$$

and

$$\nabla u_i^* = \frac{1}{W_i} \sum_{j=1}^{k} w_j \nabla u_j, \tag{6}$$

where ψ_i is the ith P1 Lagrange shape function on element e, s is the number of shape functions of the element e (here, $s = 3$), j is the jth element connected to the vertex i, k is the number of elements connected to vertex i, w_j is the weight relative to the element j and W_i is the sum of all weights for the vertex i. Here, the weights w are defined as the geometric area of the triangular elements. We implement the ZZ error estimator for the deviatoric stress tensor (τ), written in a vectorized form, i.e., for SSA we have $\nabla u \rightarrow \boldsymbol{\tau} = (\tau_{xx}, \tau_{yy}, \tau_{xy})^\intercal$. We also extend the estimator for the ice thickness ($u = H$). The ZZ estimator was conceived by Zienkiewicz and Zhu (1987) for linear elasticity, which involves elliptic equations. Applying the ZZ error estimator to the deviatoric stress tensor is therefore a natural extension, since the SSA equations are also elliptic. The ZZ estimator for the ice thickness highlights the regions of sharp bedrock gradient, and could be used to improve the resolution of the bedrock geometry (e.g., see Figure 8). See Section 2.4 and Algorithm 2 for an explanation of how these error estimates are combined.

3 Numerical experiments

We run 2 different benchmark experiments to evaluate the adaptive mesh refinement capabilities based on the MISMIP3D (Pattyn et al., 2013) and MISMIP+ (Asay-Davis et al., 2016) experiments. The following subsections describe briefly each setup. More details can be found in the respective references. All experiments are performed using the vertically integrated Shelfy-Stream Approximation equations (SSA, Morland, 1987; MacAyeal, 1989).

3.1 MISMIP3d setup

The MISMIP3d domain setup is rectangular, and extends from 0 to 800 km in the x direction and from 0 to 50 km in the y direction. The bed elevation (b) varies only in the x direction, as follows:

$$b\,(x, y) = -100 - x. \tag{7}$$

Boundary conditions are applied as follows: a symmetric condition at $x = 0$ so that ice velocity is equal to zero, a symmetric condition at $y = 0$ (which represents the centerline of the ice stream), and free slip condition at $y = 50$ km so that the flux through these surfaces is zero. Water pressure is applied at the ice front at $x = 800$ km.

The ice viscosity, μ, is considered to be isotropic and to follow the Glen's flow law (Cuffey and Paterson, 2010):

$$\mu = \frac{B}{2\dot{\epsilon_e}^{\frac{n-1}{n}}}, \tag{8}$$

where B ($= A^{1/n}$, being A the Glen's flow law factor) is the ice viscosity parameter, $\dot{\epsilon_e}$ is the effective strain rate and $n = 3$~~is the~~ , a commonly used value for the exponent in Glen's ~~exponent~~flow law. The ice viscosity parameter, B, is uniform and constant over the domain and the time, and its value is equal to $2.15 \times 10^8\,\mathrm{Pa\,s^{-1/3}}$. A non-linear friction (Weertman) law is applied on grounded ice:

$$\boldsymbol{\tau}_b = C\,|\boldsymbol{u}_b|^{m-1}\,\boldsymbol{u}_b, \tag{9}$$

where $\boldsymbol{\tau}_b$ is the basal shear stress, $\boldsymbol{u}_b$ is the basal sliding velocity, C is the friction coefficient, and $m = 1/3$ is the sliding law exponent. The basal friction coefficient, C, is also spatially uniform for all grounded ice, and equal to $10^7\,\mathrm{Pa\,m^{-1/3}s^{1/3}}$.

The experiments are run starting from an initial configuration with a thin layer (100 m) of ice and ~~run~~ with a constant accumulation rate of $0.5\ \mathrm{m\,yr^{-1}}$ applied over the whole domain. The experiments run forward in time until a steady state condition is reached, which occurs after 30,000 years. We compare the GL positions from different meshes at t=30,000 yr.

We investigate the sensitivity of the AMR for which the refinement method is based on the element distance to the GL, R_{gl} (criterion (a), Section 2.4). For comparison analysis, three different distances are used for the highest refinement level: $R_{gl} = 5$, 10 and 15 km. These different meshes are labeled as R5, R10 and R15, respectively. The distance R_{gl} refers to the region with the highest level of refinement. For example, R5 means that 5 km on both sides of the GL (upstream and downstream) are refined with the highest level. Table 1 summarizes the criteria used for all experiments. The coarse mesh, that has a resolution of 5 km, is used as an initial mesh[1] for all simulations and mesh generators (Bamg and NeoPZ). To analyze the convergence, we refine the coarse mesh $1\times$, $2\times$ and $3\times$. These 3 levels of refinement are applied to both uniform and adaptive meshes, and correspond to elements with 2.5, 1.25 and 0.63 km resolution, respectively. Table 2 presents the correspondence between level and resolution at the GL used in the experiments.

We also investigate the sensitivity of the AMR to GL parameterization into the elements (Seroussi et al., 2014a). Three sub-element parameterizations are tested: no sub-element parameterization (NSEP), sub-element parameterization 1 (SEP1) and sub-element parameterization 2 (SEP2). In the NSEP method, each element of the mesh is either grounded or floating and the grounding line position is defined as the last grounded point. In SEP1 and SEP2 methods, the grounding line position is located anywhere within an element and defined by the implicit level set function, ϕ_{gl}, which is based on the floating condition (see Section 2.4). The difference between SEP1 and SEP2 is how each one of these methods computes the basal friction to match the amount of grounded ice in the element. In the SEP1 approach, the basal friction coefficient (C) is reduced as $C_g = C\,A_g/A$, where C_g is the new basal friction coefficient for the element partially grounded, A_g is the area of grounded ice of this element and A is the total area of the element. In the ~~SPE2~~ SEP2 technique, the basal friction is integrated (in the sense of the finite element method) only on the part where the element is grounded. This is done by changing the integration area

[1] Here, setting the coarse mesh as the initial mesh does not produce numerical artifacts because the experiments are run until a steady state is reached. However, for general simulations (e.g., the experiment Ice1r, Section 4.2), the initial conditions should be self-consistent with the AMR mesh. See Algorithm 1.

from the original element to the grounded part of the element. We refer to Seroussi et al. (2014a) for a complete description of these sub-element parameterizations.

3.2 MISMIP+ setup

The MISMIP+ domain is also rectangular, whose dimensions are: $0 \leq x \leq 640$ km and $0 \leq y \leq 80$ km. The bed elevation is defined as follows:

$$b(x,y) = \max\left(b_x(x) + b_y(y), b_{deep}\right), \tag{10}$$

with:

$$b_x(x) = b_0 + b_2\left(\frac{x}{\bar{x}}\right)^2 + b_4\left(\frac{x}{\bar{x}}\right)^4 + b_6\left(\frac{x}{\bar{x}}\right)^6, \tag{11}$$

and

$$b_y(y) = \frac{d}{1+\exp\left[-2(y - L_y/2 - w_c)/f_c\right]} + \frac{d}{1+\exp\left[2(y - L_y/2 + w_c)/f_c\right]}, \tag{12}$$

where $b_{deep} = -720$ m, $b_0 = -150.0$ m, $b_2 = -728.8$ m, $b_4 = 343.91$ m, $b_6 = -50.57$ m, $\bar{x} = 300$ km, $d = 500$ m, $L_y = 80$ km, $w_c = 24$ km, $f_c = 4$ km. Figure 4 shows the bed elevation calculated with Eqs. (10), (11) and (12).

The ice is isothermal and the ice viscosity parameter, B, is equal to $1.1642 \times 10^8\,\mathrm{Pa\,s^{-1/3}}$ (uniform and constant over the domain and the time). The boundary conditions are similar to MISMIP3d. The friction model used here is a power law, Eq. (9), with a coefficient, C, equal to $3.160 \times 10^6\,\mathrm{Pa\,m^{-1/3}s^{1/3}}$ (spatially uniform for all grounded ice) and sliding law exponent, m, equal to $1/3$.

We run the experiments starting from an initial configuration with a 100 m thick layer of ice, and run the simulations until a steady state condition is ~~reach~~ reached (after 20,000 years). A constant accumulation rate of 0.3 $\mathrm{m\,yr^{-1}}$ is applied over the entire domain. The GL positions are compared at t=20,000 yr.

To investigate further the sensitivity of the GL position to the refinement distance, R_{gl}, we choose distances with the highest refinement level equal to $R_{gl} = 5$, 15 and 30 km, with meshes labeled as R5, R15 and R30, respectively (see Table 1). As for the MISMIP3d simulations, these distances refer to the region around the GL with the highest level of refinement. The same coarse mesh[2] with a resolution of 4 km is used for Bamg and NeoPZ, and it is refined up to four times for both adaptive and uniform refinement approaches. The respective resolutions for the four refinement levels are 2, 1, 0.5 and 0.25 km. Table 2 summarizes the levels and the respective resolutions at the GL. All the MISMIP+ simulations are performed with sub-element parameterization type I, SEP1 (Seroussi et al., 2014a).

It is important to emphasize that the MISMIP+ bed elevation (Figure 4) is calculated directly in the code every time AMR is called (step 'e.5', Algorithm 1). This procedure avoids excessive smoothing of the complex bedrock topography in the refined region.

[2] See footnote 1.

4 Results

For a given problem, the results from an AMR mesh should be as close as possible (within an acceptable tolerance) to those obtained with an uniformly refined mesh, for the same level of refinement (element resolution) in both meshes. This comparison is an indicator of the AMR performance to that given problem. Since Bamg and NeoPZ adapt the mesh in different ways, it is important to analyze how their differences impact the numerical solutions. Therefore, we first compare the results from the adaptive and uniform meshes using both Bamg and NeoPZ for the MISMIP3d and MISMIP+ experiments, and then we assess the time performance of the AMR in comparison with the uniformly refined mesh.

4.1 GL position comparison

4.1.1 MISMIP3d setup

Figure 5 presents the GL positions and the ice volume above floatation (VAF[3]) for different AMR meshes and sub-element parameterizations as a function of element resolutions. The refinement criterion used is the element distance to the GL, R_{gl} (see Table 1 and Section 2.4). GL positions and VAF obtained with uniformly refined meshes are also shown in Figure 5. For NSEP, GL position varies between 200 km and 520 km for meshes L0 (coarse mesh) and L3 (level of refinement equal to 3), respectively. For these same meshes, GL position varies between 620 km and 600 km for SEP1, and 550 km and 600 km for SEP2.

We note that AMR meshes with NeoPZ produce GL positions that are very similar to the ones produced with uniformly refined mesh. This holds for all sub-element parameterizations. AMR with Bamg is more sensitive to NSEP, for which GL positions depend on the element distance to the GL (R_{gl}) used, especially for the lower refinement level (level equal to 1). Despite this, GL positions from AMR with Bamg are in agreement with uniformly refined meshes for SEP1 and SEP2. Similar behaviour is observed in the VAF amounts.

4.1.2 MISMIP+ setup

The MISMIP+ bed topography (see Section 3.2 and Figure 4) is designed to introduce a strong buttressing on the ice stream from the confined ice shelf. It is therefore expected that the results are more sensitive to the mesh refinement compared to simpler bedrock descriptions (e.g., MISMIP3d), since refining the mesh also improves the resolution of the bedrock geometry (see Section 3.2).

Figure 6 presents the coarse mesh and 3 examples of adaptive meshes obtained with Bamg and NeoPZ and different criteria: element distance to the GL, R_{gl} ($= 5$ km, R5) and error estimator ZZ (see Table 1). The figure also shows the GL positions obtained with these meshes and with the most refined uniform mesh (250 m resolution). Figure 6 provides an example of a case for which the GL position remains resolution-dependent and refinement criterion-dependent. We can note that, using the same criterion based on the element distance the to GL (meshes R5), Bamg and NeoPZ produce different meshes, as expected.

[3]The ice volume above floatation is the ice volume that contributes to sea level (Bindschadler et al., 2013).

For Bamg, the mesh transition zone between the lowest and highest resolution is smoother than NeoPZ's mesh, since the resolutions in NeoPZ are obtained stepwise by nested elements. In Figure 6, at the center of the domain (y=40 km), the GL position ~~varies~~ differs by 12 and 13 km between the most refined uniform mesh and the adaptive meshes generated by Bamg and NeoPZ, respectively. Between the coarse mesh and the adaptive meshes, the GL position ~~varies~~ differs by about 10 km (for both Bamg and NeoPZ). When the ZZ criterion is used, the GL positions differ by 6 km (17 km) in comparison with the one obtained from the most refined uniform mesh (coarse mesh).

Figure 7 presents a set of results for the grounding line position and the ice volume above floatation as a function of mesh resolution. AMR mesh-dependency is clear in Figure 7. For AMR with NeoPZ, GL positions obtained with AMR R5 ~~are below~~ differ from the ones produced by AMR R15 and AMR R30. ~~Marginally~~ Virtually AMR R15 and AMR R30 produce the same GL positions. For AMR with Bamg, AMR R5 and AMR R15 do not improve the position of the GL as the resolution increases. We can note the differences of GL positions from AMR (with both Bamg and NeoPZ) and from uniformly refined meshes are higher in comparison to the MISMIP3d experiment. The same AMR mesh-dependency is observed in the VAF values.

To investigate the possible causes of this AMR mesh-dependency, we perform the AMR using the ZZ error estimator calculated for the deviatoric stress tensor, τ (Table 1). The GL positions obtained with AMR ZZ are presented in Figure 7. We observe that GL positions with AMR ZZ are closer to the ones obtained with uniform meshes, for all mesh resolutions. To understand this AMR ZZ result, we plot the spatial distributions of the ZZ error estimator for the coarse and adaptive meshes (using NeoPZ), as illustrated in Figure 8 (see also the movies in the supporting information). The ZZ error values are normalized between 0 and 1. For the coarse mesh, we see in Figure 8 that the error estimators calculated for the deviatoric stress tensor and the ice thickness present high values around the GL. In particular, for the ice thickness, the estimator also presents high values in the grounded part of the marine ice sheet, following the high gradient in the side walls of the bed topography (see Figure 4). For AMR R5 meshes, there are high ZZ error values around the refined region. This is not observed when the refinement criterion used is the ZZ estimator (AMR ZZ, see Table 1), as expected. Using the ZZ criterion induces an equalization in the spatial distribution of the estimated errors, improving the solutions (e.g., GL position, see Figure 7). In terms of ~~performance~~efficiency, AMR ZZ generates fewer elements than AMR R30. At the end of the experiment and for a level of refinement equal to 4 (resolution equal to 250 m), using NeoPZ, AMR R30 mesh has 464,712 elements, while AMR ZZ mesh has 24,428 elements (i.e., only $\sim$5% of the number of elements in AMR R30).

4.2 AMR time performance

To analyze the AMR performance in terms of computational time, we run the experiment Ice1r of MISMIP+ (Asay-Davis et al., 2016). The experiment starts from the steady state condition and runs forward in time for 100 years with a basal melt rate applied. The time step is equal to 0.2 yr (computed to fulfil the CFL condition for the highest resolution mesh). The nonlinear SSA equations are solved using the Picard scheme and the Multifrontal Massively Parallel sparse direct Solver, MUMPS (Amestoy et al., 2001, 2006).

The purpose of the experiments described here is to assess the computational overhead when AMR is active. We initialize all the models using the steady state solution obtained with the same AMR mesh (level of refinement and criteria) used to carry

out the experiment Ice1r. This procedure emulates a common modeling practice (e.g., Cornford et al., 2013; Lee et al., 2015): the initial conditions are self-consistent with the AMR mesh, avoiding numerical artifacts during the transient simulation. All the experiments are run in parallel (16 cores) in a 2x Intel Xeon E5-2630 v3 2.40 GHz with 64 GB of RAM.

Table 3 presents GL positions obtained with different meshes at the end of experiment Ice1r, and the computational time and number of elements required for each mesh, as well as the criterion used. The levels of refinement are labeled as 'L#', e.g., L3 means level 3 (see Table 2). Considering the GL position obtained from the highest resolution mesh (L4 uniform) as a reference result, we compare the computational cost using uniform and AMR meshes to obtain the same result within a deviation of 1.5%. In Table 3, only L3 uniform, L3 AMR R30, L3 AMR ZZ and L3 AMR R5+ZZ meshes produce this required accuracy. ~~L3 uniform~~ AMR R30 mesh has at least ~~4× more elements than the AMR R30~~ 25% of the number of elements of the L3 uniform mesh, which represents ~~a computational time 24%× higher in comparison with the adaptive approach~~virtually 80% of the computational time using the uniform mesh. In terms of refinement criteria, AMR ZZ generates ~~one-fifth~~ 20% of the number of elements in comparison to AMR R30, which means virtually ~~at least a quarter~~ 25% of computational time. Comparing AMR ZZ and L3 uniform, the computational time using the adaptive mesh ~~is at least 4.5× less. The performances~~ represents at least 25% of the computational time using the uniform mesh. The performance of Bamg and NeoPZ ~~are similar, once~~ is similar, and the ratio of computational time and number of elements is virtually equal for both packages (not shown here).

Figure 9 shows the element counts and the solution time for the AMR meshes normalized against the values for the equivalent uniform meshes. In Figure 9, the solution time curve represents the relative savings due to AMR, while the gap between the two curves (solution time minus element counts) illustrates the overhead due to the AMR procedure. We note the AMR overhead decreases with the level of refinement and becomes reasonable for level 2 or higher.

5 Discussion

In this work, we describe the implementation of an adaptive mesh refinement approach in the Ice Sheet System Model (v4.14) as well as the performance of our implementation in terms of accuracy of the simulated grounding line position and simulation time. We investigate the adaptive meshes performance using a heuristic criterion based on the distance to the GL (Durand et al., 2009; Goldberg et al., 2009; Gudmundsson et al., 2012; Cornford et al., 2013), and we compare with an error estimator (ZZ, Zienkiewicz and Zhu, 1987) based on the a posteriori analysis of the transient solutions (e.g., Goldberg et al., 2009; Gudmundsson et al., 2012; Cornford et al., 2013).

We rely on two different mesh generators, Bamg (Hecht, 2006) and NeoPZ (Devloo, 1997) that have different properties. It is therefore expected that their solutions are not identical. This explains the difference observed in the GL positions (and VAF) compared to uniform meshes for the 3 sub-element parameterizations (e.g., the MISMIP3d setup, Figure 5).

NeoPZ generates nested meshes, which reduces errors in the interpolation step, ~~which~~ and is useful to assess AMR performance in comparison to uniformly refined mesh. Bamg's algorithm works differently: the fact that some vertices positions change produces at least two side effects: (1) induced errors in the interpolation process; (2) positive or negative impact on

the convergence of the solutions. The weight of the first side effect can be reduced using higher element distance to the GL (R_{gl}), for which the highest resolution is applied, and increasing the length of the mesh transition zone between fine and coarse elements. Higher-order interpolative schemes can be also used, as pointed out by Goldberg et al. (2009), to avoid solution diffusion. In ISSM, the interpolation scheme is carried out by P0 and P1 Lagrange polynomials, and we suspect these are enough for our AMR procedure. The weight of the second side effect depends on the problem considered. We suspect that for GL dynamics this effect has overall a positive impact, once updating vertex positions is somewhat similar to the moving mesh technique, although the GL is not explicitly defined in our approach as in other studies (e.g., Vieli and Payne, 2005). This argument is based on the results shown here, for both MISMIP3d and MISMIP+ setups. Some mesh packages and finite element libraries related to NeoPZ are: Deal II (Bangerth et al., 2007), Hermes (Šolín et al., 2008), libMesh (Kirk et al., 2006) and HP90 (Demkowicz et al., 1998). Mesh generators related to Bamg are: MMG (Dapogny et al., 2014), Yams (Frey, 2001) and Gmsh (Geuzaine and Remacle, 2009). So, we expect that the results shown here in this work would be reproduced with these related packages.

The results from MISMIP3d suggest that independently of the sub-element parameterization and refinement level, refining elements within a 5 km region with highest resolution around the GL is enough to generate solutions similar to the ones produced by uniform meshes. This holds for Bamg and NeoPZ (Figure 5). Cornford et al. (2013) presented similar results for MISMIP3d using SSA equations through BISICLES, an AMR finite volume-based ice sheet ~~simulator. They~~ model. Based on the MISMIP3d experiment, they concluded that refining 4 cells on either sides of the GL was enough to achieve results similar to uniform meshes for all levels of refinement.

For MISMIP+, a minimal distance of 30 km for the highest resolution around the GL is necessary to accurately capture the GL position (Figure 7). Nevertheless, there is a residual between GL positions from AMR and uniform meshes. This AMR mesh-dependency can be explained by the bed topography of MISMIP+ (Figure 4): the high gradient in the side walls induces numerical errors on the gradients of the velocity field (deviatoric stress tensor, near the GL) and ice thickness (on grounded ice), as illustrated by the spatial distribution of the a posteriori error estimator used here (Figure 8). For the MISMIP3d setup, the highest values of the error estimate concentrate only around the GL (not shown here), which explains why a few kilometers of high resolution near the GL improves the GL positions.

Figures 5 and 7 present a picture of the impact of mesh resolution in integrated quantities like VAF. The VAF curves follow the GL position behaviour, presenting the same AMR mesh-dependency in the MISMIP+ setup. Therefore, the accuracy of VAF depends on the accuracy of the GL dynamics. Since VAF changes represent potential sea level rise, we highlight that the GL movement should be accurately tracked in ice sheet models.

Since numerical errors are not only concentrated near the GL for the MISMIP+ setup, an error estimator is likely more appropriate to understand the error structure of the problem, to guide the refinement and to reduce the error estimates along the domain, improving AMR performance. This explains why a simple test with the AMR ZZ produces better convergence with much less elements than AMR based on the heuristic criterion (element distance to the GL, Figure 7). Related works have used proxies of error estimators: Goldberg et al. (2009) used the jumps in strain rate between adjacent cells; Gudmundsson et al. (2012) used the second derivative of the ice thickness; Cornford et al. (2013) used the Laplacian of the velocity field

and Gillet-Chaulet et al. (2017) used the estimator proposed by Frey and Alauzet (2005), whose metric is based on a priori interpolation error calculated by the field's Hessian matrix (second derivative). The ZZ used here is a true a posteriori error estimator based on the recovered gradient (Ainsworth and Oden, 2000, p. 3), widely used in the finite element community (Ainsworth et al., 1989; Grätsch and Bathe, 2005) and suitable to be implemented in ice sheet models, ~~or the ones~~ including those based on finite volumes or finite differences. As the MISMIP+ bed geometry is more realistic than MISMIP3d, we can expect a similar result for real glaciers, i.e., high numerical errors present in regions not necessarily adjacent to the GL.

Further analysis with ZZ or another error estimator should be developed to improve the AMR criterion used in ice sheet modeling. An important issue to be investigated is the interpolation of real bed topography directly from a dataset every time AMR is carried out. This interpolation increases bed resolution according to mesh adaptation, which reduces the smoothness of the bed in the model (since real beds are not necessarily smooth). The reduction of the bed smoothness induces some numerical errors and counterbalances the effect of mesh adaptation, increasing AMR mesh-dependency. Real bed topographies should be analyzed in benchmark models as well as in real ice sheet domains. Our current AMR implementation interpolates the bed elevation from the coarse (initial) mesh, except for the MISMIP+ experiment, for which we hard-coded the calculation of the bed topography directly in the code (in this case, AMR reduces the smoothness of the bed in the model, but as there is no ~~noise~~small-scale bed topography, the numerical error based on the ZZ error estimator for the ice thickness is reduced). The interpolation from a dataset will be implemented in ISSM in the future. Based on this discussion and the results shown in this study, we recommend AMR with the combination of the heuristic criterion (using a minimal distance, e.g., 5 km) with an associated error estimator. Our recommendation is based on the following: we know a priori that applying high resolution around the GL would reduce the error caused by the basal friction discretization within the elements. In fact, applying only an error estimator does not guarantee that the elements around the GL are refined until the highest (desired) resolution. We noted this for the MISMIP+ setup (see the last mesh in Figure 6). Otherwise, only imposing fine mesh resolution near the GL does not ensure that the GL position is correctly captured because the extension of the ~~region (around the GL) where the velocity field changes significantly~~ grounding zone (where the deviatoric stress dominates the stress balance in the ice sheet-shelf transition; e.g., see Figure 11 in Schoof, 2007b) depends on the physical parameters of the ice sheet. Interestingly, for the MISMIP+ setup, the combination of the heuristic criterion with the ZZ error estimator (AMR R5+ZZ) and the AMR ZZ produce similar results (as shown in Table 4), which does not mean that it would be the case for real ice sheets. Therefore, for real ice sheets, we suspect that using both criteria (R5+ZZ) should work properly. Tests varying AMR parameters (distance to the GL, maximum thresholds for the error estimator, level of refinement, etc.) should be carried before any ice sheet simulation to optimize AMR performance in terms of both solutions and computational time.

The grounding ~~line~~ zone is not the only place where AMR can be applied. Ice front and calving dynamics (Todd et al., 2018) as well as shear margins in ice streams (Haseloff et al., 2015) are examples for which adaptive meshes can improve numerical solutions with reduced computational efforts. In ISSM, the AMR can be applied to these regions through extension of Algorithm 2. Other experiments (not shown here) testing the AMR to refine the ice front region show promising results (Santos et al., 2018).

Our AMR performance analysis shows that the computational time in AMR simulations reaches up to one order of magnitude less in comparison to models based on uniform meshes. Computational time and solution accuracy of AMR depend on the physical problem and the refinement criterion used. In this work, even with hundreds of elements generated (e.g., meshes AMR R30), the computational time is satisfactory. This is observed for both NeoPZ and Bamg. Further analysis should be carried out to check the performance in real ice sheets and in higher computational scale (thousand of elements), but the results presented in this study suggest that our AMR implementation strategy is adapted to the modeling questions being investigated. Our AMR computation time compares to Cornford et al. (2013), in which AMR simulations spend $\sim$1/3 of CPU time needed in simulations performed by uniform meshes.

6 Conclusions

We implemented dynamic AMR into ISSM and tested its performance on two different experiments with different refinement criteria. The comparison between Bamg and NeoPZ shows that they present similar performance, and the choice of which to be used is up to the user. Moreover, users using Bamg (or similar mesh generator) should pay attention in the minimal extension of the mesh transition zone to reduce numerical errors (e.g., in the interpolation step). NeoPZ is more suitable with error estimators, as well as in AMR performance comparison. Based on the AMR mesh-sensitivity observed here, we conclude that AMR without an error estimator should be avoided, mainly in setups where bedrock induces complex stress distributions and/or strong buttressing. In real bedrock topographies, where small scale features may play an important role, an error estimator is suitable to guide the AMR. Further research should be carried out in order to evaluate AMR performance in real bed geometries. Our recommendation to improve the AMR performance while minimizing computational effort is the combination of the heuristic criteria, applying a minimal distance around the GL (e.g., 5 km), with an error estimator. The simple tests with the ZZ error estimator show a significant potential, mostly due to its simple implementation and performance. The AMR technique in ISSM can be extended to others physical processes such that the evolution of ice sheets and, consequently the sea level rise, can be accurately modeled and projected.

Code availability. The adaptive mesh refinement are currently implemented in the ISSM code for triangular elements. The code can be download, compiled and executed following the instructions avaiable on the ISSM website: https://issm.jpl.nasa.gov/download.

Competing interests. Authors declare no competing interests.

Acknowledgements. This work was performed at the University of Campinas (UNICAMP) and Federal University of Rio Grande do Sul (UFRGS) with financial support from CNPq - Conselho Nacional de Desenvolvimento Científico e Tecnológico, Brazil, PhD scholarship

N^o 140186/2015-8 - and at the University of California, Irvine, under a contract with the National Aeronautics and Space Administration (NASA), Cryospheric Sciences Program (N^o NNX14AN03G).

References

Ainsworth, M. and Oden, J. T.: A Posterori Error Estimation in Finite Element Analysis, Pure and Applied Mathematics: A Wiley Series of Texts, Monographs and Tracts, Wiley-Interscience, New York, NY, USA, 1st edn., 2000.

Ainsworth, M., Zhu, J. Z., Craig, A. W., and Zienkiewicz, O. C.: Analysis of the Zienkiewicz–Zhu a-posteriori error estimator in the finite element method, International Journal for Numerical Methods in Engineering, 28, 2161–2174, https://doi.org/10.1002/nme.1620280912, https://onlinelibrary.wiley.com/doi/abs/10.1002/nme.1620280912, 1989.

Amestoy, P. R., Duff, I. S., L'Excellent, J.-Y., and Koster, J.: A Fully Asynchronous Multifrontal Solver Using Distributed Dynamic Scheduling, SIAM Journal on Matrix Analysis and Applications, 23, 15–41, https://doi.org/10.1137/S0895479899358194, 2001.

Amestoy, P. R., Guermouche, A., L'Excellent, J.-Y., and Pralet, S.: Hybrid scheduling for the parallel solution of linear systems, Parallel Computing, 32, 136–156, https://doi.org/https://doi.org/10.1016/j.parco.2005.07.004, http://www.sciencedirect.com/science/article/pii/S0167819105001328, parallel Matrix Algorithms and Applications (PMAA'04), 2006.

Anderson, D. A., Tannehill, J. C., and Pletcher, R. H.: Computational Fluid Mechanics and Heat Transfer, Series in computational methods in mechanics and thermal sciences, McGraw-Hill Book Company, USA, 1984.

Asay-Davis, X. S., Cornford, S. L., Durand, G., Galton-Fenzi, B. K., Gladstone, R. M., Gudmundsson, G. H., Hattermann, T., Holland, D. M., Holland, D., Holland, P. R., Martin, D. F., Mathiot, P., Pattyn, F., and Seroussi, H.: Experimental design for three interrelated marine ice sheet and ocean model intercomparison projects: MISMIP v. 3 (MISMIP+), ISOMIP v. 2 (ISOMIP+) and MISOMIP v. 1 (MISOMIP1), Geoscientific Model Development, 9, 2471–2497, https://doi.org/10.5194/gmd-9-2471-2016, https://www.geosci-model-dev.net/9/2471/2016/, 2016.

Bangerth, W., Hartmann, R., and Kanschat, G.: Deal.II&Mdash;A General-purpose Object-oriented Finite Element Library, ACM Trans. Math. Softw., 33, https://doi.org/10.1145/1268776.1268779, http://doi.acm.org/10.1145/1268776.1268779, 2007.

Berger, M. and Colella, P.: Local adaptive mesh refinement for shock hydrodynamics, Journal of Computational Physics, 82, 64–84, https://doi.org/https://doi.org/10.1016/0021-9991(89)90035-1, http://www.sciencedirect.com/science/article/pii/0021999189900351, 1989.

Bindschadler, R. A., Nowicki, S., Abe-Ouchi, A., Aschwanden, A., Choi, H., Fastook, J., Granzow, G., Greve, R., Gutowski, G., Herzfeld, U., and et al.: Ice-sheet model sensitivities to environmental forcing and their use in projecting future sea level (the SeaRISE project), Journal of Glaciology, 59, 195–224, https://doi.org/10.3189/2013JoG12J125, 2013.

Calle, J. L. D., Devloo, P. R., and Gomes, S. M.: Implementation of continuous hp-adaptive finite element spaces without limitations on hanging sides and distribution of approximation orders, Computers & Mathematics with Applications, 70, 1051–1069, https://doi.org/https://doi.org/10.1016/j.camwa.2015.06.033, http://www.sciencedirect.com/science/article/pii/S0898122115003193, 2015.

Christie, F. D. W., Bingham, R. G., Gourmelen, N., Tett, S. F. B., and Muto, A.: Four-decade record of pervasive grounding line retreat along the Bellingshausen margin of West Antarctica, Geophysical Research Letters, 43, 5741–5749, https://doi.org/10.1002/2016GL068972, https://agupubs.onlinelibrary.wiley.com/doi/abs/10.1002/2016GL068972, 2016.

Church, J., Clark, P., Cazenave, A., Gregory, J., Jevrejeva, S., Levermann, A., Merrifield, M., Milne, G., Nerem, R., Nunn, P., Payne, A., Pfeffer, W., Stammer, D., and Unnikrishnan, A.: Sea Level Change, in: Climate Change 2013: The Physical Science Basis. Contribution of Working Group I to the Fifth Assessment Report of the Intergovernmental Panel on Climate Change, edited by Stocker, T., Qin, D., Plattner, G.-K., Tignor, M., Allen, S., Boschung, J., Nauels, A., Xia, Y., Bex, V., and Midgley, P., pp. 1137–1216, Cambridge University

Press, Cambridge, United Kingdom and New York, NY, USA, http://www.ipcc.ch/pdf/assessment-report/ar5/wg1/WG1AR5_Chapter13_FINAL.pdf, 2013.

Cornford, S. L., Martin, D. F., Graves, D. T., Ranken, D. F., Brocq, A. M. L., Gladstone, R. M., Payne, A. J., Ng, E. G., and Lipscomb, W. H.: Adaptive mesh, finite volume modeling of marine ice sheets, Journal of Computational Physics, 232, 529 – 549, https://doi.org/https://doi.org/10.1016/j.jcp.2012.08.037, http://www.sciencedirect.com/science/article/pii/S0021999112005050, 2013.

Cuffey, K. and Paterson, W. S. B.: The Physics of Glaciers, Elsevier, Oxford, 4th edn., 2010.

Dapogny, C., Dobrzynski, C., and Frey, P.: Three-dimensional adaptive domain remeshing, implicit domain meshing, and applications to free and moving boundary problems, Journal of Computational Physics, 262, 358–378, https://doi.org/https://doi.org/10.1016/j.jcp.2014.01.005, http://www.sciencedirect.com/science/article/pii/S0021999114000266, 2014.

DeConto, R. and Pollard, D.: Contribution of Antarctica to past and future sea-level rise, Nature, 531, 591–597, https://doi.org/10.1038/nature17145, http://dx.doi.org/10.1038/nature17145, 2016.

Demkowicz, L., Gerdes, K., Schwab, C., Bajer, A., and Walsh, T.: HP90: A general and flexible Fortran 90 hp-FE code, Computing and Visualization in Science, 1, 145–163, https://doi.org/10.1007/s007910050014, https://doi.org/10.1007/s007910050014, 1998.

Devloo, P., Oden, J., and Strouboulis, T.: Implementation of an adaptive refinement technique for the SUPG algorithm, Computer Methods in Applied Mechanics and Engineering, 61, 339–358, https://doi.org/https://doi.org/10.1016/0045-7825(87)90099-5, http://www.sciencedirect.com/science/article/pii/0045782587900995, 1987.

Devloo, P. R. B.: PZ: An object oriented environment for scientific programming, Computer Methods in Applied Mechanics and Engineering, 150, 133–153, https://doi.org/https://doi.org/10.1016/S0045-7825(97)00097-2, http://www.sciencedirect.com/science/article/pii/S0045782597000972, symposium on Advances in Computational Mechanics, 1997.

Durand, G., Gagliardini, O., Zwinger, T., Meur, E. L., and Hindmarsh, R. C.: Full Stokes modeling of marine ice sheets: influence of the grid size, Annals of Glaciology, 50, 109–114, https://doi.org/10.3189/172756409789624283, 2009.

Dutrieux, P., De Rydt, J., Jenkins, A., Holland, P. R., Ha, H. K., Lee, S. H., Steig, E. J., Ding, Q., Abrahamsen, E. P., and Schröder, M.: Strong Sensitivity of Pine Island Ice-Shelf Melting to Climatic Variability, Science, 343, 174–178, https://doi.org/10.1126/science.1244341, http://science.sciencemag.org/content/343/6167/174, 2014.

Favier, L., Durand, G., Cornford, S. L., Gudmundsson, G. H., Gagliardini, O., Gillet-Chaulet, F., Zwinger, T., Payne, A. J., and Le Brocq, A. M.: Retreat of Pine Island Glacier controlled by marine ice-sheet instability, Nature Climate Change, 4, 117–121, https://doi.org/10.1038/nclimate2094, https://www.nature.com/articles/nclimate2094#supplementary-information, 2014.

Feldmann, J., Albrecht, T., Khroulev, C., Pattyn, F., and Levermann, A.: Resolution-dependent performance of grounding line motion in a shallow model compared with a full-Stokes model according to the MISMIP3d intercomparison, Journal of Glaciology, 60, 353–360, https://doi.org/10.3189/2014JoG13J093, 2014.

Fretwell, P., Pritchard, H. D., Vaughan, D. G., Bamber, J. L., Barrand, N. E., Bell, R., Bianchi, C., Bingham, R. G., Blankenship, D. D., Casassa, G., Catania, G., Callens, D., Conway, H., Cook, A. J., Corr, H. F. J., Damaske, D., Damm, V., Ferraccioli, F., Forsberg, R., Fujita, S., Gim, Y., Gogineni, P., Griggs, J. A., Hindmarsh, R. C. A., Holmlund, P., Holt, J. W., Jacobel, R. W., Jenkins, A., Jokat, W., Jordan, T., King, E. C., Kohler, J., Krabill, W., Riger-Kusk, M., Langley, K. A., Leitchenkov, G., Leuschen, C., Luyendyk, B. P., Matsuoka, K., Mouginot, J., Nitsche, F. O., Nogi, Y., Nost, O. A., Popov, S. V., Rignot, E., Rippin, D. M., Rivera, A., Roberts, J., Ross, N., Siegert, M. J., Smith, A. M., Steinhage, D., Studinger, M., Sun, B., Tinto, B. K., Welch, B. C., Wilson, D., Young, D. A., Xiangbin, C., and Zirizzotti, A.: Bedmap2: improved ice bed, surface and thickness datasets for Antarctica, The Cryosphere, 7, 375–393, https://doi.org/10.5194/tc-7-375-2013, https://www.the-cryosphere.net/7/375/2013/, 2013.

Frey, P.: YAMS A fully Automatic Adaptive Isotropic Surface Remeshing Procedure, Tech. rep., INRIA, 2001.

Frey, P. and Alauzet, F.: Anisotropic mesh adaptation for CFD computations, Computer Methods in Applied Mechanics and Engineering, 194, 5068–5082, https://doi.org/https://doi.org/10.1016/j.cma.2004.11.025, http://www.sciencedirect.com/science/article/pii/S0045782505000794, unstructured Mesh Generation, 2005.

Gagliardini, O., Zwinger, T., Gillet-Chaulet, F., Durand, G., Favier, L., de Fleurian, B., Greve, R., Malinen, M., Martín, C., Råback, P., Ruokolainen, J., Sacchettini, M., Schäfer, M., Seddik, H., and Thies, J.: Capabilities and performance of Elmer/Ice, a new-generation ice sheet model, Geoscientific Model Development, 6, 1299–1318, https://doi.org/10.5194/gmd-6-1299-2013, https://www.geosci-model-dev.net/6/1299/2013/, 2013.

Geuzaine, C. and Remacle, J.-F.: Gmsh: A 3-D finite element mesh generator with built-in pre- and post-processing facilities, International Journal for Numerical Methods in Engineering, 79, 1309–1331, https://doi.org/10.1002/nme.2579, https://onlinelibrary.wiley.com/doi/abs/10.1002/nme.2579, 2009.

Gillet-Chaulet, F., Tavard, L., Merino, N., Peyaud, V., Brondex, J., Durand, G., and Gagliardini, O.: Anisotropic mesh adaptation for marine ice-sheet modelling, in: EGU General Assembly 2017, vol. 19, Geophysical Research Abstracts, Vienna, Austria, https://meetingorganizer.copernicus.org/EGU2017/EGU2017-2048.pdf, 2017.

Gladstone, R. M., Lee, V., Vieli, A., and Payne, A. J.: Grounding line migration in an adaptive mesh ice sheet model, Journal of Geophysical Research: Earth Surface, 115, https://doi.org/10.1029/2009JF001615, https://agupubs.onlinelibrary.wiley.com/doi/abs/10.1029/2009JF001615, 2010.

Goldberg, D., Holland, D. M., and Schoof, C.: Grounding line movement and ice shelf buttressing in marine ice sheets, Journal of Geophysical Research: Earth Surface, 114, https://doi.org/10.1029/2008JF001227, https://agupubs.onlinelibrary.wiley.com/doi/abs/10.1029/2008JF001227, 2009.

Grätsch, T. and Bathe, K.-J.: A posteriori error estimation techniques in practical finite element analysis, Computers & Structures, 83, 235–265, https://doi.org/https://doi.org/10.1016/j.compstruc.2004.08.011, http://www.sciencedirect.com/science/article/pii/S0045794904003165, 2005.

Gudmundsson, G. H., Krug, J., Durand, G., Favier, L., and Gagliardini, O.: The stability of grounding lines on retrograde slopes, The Cryosphere, 6, 1497–1505, https://doi.org/10.5194/tc-6-1497-2012, https://www.the-cryosphere.net/6/1497/2012/, 2012.

Haseloff, M., Schoof, C., and Gagliardini, O.: A boundary layer model for ice stream margins, Journal of Fluid Mechanics, 781, 353–387, https://doi.org/10.1017/jfm.2015.503, 2015.

Hecht, F.: A few snags in mesh adaptation loops, in: Proceedings of the 14th International Meshing Roundtable, edited by Hanks, B. W., pp. 301–311, Springer-Verlag Berlin Heidelberg, Germany, 2005.

Hecht, F.: BAMG: Bidimensional Anisotropic Mesh Generator, Tech. rep., FreeFem++, 2006.

Jacobs, S. S., Jenkins, A., Giulivi, C. F., and Dutrieux, P.: Stronger ocean circulation and increased melting under Pine Island Glacier ice shelf, Nature Geoscience, 4, 519–523, https://doi.org/10.1038/ngeo1188, 2011.

Jevrejeva, S., Grinsted, A., and Moore, J. C.: Upper limit for sea level projections by 2100, Environmental Research Letters, 9, 104 008, http://stacks.iop.org/1748-9326/9/i=10/a=104008, 2014.

Jouvet, G. and Gräser, C.: An adaptive Newton multigrid method for a model of marine ice sheets, Journal of Computational Physics, 252, 419 – 437, https://doi.org/https://doi.org/10.1016/j.jcp.2013.06.032, http://www.sciencedirect.com/science/article/pii/S0021999113004622, 2013.

Katz, R. F. and Worster, M. G.: Stability of ice-sheet grounding lines, Proceedings of the Royal Society of London A: Mathematical, Physical and Engineering Sciences, 466, 1597–1620, https://doi.org/10.1098/rspa.2009.0434, http://rspa.royalsocietypublishing.org/content/466/2118/1597, 2010.

Kimura, S., Jenkins, A., Dutrieux, P., Forryan, A., Naveira Garabato, A. C., and Firing, Y.: Ocean mixing beneath Pine Island Glacier ice shelf, West Antarctica, Journal of Geophysical Research: Oceans, 121, 8496–8510, https://doi.org/10.1002/2016JC012149, https://agupubs.onlinelibrary.wiley.com/doi/abs/10.1002/2016JC012149, 2016.

Kirk, B. S., Peterson, J. W., Stogner, R. H., and Carey, G. F.: libMesh : a C++ library for parallel adaptive mesh refinement/coarsening simulations, Engineering with Computers, 22, 237–254, https://doi.org/10.1007/s00366-006-0049-3, https://doi.org/10.1007/s00366-006-0049-3, 2006.

Larour, E., Seroussi, H., Morlighem, M., and Rignot, E.: Continental scale, high order, high spatial resolution, ice sheet modeling using the Ice Sheet System Model (ISSM), Journal of Geophysical Research: Earth Surface, 117, https://doi.org/10.1029/2011JF002140, https://agupubs.onlinelibrary.wiley.com/doi/abs/10.1029/2011JF002140, 2012.

Lee, V., Cornford, S. L., and Payne, A. J.: Initialization of an ice-sheet model for present-day Greenland, Annals of Glaciology, 56, 129–140, https://doi.org/10.3189/2015AoG70A121, 2015.

Leguy, G. R., Asay-Davis, X. S., and Lipscomb, W. H.: Parameterization of basal friction near grounding lines in a one-dimensional ice sheet model, The Cryosphere, 8, 1239–1259, https://doi.org/10.5194/tc-8-1239-2014, https://www.the-cryosphere.net/8/1239/2014/, 2014.

MacAyeal, D.: Large-scale ice flow over a viscous basal sediment: Theory and application to ice stream B, Antarctica, Journal of Geophysical Research: Solid Earth, 94, 4071–4087, https://doi.org/10.1029/JB094iB04p04071, https://agupubs.onlinelibrary.wiley.com/doi/abs/10.1029/JB094iB04p04071, 1989.

Mercer, J. H.: West Antarctic ice sheet and CO2 greenhouse effect: a threat of disaster, Nature, 271, 321–325, https://doi.org/10.1038/271321a0, 1978.

Morland, L. W.: Unconfined ice shelf flow, in: Dynamics of the West Antarctic Ice Sheet, edited by Van der Veen, C. and Oerlemans, J., vol. 4 of *Glaciology and Quaternary Geology*, pp. 99–116, Springer, Dordrecht, The Netherlands, 1987.

Morlighem, M., Rignot, E., Seroussi, H., Larour, E., Ben Dhia, H., and Aubry, D.: Spatial patterns of basal drag inferred using control methods from a full-Stokes and simpler models for Pine Island Glacier, West Antarctica, Geophysical Research Letters, 37, https://doi.org/10.1029/2010GL043853, https://agupubs.onlinelibrary.wiley.com/doi/abs/10.1029/2010GL043853, 2010.

Oden, J., Strouboulis, T., and Devloo, P.: Adaptive finite element methods for the analysis of inviscid compressible flow: Part I. Fast refinement/unrefinement and moving mesh methods for unstructured meshes, Computer Methods in Applied Mechanics and Engineering, 59, 327–362, https://doi.org/https://doi.org/10.1016/0045-7825(86)90004-6, http://www.sciencedirect.com/science/article/pii/0045782586900046, 1986.

Pattyn, F.: A new three-dimensional higher-order thermomechanical ice sheet model: Basic sensitivity, ice stream development, and ice flow across subglacial lakes, Journal of Geophysical Research, 108, 1–15, 2003.

Pattyn, F.: Sea-level response to melting of Antarctic ice shelves on multi-centennial timescales with the fast Elementary Thermomechanical Ice Sheet model (f.ETISh v1.0), The Cryosphere, 11, 1851–1878, https://doi.org/10.5194/tc-11-1851-2017, https://www.the-cryosphere.net/11/1851/2017/, 2017.

Pattyn, F., Schoof, C., Perichon, L., Hindmarsh, R. C. A., Bueler, E., de Fleurian, B., Durand, G., Gagliardini, O., Gladstone, R., Goldberg, D., Gudmundsson, G. H., Huybrechts, P., Lee, V., Nick, F. M., Payne, A. J., Pollard, D., Rybak, O., Saito, F., and Vieli, A.: Results

of the Marine Ice Sheet Model Intercomparison Project, MISMIP, The Cryosphere, 6, 573–588, https://doi.org/10.5194/tc-6-573-2012, https://www.the-cryosphere.net/6/573/2012/, 2012.

Pattyn, F., Perichon, L., Durand, G., Favier, L., Gagliardini, O., Hindmarsh, R. C., Zwinger, T., Albrecht, T., Cornford, S., Docquier, D., and et al.: Grounding-line migration in plan-view marine ice-sheet models: results of the ice2sea MISMIP3d intercomparison, Journal of Glaciology, 59, 410–422, https://doi.org/10.3189/2013JoG12J129, 2013.

Pollard, D. and DeConto, R. M.: Modelling West Antarctic ice sheet growth and collapse through the past five million years, Nature, 458, 329–332, https://doi.org/10.1038/nature07809, https://www.nature.com/articles/nature07809#supplementary-information, 2009.

Pollard, D. and DeConto, R. M.: Description of a hybrid ice sheet-shelf model, and application to Antarctica, Geoscientific Model Development, 5, 1273–1295, https://doi.org/10.5194/gmd-5-1273-2012, https://www.geosci-model-dev.net/5/1273/2012/, 2012.

Reinders, J. and Jeffers, J.: High Performance Parallelism Pearls, vol. 2, Morgan Kaufmann, Waltham, MA, USA, 2015.

Rignot, E., Mouginot, J., Morlighem, M., Seroussi, H., and Scheuchl, B.: Widespread, rapid grounding line retreat of Pine Island, Thwaites, Smith, and Kohler glaciers, West Antarctica, from 1992 to 2011, Geophysical Research Letters, 41, 3502–3509, https://doi.org/10.1002/2014GL060140, https://agupubs.onlinelibrary.wiley.com/doi/abs/10.1002/2014GL060140, 2014.

Ritz, C., Edwards, T., Durand, G., Payne, A., Peyaud, V., and Hindmarsh, R.: Potential sea-level rise from Antarctic ice-sheet instability constrained by observations, Nature, 528, 115–118, https://doi.org/10.1038/nature16147, http://dx.doi.org/10.1038/nature16147, 2015.

Santos, T. D., Devloo, P. R. B., Simões, J. C., Morlighem, M., and Seroussi, H.: Adaptive Mesh Refinement Applied to Grounding Line and Ice Front Dynamics, in: EGU General Assembly 2018, vol. 20, Geophysical Research Abstracts, Vienna, Austria, https://meetingorganizer.copernicus.org/EGU2018/EGU2018-1886.pdf, 2018.

Schoof, C.: Marine ice-sheet dynamics. Part 1. The case of rapid sliding, Journal of Fluid Mechanics, 573, 27–55, https://doi.org/10.1017/S0022112006003570, 2007a.

Schoof, C.: Ice sheet grounding line dynamics: Steady states, stability, and hysteresis, Journal of Geophysical Research: Earth Surface, 112, https://doi.org/10.1029/2006JF000664, https://agupubs.onlinelibrary.wiley.com/doi/abs/10.1029/2006JF000664, 2007b.

Seroussi, H., Morlighem, M., Larour, E., Rignot, E., and Khazendar, A.: Hydrostatic grounding line parameterization in ice sheet models, The Cryosphere, 8, 2075–2087, https://doi.org/10.5194/tc-8-2075-2014, https://www.the-cryosphere.net/8/2075/2014/, 2014a.

Seroussi, H., Morlighem, M., Rignot, E., Mouginot, J., Larour, E., Schodlok, M., and Khazendar, A.: Sensitivity of the dynamics of Pine Island Glacier, West Antarctica, to climate forcing for the next 50 years, The Cryosphere, 8, 1699–1710, https://doi.org/10.5194/tc-8-1699-2014, https://www.the-cryosphere.net/8/1699/2014/, 2014b.

Seroussi, H., Nakayama, Y., Larour, E., Menemenlis, D., Morlighem, M., Rignot, E., and Khazendar, A.: Continued retreat of Thwaites Glacier, West Antarctica, controlled by bed topography and ocean circulation, Geophysical Research Letters, 44, 6191–6199, https://doi.org/10.1002/2017GL072910, https://agupubs.onlinelibrary.wiley.com/doi/abs/10.1002/2017GL072910, 2017.

Szabó, B. and Babuška, I.: Finite Element Analysis, John Wiley & Sons, USA, 1991.

Thomas, R.: The Dynamics of Marine Ice Sheet, Journal of Glaciology, 24, 167–177, https://doi.org/10.3189/S0022143000014726, 1979.

Todd, J., Christoffersen, P., Zwinger, T., Råback, P., Chauché, N., Benn, D., Luckman, A., Ryan, J., Toberg, N., Slater, D., and Hubbard, A.: A Full-Stokes 3-D Calving Model Applied to a Large Greenlandic Glacier, Journal of Geophysical Research: Earth Surface, 123, 410–432, https://doi.org/10.1002/2017JF004349, https://agupubs.onlinelibrary.wiley.com/doi/abs/10.1002/2017JF004349, 2018.

Vieli, A. and Payne, A. J.: Assessing the ability of numerical ice sheet models to simulate grounding line migration, Journal of Geophysical Research: Earth Surface, 110, https://doi.org/10.1029/2004JF000202, https://agupubs.onlinelibrary.wiley.com/doi/abs/10.1029/2004JF000202, 2005.

Šolín, P., Červený, J., and Doležel, I.: Arbitrary-level hanging nodes and automatic adaptivity in the hp-FEM, Mathematics and Computers in Simulation, 77, 117–132, https://doi.org/https://doi.org/10.1016/j.matcom.2007.02.011, http://www.sciencedirect.com/science/article/pii/S0378475407001504, 2008.

Weertman, J.: Stability of the junction of an ice sheet and an ice shelf, Journal of Glaciology, 13, 3–11, https://doi.org/10.3189/S0022143000023327, 1974.

Zienkiewicz, O. C. and Zhu, J. Z.: A simple error estimator and adaptive procedure for practical engineerng analysis, International Journal for Numerical Methods in Engineering, 24, 337–357, https://doi.org/10.1002/nme.1620240206, https://onlinelibrary.wiley.com/doi/abs/10.1002/nme.1620240206, 1987.

Figure 1. Vertical cross-section of a marine ice sheet: **marine ice sheet**, **ocean** and **bed**. The position of the grounding line is implicitly defined by the level set function, ϕ_{gl}, based on a hydrostatic floatation criterion (Seroussi et al., 2014a).

Figure 2. Solution sequence for ice sheet transient simulation with adaptive mesh refinement.

Figure 3. Examples of adaptive meshes using Bamg and NeoPZ. **Blue line**: grounding line position. **Black lines**: coarse mesh, common for Bamg and NeoPZ. **Green lines**: adaptive meshes with level of refinement equal to 2 (L2). Bamg keeps vertices and connectivities unchanged as much as possible compared to the coarse mesh. NeoPZ generates nested meshes: vertices and connectivities of the coarse mesh are kept unchanged.

Algorithm 1 Transient simulation with AMR

1. set initial solution state and initial mesh[4]
2. while $t_n \leq t_{max}$ do:
    a. call stress balance core (diagnostic)
    b. call thickness balance core (prognostic)
    c. call ice front migration core (level set adjustment)
    d. call grounding line migration core (hydrostatic adjustment)
    e. call remesh core (AMR)
        e.1. call AMR core (refine/coarsen mesh, Bamg or NeoPZ, serial in CPU #0)
        e.2. call mesh partitioning (over all CPU's, serial)
        e.3. build new data structures (all CPU's, parallel)
        e.4. interpolate solutions (all CPU's, parallel)
        e.5. call geometry adjustment core (all CPU's, parallel)
    f. time increment $t_{n+1} = t_n + dt$
3. post processing

[4]The setup of the inital solution into the initial mesh is important to reduce numerical artifacts in the first time steps. Therefore, the initial mesh should be defined using AMR with the same level of refinement chosen in Algorithm 1 (e.g., see Cornford et al., 2013; Lee et al., 2015).

Algorithm 2 AMR core: refinement criteria calculation, refinement and coarsening processes. e = element. g = group of elements that are nested and derived from a refined element. $L(e)$ = level of refinement of the element e. L^{max} = maximum level of refinement. R^{max} = maximum threshold for element/group distance to the grounding line. ϵ^{max} = maximum threshold for element/group error estimator (thickness/deviatoric stress). θ = binary flags that define the criteria.

1. if $\theta_{gl} = 1$, then **compute** the element and group distances to the grounding line, $R_{gl}(e)$ and $R_{gl}(g)$.
2. if $\theta_{\tau} = 1$, then **compute** the element and group deviatoric stress error estimators, $\epsilon_{\tau}(e)$ and $\epsilon_{\tau}(g)$.
3. if $\theta_{H} = 1$, then **compute** the element and group thickness error estimators, $\epsilon_{H}(e)$ and $\epsilon_{H}(g)$.
4. for each element e such that $L(e) < L^{max}$, do:
   if $\left[R_{gl}(e) < \theta_{gl} \cdot R_{gl,e}^{max}\right]$ or if $\left[\theta_{\tau} \cdot \epsilon_{\tau}(e) > \epsilon_{\tau,e}^{max}\right]$ or if $\left[\theta_{H} \cdot \epsilon_{H}(e) > \epsilon_{H,e}^{max}\right]$,
   then **refine** e.
5. for each group g, do:
   if $\left[R_{gl}(g) > \theta_{gl} \cdot R_{gl,g}^{max}\right]$ and if $\left[\theta_{\tau} \cdot \epsilon_{\tau}(g) < \epsilon_{\tau,g}^{max}\right]$ and if $\left[\theta_{H} \cdot \epsilon_{H}(g) < \epsilon_{H,g}^{max}\right]$,
   then **coarsen** g.

Table 1. Refinement criteria for the adaptive mesh refinement (AMR) simulations.

Experiment	Label	Criterion
MISMIP3d	AMR R5	distance of 5 km to the GL
MISMIP3d	AMR R10	distance of 10 km to the GL
MISMIP3d	AMR R15	distance of 15 km to the GL
MISMIP+	AMR R5	distance of 5 km to the GL
MISMIP+	AMR R15	distance of 15 km to the GL
MISMIP+	AMR R30	distance of 30 km to the GL
MISMIP+	AMR ZZ	ZZ error estimator for τ

GL = grounding line. τ = deviatoric stress tensor. The distance to the GL refers to the region with the highest level of refinement. For example, AMR R5 means that 5 km on both sides of the GL (upstream and downstream) are refined with the highest level.

Table 2. Levels of refinement tested in the experiments.

Experiment	Level	Label	Resolution
MISMIP3d	0 (CM)	L0	5 km
MISMIP3d	1	L1	2.5 km
MISMIP3d	2	L2	1.25 km
MISMIP3d	3	L3	625 m
MISMIP+	0 (CM)	L0	4 km
MISMIP+	1	L1	2 km
MISMIP+	2	L2	1 km
MISMIP+	3	L3	500 m
MISMIP+	4	L4	250 m

CM = coarse mesh, common for Bamg and NeoPZ.

Figure 4. The bedrock topography for the MISMIP+ experiment (Asay-Davis et al., 2016).

Figure 5. Grounding line (GL) positions and ice volume above floatation (VAF) at steady state obtained from the coarse mesh and from adaptive mesh refinement (AMR) using the refinement criterion based on the element distance to the GL, R_{gl}. Three element distances are used and compared: $R_{gl} = 5, = 10$ and $= 15$ km. The meshes generated with these distances are labeled as AMR R5, AMR R10 and AMR R15, respectively (see Tables 1 and 2). Results from uniformly refined meshes (labeled as uniform) are also shown. The simulations are carried out through the mesh generators Bamg (left) and NeoPZ (right) using 3 sub-element parameterizations: NSEP, SEP1 and SEP2.

Figure 6. Examples of adaptive meshes for the MISMIP+ experiment using different refinement criteria and mesh generators (see Tables 1 and 2). **Red line**: grounding line position at steady state obtained with the coarse mesh. **Black dots**: grounding line position at steady state obtained with each adaptive mesh. **Blue line**: grounding line position at steady state obtained with the most refined mesh (L4, uniform). The thresholds used in the ZZ crterion are described in the legend of Figure 7.

Figure 7. Grounding line (GL) positions and ice volume above floatation (VAF) at steady state obtained from the coarse mesh and from adaptive mesh refinement (AMR) for 4 refinement criteria: R5, R15, R30 and ZZ (see Tables 1 and 2). Results from uniformly refined meshes (uniform) are also shown. The simulations are carried out through the mesh generators Bamg (left) and NeoPZ (right) using sub-element parameterization type 1 (SEP1). The thresholds for element/group used in the ZZ criterion are, respectively, $\epsilon_{\tau,e}^{max} = 0.08\epsilon_{\tau}^{max}$ (for both Bamg and NeoPZ) and $\epsilon_{\tau,g}^{max} = 0.04\epsilon_{\tau}^{max}$ for NeoPZ and $\epsilon_{\tau,g}^{max} = 0.008\epsilon_{\tau}^{max}$ for Bamg, where ϵ_{τ}^{max} is the maximum error value observed in the coarse mesh.

Figure 8. Spatial distribution of the ZZ error estimator in the coarse and refined meshes (uniform and AMR) used in the MISMIP+ experiments. The ZZ error values are normalized between 0 and 1 using the maximum error value observed in the coarse mesh. **Black lines** are the grounding line positions at steady state obtained with the respective meshes. The refined meshes (uniform and AMR) are generated by NeoPZ considering level of refinement equal to 2 (L2, see Table 2), and the criteria used (R5 and ZZ) are summarized in Table 1. The thresholds used in the AMR ZZ are described in the legend of Figure 7.

Table 3. AMR time performance comparison for the experiment Ice1r, MISMIP+.

Level	CPU time (s)	Nb elem.	GL pos. (km)
L0 uniform	40	6,780	396.5
L1 uniform	188	27,706	407.0
L2 uniform	857	107,722	411.9
L3 uniform	1,705	473,446	416.0
L4 uniform	9,035	1,780,012	419.0
L3 AMR R5	498	33,794	405.2
L3 AMR R30	1,376	110,332	413.7
L3 AMR ZZ	369	21,088	415.7
L3 AMR R5+ZZ	807	56,267	413.7

Level = level of refinement. Nb elem. = number of elements. GL pos. = grounding line position at the end of the experiment Ice1r, MISMIP+. AMR R5+ZZ = combination of the criteria ZZ error estimator (deviatoric stress tensor) and element distance to the GL ($R_{gl} = 5$ km, R5). Mesher used: Bamg. The thresholds for element/group used in the ZZ criterion are, respectively, $\epsilon^{max}_{\tau,e} = 0.16\epsilon^{max}_{\tau}$ and $\epsilon^{max}_{\tau,g} = 0.016\epsilon^{max}_{\tau}$ for AMR ZZ, and $\epsilon^{max}_{\tau,e} = 0.48\epsilon^{max}_{\tau}$ and $\epsilon^{max}_{\tau,g} = 0.08\epsilon^{max}_{\tau}$ for AMR R5+ZZ, where ϵ^{max}_{τ} is the maximum error value observed in the coarse mesh.

Figure 9. Number of elements and CPU time for AMR meshes using the ZZ error estimator (AMR ZZ). The number of elements and CPU time are normalized by the respective values of the uniformly refined meshes. The normalized CPU time curve represents the AMR savings, while the difference between the two curves represents the adaptive mesh procedure cost. Mesher used: Bamg. The thresholds for element/group used in the AMR ZZ are, respectively, $\epsilon_{\tau,e}^{max} = 0.64\epsilon_{\tau}^{max}$ and $\epsilon_{\tau,g}^{max} = 0.32\epsilon_{\tau}^{max}$ for L1, $\epsilon_{\tau,e}^{max} = 0.24\epsilon_{\tau}^{max}$ and $\epsilon_{\tau,g}^{max} = 0.08\epsilon_{\tau}^{max}$ for L2, $\epsilon_{\tau,e}^{max} = 0.16\epsilon_{\tau}^{max}$ and $\epsilon_{\tau,g}^{max} = 0.016\epsilon_{\tau}^{max}$ for L3, $\epsilon_{\tau,e}^{max} = 0.048\epsilon_{\tau}^{max}$ and $\epsilon_{\tau,g}^{max} = 0.0064\epsilon_{\tau}^{max}$ for L4, where ϵ_{τ}^{max} is the maximum error value observed in the coarse mesh.

Table 4. AMR criteria comparison for the experiment MISMIP+.

Level	Criteria	GL pos. (km)	Nb elem.
L0	(coarse mesh)	435.6	6,780
L1	AMR ZZ	446.8	15,864
L1	AMR R5+ZZ	446.7	15,976
L1	Uniform	447.0	27,120
L2	AMR ZZ	452.6	20,891
L2	AMR R5+ZZ	452.2	22,692
L2	Uniform	451.9	108,480
L3	AMR ZZ	455.3	21,936
L3	AMR R5+ZZ	455.6	42,617
L3	Uniform	456.3	433,920
L4	AMR ZZ	455.8	24,428
L4	AMR R5+ZZ	455.4	192,149
L4	Uniform	459.0	1,735,680

Level = level of refinement. GL pos. = grounding line position at the end of the experiment. Nb elem. = number of elements. AMR R5+ZZ = combination of the criteria ZZ error estimator (deviatoric stress tensor) and element distance to the GL ($R_{gl} = 5$ km, R5). Mesher used: NeoPZ. The thresholds used in the ZZ crterion are described in the legend of Figure 7.

Binary file (standard input) matches